Control of liquid crystallinity and rheological property of clay mineral nanosheet colloids by adding biopolymer and organic molecules

THESIS SUBMITTED TO FUKUOKA INSTITUTE OF TECHNOLOGY

Riki Kato

CONTENTS

CHAPTER1

Introduction

CHAPTER1

Introduction

1.1. General introduction

A colloidal dispersion of anisotropic particles forms liquid crystal phases at higher particle concentration due to spontaneous orientation of the particles. This type of liquid crystal is classified as lyotropic liquid crystals and are distinguished from organic thermotropic liquid crystals widely used in display applications. Among them, "nanosheet liquid crystals" is composed of ultrathin plate-shaped nanosheets with high aspect ratio (~1nm thickness and several μm width); they form liquid crystal phase at exceptionally low concentration less than 1 wt%. Many applications of nanosheet liquid crystals are expected such as fabrication of nanocomposite material with good mechanical and gas-barrier properties and mechanochromic structural color materials. For the future applications, control of liquid crystal structure and rheological property are strongly desired. In this situation, this thesis demonstrates that the structure and rheological property of the nanosheet liquid crystal is effectively controllable by adding organic molecules and biopolymers.

This thesis is composed of 7 chapters as follows.

In Chapter 1, background of this thesis is described. Overview of liquid crystalline nanosheet materials, including structural control and applications for composite materials fabrication are reviewed.

In Chapter 2, liquid crystal phase of clay nanosheets dispersed in water/*N*,*N*-dimethylformaide (DMF) mixture solution is investigated by using small angle X-ray scattering and rheometer. The liquid crystal phase similar to conventional water system was obtained in the mixed solvent, leading to future application for fabrication of hydrophobic polymer/nanosheet composites. With the increase of DMF concentration, viscosity and nanosheet-nanosheet distance tended to increase compared to water system.

Chapter 3 demonstrates control of rheological property of nanosheet colloid by adding carbonyl compounds. Even at high nanosheet concentration, some kinds of carbonyl compounds inhibited gelation and the viscosity was largely decreased.

In Chapter 4, montmorillonite nanosheets colloid was found to form defect-free liquid crystal domain of cm-scale and this behavior was related to rheological property of the colloid. Furthermore, uniformly orientated nanosheet/polymer composite gel with high mechanical strength was obtained by in-situ polymerization of *N*-isopropylacrylamide in this liquid crystalline nanosheet colloid.

In Chapter 5, liquid crystalline colloid mixture system of nanosheet and cellulose nanofiber was investigated. When very small amount of cellulose nanofiber was added to isotropic nanosheet colloid, liquid crystal phase with very high structural order was obtained. The composite materials with high transmittance and mechanical property were successfully obtained from the colloidal mixture.

In Chapter 6, the mixture of motor protein tubulin with nanosheet was investigated. Tubulin reversibly formed microtubules in the presence of nanosheets as

triggered by temperature change, resulting in reversible structural change of the liquid crystal phase of the nanosheets.

Chapter 7 shows conclusions of this thesis.

1.2. Nanosheet colloids

1.2.1. *Overview*

Inorganic layered crystals are composed of a few nanometer-thick layers of inorganic crystals sandwiching counter cations. The interlayer spaces can be intercalated with variety of species such as solvents, other counter cations and polymers. When specific counter cation and solvent molecules are intercalated, inorganic layered crystals are infinity swollen and exfoliated to monolayer crystals which are called nanosheets. The nanosheets with high aspect ratio (~1nm in thickness and several μm in width) having various inorganic function (photocatalytic activity, semiconductor property, conductivity, magnetic property, fluorescence etc.) are available as functional nanomodules for many applications. By spin coating and a Langmuir-Blodgett method, the nanosheets are restacked with counter cation or polymers as multi-layered thin film with regulated nanostructure. It is also interesting to use the nanosheets as the framework of porous materials. All of these nanomaterials are synthesized via nanosheet colloids. Hence, it is important to control the rheological property and microstructure of the nanosheet colloids.

Highly swelling layered clay minerals are spontaneously exfoliated just by dispersing in a water so that the clay minerals are widely used in many industrial application. Many clay mineral nanosheet colloids often form physical gel at low nanosheet concentration. Two-dimensional nanosheet colloids exhibit specific rheological properties. A detailed review will be presented in the next Section ***1.2.2***.

Some of transition metal oxides nanosheet and graphene oxide forms high fluidity nanosheet colloids even at high nanosheet concentration. In these fluid nanosheet colloid, when nanosheet concentration increases, the free rotational motion of the nanosheets is restricted and orient along a certain direction, so the nanosheets form a liquid crystal phase. These nanosheet colloids are distinguished as rare example of liquid crystal formed by two-dimensional colloid so that they have been experimentally and theoretically investigated recently. The Sections ***1.2.3.*** and ***1.2.4.*** introduces several kinds of nanosheet liquid crystals dispersed in water or non-aqueous solvents.

Nanoplates or nanorods as well as nanosheets exhibits an isotopic and a nematic (and columnar) liquid crystal phases upon increasing the particle concentration as investigated experimentally and theoretically. Adding a second component to these anisotropic colloid causes new phenomena such as demixing depending on size ratio and

phase transitions due to the depletion interaction. The phase behavior of mixtures is richer and more complicated than single component colloids because the behavior originates from the subtle balance between the mixtures of entropy, orientation of particles, excluded volume and depletion interaction. In the Section ***1.2.5.*** section, liquid crystalinity and rheological property of double-component mixture system with other particles are reviewed.

1.2.2. Rheology of nanosheet colloids

Many clay mineral nanosheet colloids form physical gel above a concentration of several wt% and thixotropy is observed. Freundlich et al. first reported on the thixotropic behavior of gels of Wyoming bentonite in 1928.[11] The rheological behavior is important in view of the rheology modifiers for paints or cosmetics. However, it is difficult to explain a rational model for the behavior by a classical theory. This section reviews current research of clay colloid rheology strating from a historical background.

Broughton and Squires investigated the effects of clay concentration of Wyoming dispersions on colloid rheology.[12] They interpreted that the gelation occurred through edge-edge connection of nanosheets. Van Olphen suggested the formation of a 3D house of cards network that may occur through face-face, edge-edge, or edge-face connection of nanosheets[13] because the face of nanosheet has a negative permanent charge, whereas

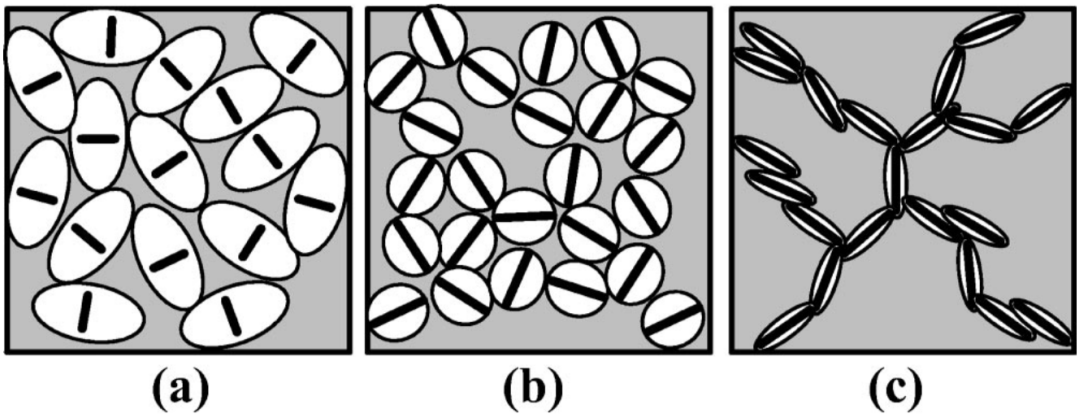

Figure 1 Schematic figures representing repulsive (‘‘Wigner’’) colloidal glass (a), attractive glass (b), and gel (c). Each thick line represents a Laponite disk, while a white ellipsoid represents the range of electrostatic repulsions. In (a), long-range electrostatic repulsions dominate. In (b), attractive interactions affect the spatial distribution (i.e., the structure factor) but repulsive interactions still play the predominant role in the slow dynamics of the system. In (c), attractive interactions play a dominant role; a percolated net- work forms, which gives the system its elasticity. [6]

the edge has hydroxyl groups, which are positively or negatively charged depending on pH of the solution. However, it remains question that nanosheet colloid at high pH also formed gel although edge-face interactions (formation of 3D house of cards network) should have only occurer at low pH.

In contrast, a completely different view was proposed by Hauser et al. According to them, the gel structure is stabilized by repulsive forces between the

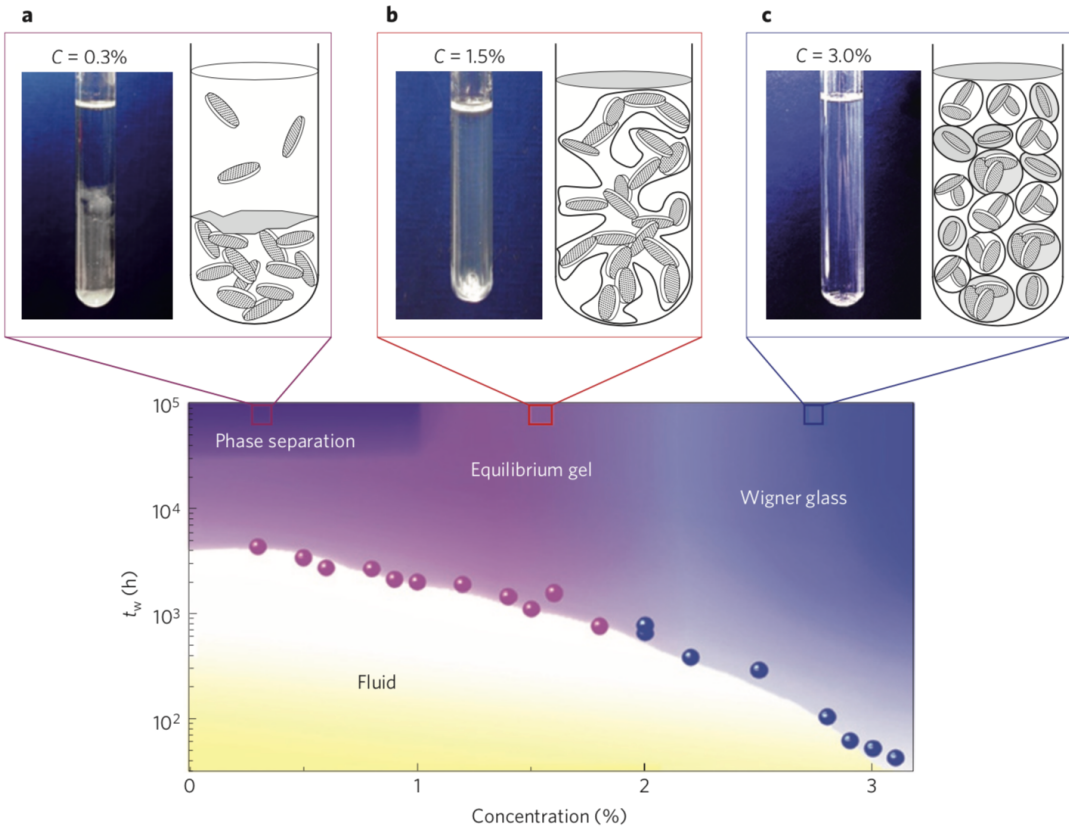

Figure2 Phase diagram of diluted Laponite suspensions, in the waiting-time-versus-concentration plane, resulting from the combined experimental and numerical results. Lower panel, Symbols correspond to experimental tw values required to observe non-ergodic behavior by dynamic light scattering; boundaries inside colored regions are guides to the eye. For long waiting times, three different regions are identified, whose representative macroscopic behavior and a pictorial microscopic view are reported in a–c. a, Phase-separated sample with colloid-poor (upper part) and colloid-rich (lower part) regions for Cw ≤ 1.0%. b, Equilibrium gel for 1.0 < Cw < 2.0%, characterized by a spanning network of T-bonded discs. c, Wigner glass, expected for 2.0 ≤ Cw ≤ 3.0%, where disconnected platelets are stabilized in a glass structure by the electrostatic repulsion, progressively hampering the formation of T bonds. [3]

interacting electrical double layers of the platelets. [14] The model is strongly supported by the measurement of interparticle forces,[15] [16] rheological properties[17, 18] and various scattering (light, X-ray, and neutron).

Three types of models which were winger glass, attractive glass and attractive gel were proposed by Tanaka et al. (Figure1). [6] *If* the free volume is not available by effective volume of particles, thus a winger glass state can be formed. Here, the effective volume per particle is the sum of a Debye length and a particle size. If the system is added with salt, the Debye length decreases, and liquid-glass transition concentration shifts to a higher volume fraction of particles. With more salt concentration, van der Waals forces prevail over the electrostatic repulsion, leading to the colloids forming 3D network, that is attractive gel. In the intermediate region, where both repulsive and attractive interactions lead, it may form an attractive glass.

Recently, new models such as empty liquids (liquid states with vanishing density) [19] and equilibrium gels (arrested networks of bonded particles, which do not require an underlying phase separation to form)[20] [21]have been formulated by simulation; however, no experimental evidence of these predictions has been provided. In this situation, Ruzicka et al. reported the first observation of empty liquids and equilibrium gels in a complex colloidal clay (Figure2).[3] They observed at long timescales of years, a significant evolution takes place. Samples underwent an extremely slow, phase separation into nanosheet-rich and nanosheet-poor phases. The behavior was observed only at very low nanosheet concentration (0.3 %) and the nanosheets remain in a homogeneous arrested state above 0.3%. The observed behaviors were similar to those predicted in simple models of patchy particles, suggesting that nanosheet forms an empty liquid at very low concentration.

]

1.2.3. *Nanosheet liquid crystal*

In a dilute anisotropic particle colloidal dispersion, anisotropic particles are moving around in translational and rotational manners due to Brownian motion. When anisotropic particle concentration increases, the free rotational motion of anisotropic particles is restricted and the anisotropic particles orient along a certain direction, so the particles form a LC phase. This type of liquid crystals is classified as lyotropic liquid crystals and are distinguished from organic thermotropic liquid crystals widely used in display applications. A lyotropic LC is generally composed of a solvent and anisotropic dispersoids, and the LC phase formation depends on the concentration of the dispersoid.

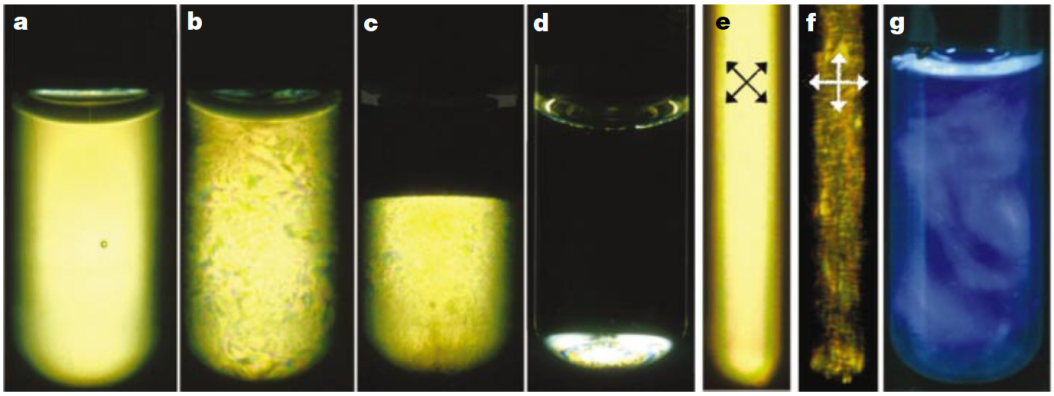

Figure 3 Naked-eye observation of samples. Test-tubes filled with aqueous suspensions of $H_3Sb_3P_3O_{14}$ single-layers, observed between crossed polarizers (a-e) (the isotropic phase in c and d appears dark). a, in 2ml of birefringent gel phase (overall volume fraction ϕ = 1.98%) the topological effects are so dense that the texture appears homogenous at the scale of this photograph. b, 2ml of birefringent fluid phase (ϕ= 0.93%). c, 2ml oof a biphasic sample (ϕ = 0.65%). d, 2ml of a biphasic sample (ϕ= 0.03%). e and f, Magnetically aligned sample observed in a 5-mm NMR tube that has been immersed for 10 min in a 18.7-T field at 50 °C, in two different orientations compared to the polarizer//analyser system, represented by arrows (ϕ = 0.75%). g, Sample iridescence (ϕ = 0.75%) observed in natural light is due to light scattering by the $H_3Sb_3P_3O_{14}$ layers stacked with a period of 225 nm. [9]

Lyotropic LCs have been reported in surfactant micelles[22], biopolymers (cellulose crystal[23] and DNA[24]), rod-shaped particles (viruses, [25] metals,[26] and oxides[27]), nanoplates (gibbsite ($Al(OH)_3$),[28] $Ni(OH)_2$, [29] and layered double hydroxides [30]). Among them, "nanosheet liquid crystals" is composed of ultrathin plate-shaped nanosheets with maximum aspect ratio (~1nm thickness and several μm width) and have been studying these materials as a new type inorganic liquid crystal.

First liquid crystalline behavior of nanosheet colloid was observed for the bentonite colloidal system by Langmuir in 1938. [31] Nevertheless, the next liquid crystallinity of nanosheet colloid has not been reported for a long time. After about 40 years, Gabriel et al. had reported liquid crystal phase of nanosheet colloid prepared from layered $K_3Sb_3P_2O_{14}$ for the first time. [9] The system showed specific interference color and phase separation (isotropic phase – biphasic phase – liquid crystal phase) as shown in

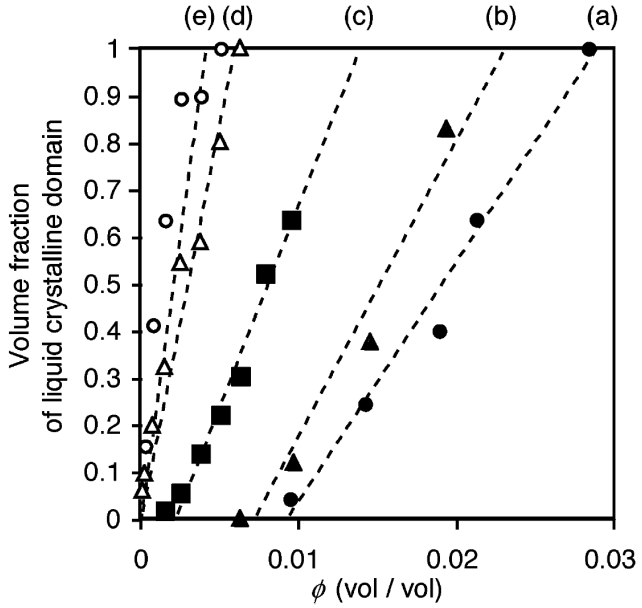

Figure 4 Relationship between colloid concentration ϕ of a colloid and the volume fraction of the liquid crystalline domain to the total volume. The colloids with *D*m = (a; filled circle) 0.15, (b; filled triangle) 0.38 and (c; filled square) 1.9 μm were observed 1 d after preparation, whereas the colloids with *D*m = (d; open triangle) 6.2 and (e; open circle) 7.8 μm were observed 5 d after preparation. [8]

Figure3. In addition, when the nanosheet concentration increased, the *d* value also decreased, following the one-dimensional swelling law.

Almost at the same time, Miyamoto et al. reported liquid crystalline Nb_6O_{17} nanosheet. [32] They synthesized large size layered crystals and exfoliated it to nanosheets with ~100μm width.[33] The large size nanosheets were broken by ultrasonication so that samples with different average nanosheet size (7.8 μm to 0.15 μm) were obtained. [8] The relationship between the aspect ratio and phase transition concentrations (isotropic-biphasic-nematic) (Figure4) indicated that the liquid crystallinity is basically explained by the excluded-volume effect, because the behavior was similar with the trends predicted by Onsager theory. [34]

In Onsager theory, a thin disk with monodisperse size and shape particle is used as a model for calculation; the behavior should be different in polydisperse experimental systems. Mejia et al. prepared α-zirconium phosphate (α-ZrP, $Zr(HPO_4)_2$) nanosheet with different particle size and polydispersity and investigated phase separation and liquid crystal phase formation by experimental and computer simulation. [35] In particular, they clarified that, as the polydispersity of suspensions increased, isotropic-biphasic transition concentration (ϕ_I) slightly decreases, while biphasic-nematic transition concentration (ϕ_N) increased. The behavior agreed with computer simulations.

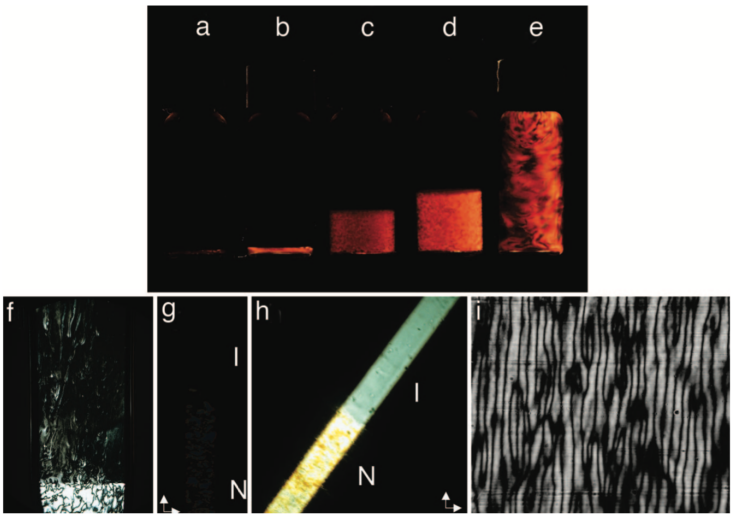

Figure 5 Visual observations of the isotropic/nematic transition in nontronite aqueous solutions. (a–e) Naked-eye observation of the samples. Vials (2 ml) were filled with aqueous suspensions of sodium nontronite (ionic strength = 10^{-4} M) and observed between crossed polarizers (the isotropic phase in a–d appears dark). (a) Isotropic liquid sample at a volume fraction $\phi = 0.5\%$. (The small bright line observed at the bottom of the vial is due to a reflection on the curved bottom.) (b) Onset of the phase separation at $\phi = 0.61\%$. (c) Biphasic sample at $\phi = 0.67\%$. (d) Biphasic sample at $\phi = 0.72\%$. (e) Birefringent gel at $\phi = 1\%$. (f) Polarized-light optical microscopy observations of a nontronite sample ($\phi = 0.7\%$, ionic strength = 10^{-3} M) at the onset of phase separation. (g and h) Polarized-light optical microscopy observations of a biphasic sample of a nontronite suspension ($\phi = 0.7\%$, ionic strength = 10^{-3} M) held in a flat capillary submitted to a horizontal 1-T magnetic field. White arrows indicate the directions of the polarizers. I, isotropic phase; N, nematic phase. (g) Extinction conditions. The capillary is barely visible because its axis is parallel to that of the polarizer. (h) Maximum transmission conditions. The nematic phase is almost uniformly bright because there are only very few defects left. The isotropic phase is not dark because of its large magnetic-field-induced anisotropy. (i) Transient hydrodynamic instability observed upon a sudden change of magnetic field direction for a nontronite suspension ($\phi = 0.7\%$, ionic strength = 10^{-3} M) held in a flat capillary. [7]

On the other hands, Layered clay minerals have been studied historically for the longest time of all layered materials and are very important materials for many types of industrial applications because of their low cost, abundant resource, and low toxicity.

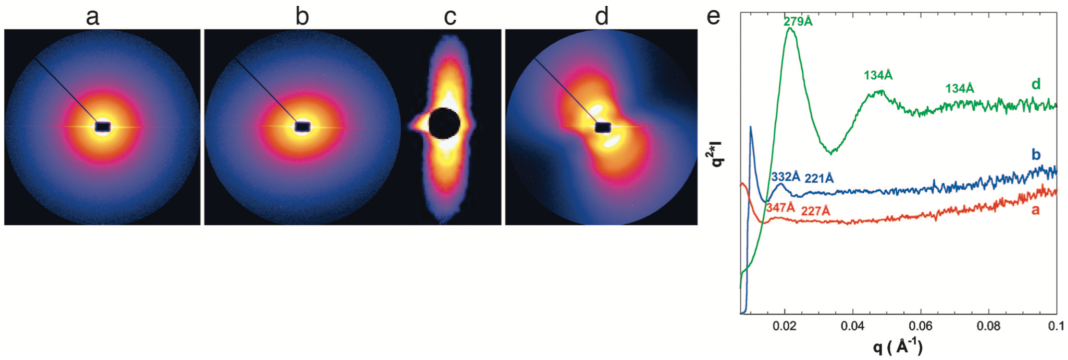

Figure 6 SAXS studies. (a) Two-dimensional SAXS pattern of the isotropic phase of a nontronite suspension (ϕ = 0.7%, ionic strength = 10^{-3} M) (b) SAXS pattern of the nematic phase of the same suspension. (c) SAXS pattern of the nematic phase of the same suspension aligned in a magnetic field of 1 T. (d) SAXS pattern of a gel sample (ϕ = 3%, ionic strength = 10^{-3} M). (e) Plots of $I \cdot q^2$ vs. q corresponding to patterns a, b, and d. For patterns a and b, the first diffuse peak is too close to the beamstop and is not observed. The intensity of pattern d was divided by 2 for enhanced readability. [7]

Smectite is composed of an octahedral sheet (Al, Fe, Mg) sandwiched between two tetrahedral sheets (Si, Al, Fe). This 2:1 structure carries a negative charge due to isomorphic substitutions that are compensated by exchangeable low valence cations present in the interlayer space. Space between the layers has counter cation such as Na^+ and Ca^{2+} for compensation charge of layer.

Suspension of clay mineral nanosheet often becomes physical gel before liquid crystal transition and the characterization as a "liquid crystal" could not be performed. In many cases, they form birefringent physical gel. First liquid crystalline behavior of nanosheet colloid was observed for the bentonite colloidal system by Langmuir in 1938. [31] However, this observation was not reproducible.

Michot et al. reported true liquid crystallinity of natural lath-shaped nontronite nanosheet colloid in 2006 for the first time (Figure5)[7]. The complete phase diagram as the functions of ionic strength and volume fraction exhibits a clear biphasic phase separation in the sol region just before the gel transition. Furthermore, the liquid crystallity was evidenced by polarized light microscopy and small angle X-ray scattering in the presence of external magnetic fields. Small angle X-ray scattering measurements of gel samples revealed strong positional and orientational orders of the particles, proving unambiguously the nematic character of the gel (Figure6). Hence, the results clearly refuted a house of cards model.

Paineau et al. reported natural beidellite nanosheet liquid crystal. Although the beidellite and the nontronite[36] have different shapes (beidellite is disk-like and nontronite is lath-like), they showed similar liquid crystallinity. By applying external fields (magnetic field or electric field) or introduced the suspension into narrow space (thickness is 0.2 mm), the nanosheets showed nematic single domains and suggested one may envision the synthesis of fully oriented clay-polymer nanocomposites with improved properties.

While natural nontronite and beidellite nanosheets, that are tetrahedrally substituted clays, showed liquid crystallinity, montmorillonite and laponite of octahedrally substituted clays showed gel transition at lower concentration that it could form liquid crystal. In this situation, Miyamoto et al. reported fluid liquid crystal phse in octahedrally substituted synthetic fluorohectorite and fluortetrasilicic mica in which all of the hydroxy groups are replaced by F atoms. [37] The samples showed permanent birefringence and formed highly ordered lamellar-like structures at wide concentration range.

In addition to the above examples, the nanosheets of $KTiNbO_5$,[38] KNb_3O_8,[38] $H_{1.07}Ti_{1.73}O_4$,[39] $KCaNb_3O_{10}$,[40] and graphene oxide[41] were also reported form liquid crystal phases. With these materials library and fundamental investigations and theories, the basis of nanosheet liquid crystal engineering has mostly been established.

1.2.4. Nanosheet liquid crystal dispersed in organic solvent

Nanosheets are commonly achieved via the control of long-range electrostatic repulsion in aqueous solutions. Dispersing nanosheets in nonaqueous solutions is much more difficult as the effective range of electrostatic repulsion is greatly reduced [42]. In this section, rare systems of nanosheets dispersed in non-aqueous solvent are reviewed.

Kim et al. synthesized graphene nanosheets reversibly transferred between aqueous and organic solutions as new type system (Figure7)[4]. First, graphene oxide nanosheets suspended in water were modified with a hydrophilic ionic liquid polymer (PIL) which consists of an imidazolium polycation and a bromide anion. Second, lithium bis(trifluoromethylsulfonyl)amide was added into the colloid; black precipitates (hydrophobic nanosheets) were formed in water by an immediate substitution of the hydrophilic anions with hydrophobic anions in the poly(1-vinyl-3-ethylimidazolium). The hydrophobic nanosheets were possible to be dispersed in propylene carbonate, dimethylformamide, acetonitrile, tetrahydrofuran, *N*-methyl-pyrollidone and nitromethane. In addition, the hydrophobic nanosheets dispersed in the non-aqueous

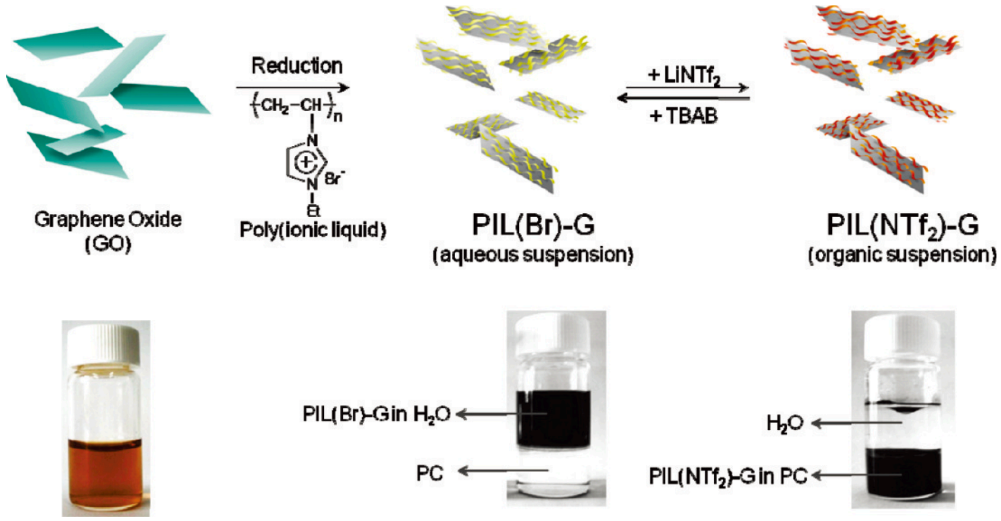

Figure 7 Schematic illustration of the synthetic process for the PIL-modified graphene sheets (PIL-G). Chemical reduction of the graphene oxide (GO) dispersion with hydrazine in the presence of water-soluble PIL(Br) produced a stable aqueous suspension of the PIL(Br)-G. Anion exchange of PIL leads to the phase transfer of PIL-modified graphene sheets between aqueous and organic solvent media (propylene carbonate). [4]

solvent were reversibly transferred from the non-aqueous phase to the aqueous phase through the addition of appropriate salts containing hydrophilic anions.

Wong et al. attached oligomeric molecules (polyoxyalkyleneamine) to attach onto α-zirconium phosphate (α-ZrP, $Zr(HPO_4)_2$) nanosheet and obtained stabilized α-ZrP nanosheets colloid dispersed in highly polar, aprotic solvents (toluene, acetone, acetonitrile and propionitrile) due to the steric stabilization effect of the adsorbed polymer layer without stacked nanosheets[43]. The system formed nematic and smectic phases at concentrations of $\phi < 0.01$ despite decreasing of aspect ratio (diameter /length) by adsorption of polymer. Furthermore, SAXS measurement revealsed basal spacings of 142 to 238 nm between the nanosheets that lead to brilliant iridescence in the visible spectrum with tunable colors attributable.

Suzuki et al. obtained montmorillonite nanosheet colloids adsorbed with ammonium or imidazolium ions having various alkyl chains (decyltrimethylammonium, trimethylstearylammonium, 1-methyl-3-decylimidazolium, 1-methyl-3-octyl imidazolium, 1-hexyl-3-methylimidazolium chloride, and 1-butyl-3-methylimidazolium chloride) and the colloids were dispersed in *N*-methylpyrrolidone solvent. [44] They achieved homogeneous dispersion of montmorillonite nanosheets exchanged by decyltrimethylammonium, 1-methyl-3-decyl imidazolium, and 1-methyl-3-

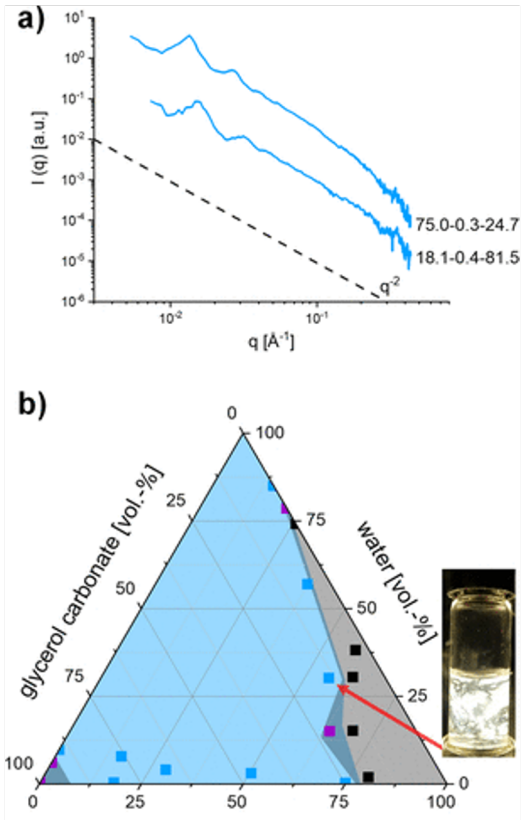

Figure 8 (a) SAXS curves of osmotically swollen clay in methanol-water-glycerolcarbonate (numbers next to the curves are vol % of the three solvents). (b) Ternary phase diagram of NaHec swollen in methanol-water-glycerolcarbonate mixtures (blue squares: osmotically swollen, purple squares: biphasic system, black squares: crystalline swollen, background colors are a guide for the eye to distinguish osmotic and crystalline swelling regimes; suspensions contained 1–2 vol % NaHec) along with an image of a representative nematic sample between crossed polarizers. [2]

octylimidazolium in *N*-methylpyrrolidone; monolayered nanosheets were observed with atomic force microscopy. The importance of the hydrophobicity of alkyl chains was suggested by the results.

Na-fluorohectorite (NaHec) nanosheets with uniformly distributed charge position and particle size of ~20 μm were synthesized by Breu et al[2] and they dispersed the nanosheets in triple mixture solvent of water-acetonitrile-methanol, water-acetonitrile-ethyleneglycol and water-methanol-glycerolcarbonate (Figure8)[45]. Dispersible amount of water in the triple mixture solvent system were smaller than double

mixture solvent systems. It is notable that the nanosheets were dispersed with very small amount of water: 0.4 vol% water, 18.1 vol% methanol, 81.5 vol% glycerolcarbonate. Furthermore, the glycerolcarbonate could be polymerized into polyglycerol carbonate, a water-soluble and biodegradable polymer, this system is an epoch-making system with a view to composite materials.

1.2.5. Double component mixture system of nanoplate or nanosheet with another particle

1.2.5.1. plate + sphere

Mixing colloidal particles with another component (differing in size or shape), may affect translational entropy and/or depletion attraction. Kleshchanok et al. selected an ideal mixture system with a narrow particle size distribution of gibbsite nanoplate (thickness is ~10 nm, diameter is ~100 nm) and silica sphere (diameter is ~16 nm). [1] The gibbsite nanoplates are able to form nematic and columnar phases. [46] Silica spheres added to gibbsite colloids acted as depletants and changed the phase behavior of gibbsite platelets (Figure9). Whereas pure gibbsite colloids showed the isotropic phase and the

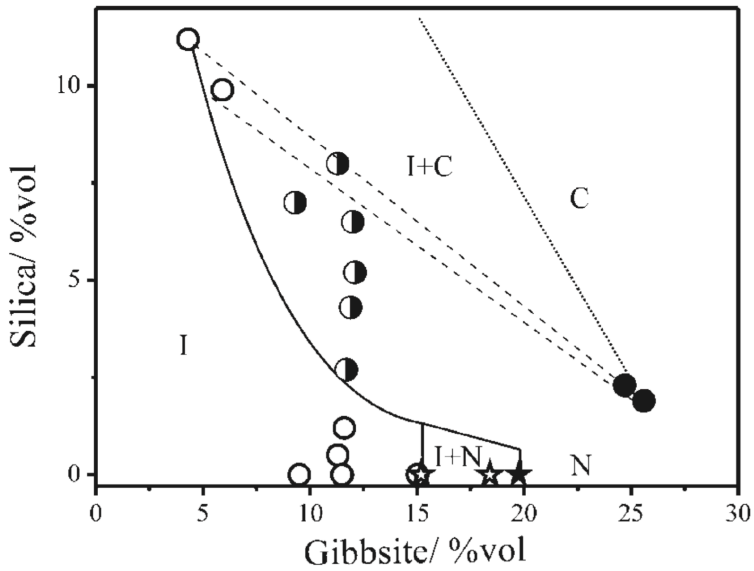

Figure 9 Experimental phase diagram of aqueous silica/gibbsite mixtures. Broken straight lines are the experimentally found tie lines, connecting coexisting phases. Phase boundaries depicted as solid curves were found from the experiment. The dotted line indicates the extrapolated columnar phase boundary. [1]

isotropic/nematic phase coexistence, the mixture system of silica spheres and gibbsite platelets showed isotropic/columnar phase coexistence. SAXS measurements show that in the columnar phase silica spheres are not located between the faces of gibbsite platelets but occupy the regions between the stacks.

Hilhorst et al. investigated the structure of the montmorillonite nanosheet colloids induced by change of the pH and by adding silica particles. [47] For the pure montmorillonite nanosheet colloids, the storage modulus at pH 5 was highest, while the modulus was low at pH 7. For all pH, addition of silica sphere led to weakening of the storage modulus. However, the underlying mechanism was different in each case. At pH 5, the shielding of the positive nanosheets-edge charges by adsorption of silica spheres led to a weakening of the attraction and lower storage modulus. The structure was observed by cryo-TEM. At pH 7, the microphase separation between nanosheets and silica spheres led to a loss of connection in the formed nanosheet structure. In the case of pH 9, the mechanism is not clear. However, the formation of a foam structure by nanosheets may have trapped silica spheres.

1.2.5.2. plate + rod

Rod-shaped boehmites and plate-shaped gibbsites were mixed and liquid crystallinity was investigated by van der Kooij and Lekkerkerker (Figure 10). [48] The

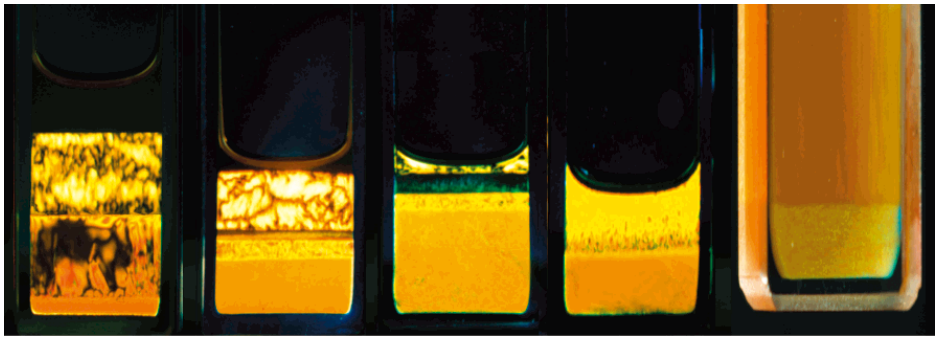

(*a*) (*b*) (*c*) (*d*) (*e*)

Figure 10 Phase-separated rod-plate mixtures as observed between crossed polarizers. Depicted are (*a*) four-phase $I + N^+ + N^- + C$ coexistence (denoted in order from top to bottom) in a sample with the composition (ϕ_{rod}, ϕ_{plate})) (0.06, 0.26), (*b*) five-phase $I + N^+ + X + N^- + C$ coexistence at (0.10,0.22), (*c*) four-phase $N^+ + X + N^- + C$ coexistence at (0.07, 0.29), and (*d*) two-phase $N^- + C$ coexistence at (0.03,0.35). Image (*e*) depicts a sample at (0.02, 0.35) exhibiting $N^- + C$ coexistence, photographed without crossed polarizers but illuminated by white light to demonstrate the Bragg reflections in the lower (*C*) phase. [5]

mixture system showed complex phase separation up to five phases such as isotropic phase (*I*), nematic phase of predominantly boehmites (N^+), nematic phase of predominantly gibbsites (N^-), columnar phase(*C*) and undecidable phase (*X*). By the phase rule of Gibbs, five-phase coexistence requires the presence of at least four different colloidal species. The authors said that "in reality, both the boehmite and gibbsite suspensions are polydisperse and hence represented by a virtually infinite number of species differing in size" (long axis and short axis of boehmite are 186 nm (30 %) 18 nm (30 %), long axis and short axis of gibbsite are 208 nm (25 %) 14 nm (20 %), respectively.). Later work by Wensink and Lekkerkerker showed that gravity have affected phase separation behavior over a centimeter scales. [49]

Liquid crystallinity of montmorillonite nanosheets mixture system with rod-shaped sepiolite was reported by Woolston and van Duijneveldt (Figure 11).[10] Initially, the samples ($\phi_{\text{sepiolite}}$ = 1.5 vol%, and $\phi_{\text{montmorillonite}}$ = 0.6 vol%) was first phase-separated to birefringent and isotropic phases. After storing over time, the birefringent phase was further separated into two phases which are nematic phase dominated by sepiolite rods and montmorillonite nanosheets-rich nematic gel phase. In contrast, pure montmorillonite nanosheet colloid of 0.6 vol% did not form gel. Sepiolite rod colloid of 1.5 vol% neither

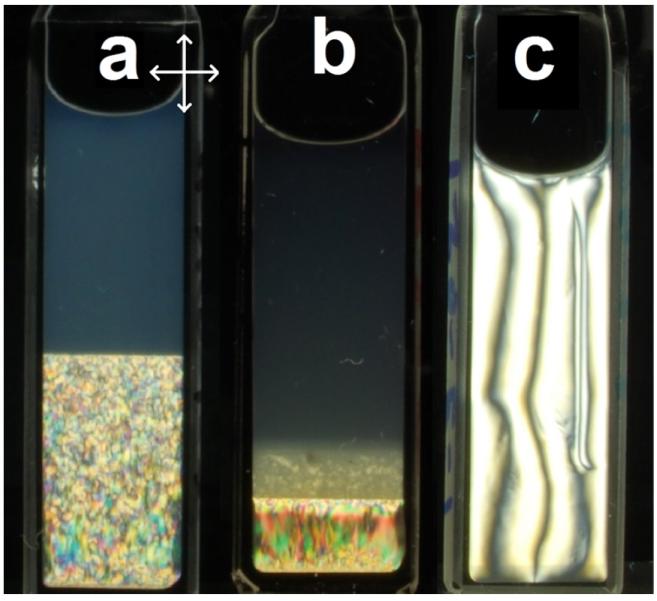

Figure 11 Illustrative examples of behavior: (a) pure Sep (ϕ_{Sep} =2.3 %), (b) three phases (ϕ_{Sep} = 1.5 %, and ϕ_{MMT} = 0.6 %), and (c) gel (ϕ_{Sep} = 0.9%, and ϕ_{MMT} = 0.9%). Arrows denote polarizer orientations. [10]

formed a gel. Those results mean, nematic sepiolite rods phase appears to drive the montmorillonite tactoids into a concentrated montmorillonite-rich phase.

1.2.5.3. plate + plate

Nakato and Miyamoto et al. investigated two kinds nanosheet mixture system (clay mineral nanosheets + transition metal oxide nanosheets). Each nanosheet formed micro liquid crystalline domain even for the same sheet-shape. [50,51] The behavior is more prominent in phase separation observation. [52] The micro phase separation could achieve controllable photoinduced electron transfer (Figure 11), [53, 54] electron accumulation, [53, 54] and photocatalytic reactions[55].

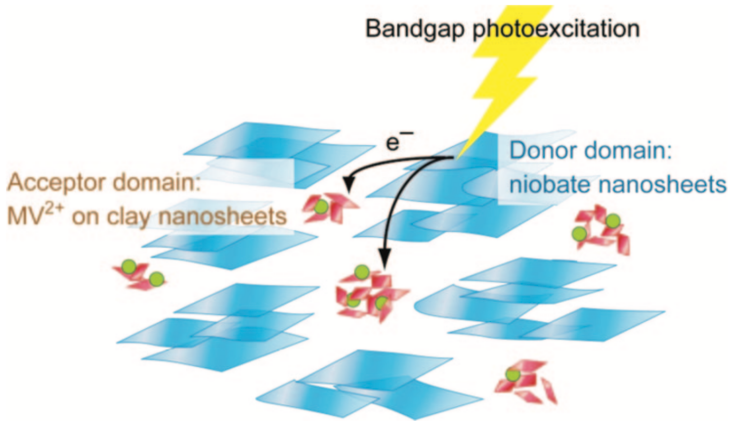

Figure 12 Schematic representation of the photoinduced electron transfer occurring in the MV/clay-niobate colloids. [51]

1.3. Reference

1. Kleshchanok, D.; Petukhov, A. V.; Holmqvist, P.; Byelov, D. V.; Lekkerkerker, H. N. W., Structures and phase behavior in mixtures of charged colloidal spheres and platelets. *Langmuir* **2010,** *26*, 13614-13621.

2. Stoter, M.; Kunz, D. A.; Schmidt, M.; Hirsemann, D.; Kalo, H.; Putz, B.; Senker, J.; Breu, J., Nanoplatelets of sodium hectorite showing aspect ratios of approximately 20,000 and superior purity. *Langmuir* **2013,** *29*, 1280-1285.

3. Ruzicka, B.; Zaccarelli, E.; Zulian, L.; Angelini, R.; Sztucki, M.; Moussaid, A.; Narayanan, T.; Sciortino, F., Observation of empty liquids and equilibrium gels in a colloidal clay. *Nat Mater* **2011,** *10*, 56-60.

4. TaeYoung Kim, H. L., JongEun Kim, and Kwang S. Suh, Synthesis of Phase Transferable Graphene Sheets Using Ionic Liquid Polymers. *ACS Nano* **2010,** *4* .

5. van der Kooij, F. M.; Lekkerkerker, H. N. W., Liquid-Crystal Phase Formed in Mixed Suspensions of Rod- and Platelike Colloids. *Langmuir* **2000,** *16*, 10144-10149.
6. Tanaka, H.; Meunier, J.; Bonn, D., Nonergodic states of charged colloidal suspensions: Repulsive and attractive glasses and gels. *Phys. Rev. E* **2004,** *69*, 031404.
7. Michot, L. J.; Bihannic, I.; Maddi, S.; Funari, S. S.; Baravian, C.; Levitz, P.; Davidson, P., Liquid–crystalline aqueous clay suspensions. *Proc. Nat. Acad. Sci.* **2006,** *103*, 16101-16104.
8. Miyamoto, N.; Nakato, T., Liquid crystalline nanosheet colloids with controlled particle size obtained by exfoliating single crystal of layered niobate $K_4Nb_6O_{17}$. *J. Phys. Chem. B* **2004,** *108*, 6152-6159.
9. Gabriel, J. C. P.; Camerel, F.; Lemaire, B. J.; Desvaux, H.; Davidson, P.; Michael, W.; Batail, P., Swollen liquid-crystalline lamellar phase based on extended solid-like sheet. *Nature* **2001,** *413*, 504-508.
10. Woolston, P.; van Duijneveldt, J. S., Three-Phase Coexistence in Colloidal Rod-Plate Mixtures. *Langmuir* **2015,** *31*, 9290-9295.
11. Freundlich, H., *Kolloid-Z.* **1928,** *46*.
12. Broughton, G.; Squires, L., *J. Phys. Chem.* **1936,** *40*, 1041–1053.
13. VanOlphen, H., *Discuss. FaradaySoc.* **1951,** *11*, 82–84.
14. A., H. E., *Chem. Rev.* **1937,** *40*, 287-321.
15. Callaghan, I. C., *Faraday Discuss.* **1947,** *57*, 110-118.
16. Lubetkin, S. D., *Trans. R. Soc. London, Sect. A* **1984,** *311*, 353-368.
17. Ramsay, J. D. F., Colloidal properties of sybthetic hectorite clay dispersions. *J. Colloid Interface Sci.* **1986,** *109*, 441-447.
18. Michot, L. J.; Bihannic, I.; Maddi, S.; Baravian, C.; Levitz, P.; Davidson, P.; , Sol/Gel and Isotropic/Nematic Transitions in Aqueous Suspensions of Natural Nontronite Clay. Influence of Particle Anisotropy. 1. Features of the I/N Transition. *Langmuir* **2008,** *24*, 3127-3139.
19. Bianchi, E.; Largo, J.; Tartaglia, P.; Zaccarelli, E.; Sciortino, F., Phase diagram of patchy colloids: towards empty liquids. *Phys. Rev. Lett.* **2006,** *97*, 168301.
20. Zaccarelli, E., Colloidal gels: Equilibrium and non-equilibrium routes. *J. Phys. Condens. Matter* **2007,** *19*, 323101–323151.
21. Lu, P. J.; Zaccarelli, E.; Ciulla, F.; Schofield, A. B.; Sciortino, F.; Weitz, D. A., Gelation of particles with short-range attraction. *Nature* **2008,** *453* (7194), 499-503.
22. Strzelecka, T. E.; Davidson, M. W.; Rill, R. L., Multiple liquid crystal phases of DNA at high concentrations. *Nature* **1988,** *331*, 457-460.

23. Xue Min Dong, T. K., Jean-Franc ¸ois Revol, and Derek G. Gray, Effects of Ionic Strength on the Isotropic-Chiral Nematic Phase Transition of Suspensions of Cellulose Crystallites. *Langmuir* **1996,** *12*, 2076-2082.

24. F.Livolant; A.M.Levelut; J.Doucet; J.P.Benoit, The highly concentrated liquid-crystalline phase of DNA is columnar hexagonal. *Nature* **1989,** *339*, 724-726.

25. Bawden, F. C.; Pirie, N. W.; Bernal, J. D.; Fankuchen, I., Liquid crystalline substances from virus-infected plants. *Nature* **1936,** *138*, 1051-1052.

26. Jana, N. R.; Gearheart, L. A.; Obare, S. O.; Johnson, C. J.; Edler, K. J.; Mann, S.; Murphy, C. J., Liquid crystalline assemblies of ordered gold nanorods. *J. Mater. Chem.* **2002,** *12*, 2909-2912.

27. Kajiwara, K.; Donkai, N.; Hiragi, Y.; Inagaki, H., Lyotropic mesophase of imogolite 1. Effect of polydispersity on phase diagram. *Macromol. Chem.* **1986,** *187*, 2883-2893.

28. van der Kooij, F. M.; Lekkerkerker, H. N. W., Formation of Nematic Liquid Crystals in Suspensions of Hard Colloidal Platelets. *J. Phys. Chem. B* **1998,** *102*, 7829-7832.

29. Brown, A. B. D.; Ferrero, C.; Narayanan, T.; Rennie, A. R., Phase separation and structure in a concentrated colloidal dispersion of uniform plates. *Eur. Phys. J. B* **1999,** *11*, 481–489.

30. Liu, S.; Zhang, J.; Wang, N.; Liu, W.; Zhang, C.; Sun, D., Liquid-crystalline phases of colloidal dispersions of layered double hydroxides. *Chem. Mater.* **2003,** *15*, 3240-3241.

31. Langmuir, I., The Role of Attractive and Repulsive Forces in the Formation of Tactoids, Thixotropic Gels, Protein Crystals and Coacervates. *The Journal of Chemical Physics* **1938,** *6*, 873-896.

32. Miyamoto, N.; Nakato, T., Liquid crystalline nature of $K_4Nb_6O_{17}$ nanosheet sols and their macroscopic alignment. *Adv. Mater.* **2002,** *14*, 1267-1270.

33. Miyamoto, N.; Yamamoto, H.; Kaito, R.; Kuroda, K., Formation of extraordinarily large nanosheets from $K_4Nb_6O_{17}$ crystals. *Chem. Commun.* **2002**, 2378-2379.

34. Onsager, L., The effect of shape on the interaction of colloidal particles. *Ann. NY Acad. Sci.* **1949,** *51*, 627-659.

35. Mejia, A. F.; Chang, Y. W.; Ng, R.; Shuai, M.; Mannan, M. S.; Cheng, Z., Aspect ratio and polydispersity dependence of isotropic-nematic transition in discotic suspensions. *Phys. Rev. E.* **2012,** *85*, 61708.

36. Paineau, E.; Antonova, K.; Baravian, C.; Bihannic, I.; Davidson, P.; Dozov, I.; Impéror-Clerc, M.; Levitz, P.; Madsen, A.; Meneau, F.; Michot, L. J., Liquid-Crystalline Nematic Phase in Aqueous Suspensions of a Disk-Shaped Natural Beidellite Clay. *J. Phys. Chem. B* **2009,** *113*, 15858-15869.

37. Miyamoto, N.; Iijima, H.; Ohkubo, H.; Yamauchi, Y., Liquid crystal phases in the aqueous colloids of size-controlled fluorinated layered clay mineral nanosheets. *Chem. Commun.* **2010,** *46*, 4166-4168.

38. Nakato, T.; Miyamoto, N.; Harada, A., Stable liquid crystalline phases of colloidally dispersed exfoliated layered niobates. *Chem. Commun.* **2004,** 1, 78-79.

39. Nakato, T.; Yamashita, Y.; Kuroda, K., Mesophase of colloidally dispersed nanosheets prepared by exfoliation of layered titanate and niobate. *Thin Solid Filims* **2006,** *495*, 24-28.

40. Miyamoto, N.; Yamamoto, S.; Shimasaki, K.; Harada, K.; Yamauchi, Y., Exfoliated Nanosheets of Layered Perovskite $KCa_2Nb_3O_{10}$ as an Inorganic Liquid Crystal. *Chem. Asian J.* **2011,** *6*, 2936-2939.

41. Kim, J. E.; Han, T. H.; Lee, S. H.; Kim, J. Y.; Ahn, C. W.; Yun, J. M.; Kim, S. O., Graphene Oxide Liquid Crystals. *Angew. Chem., Int. Ed.* **2011,** *50*, 3043-3047.

42. Hernandez, Y.; Nicolosi, V.; Lotya, M.; Blighe, F. M.; Sun, Z.; De, S.; McGovern, I. T.; Holland, B.; Byrne, M.; Gun'Ko, Y. K.; Boland, J. J.; Niraj, P.; Duesberg, G.; Krishnamurthy, S.; Goodhue, R.; Hutchison, J.; Scardaci, V.; Ferrari, A. C.; Coleman, J. N., High-yield production of graphene by liquid-phase exfoliation of graphite. *Nat. Nanotechnol.* **2008,** *3*, 563-8.

43. Wong, M.; Ishige, R.; Hoshino, T.; Hawkins, S.; Li, P.; Takahara, A.; Sue, H.-J., Solution Processable Iridescent Self-Assembled Nanoplatelets with Finely Tunable Interlayer Distances Using Charge- and Sterically Stabilizing Oligomeric Polyoxyalkyleneamine Surfactants. *Chem. Mater.* **2014,** *26*, 1528.

44. Suzuki, A.; Oaki, Y.; Imai, H., Synthesis of dispersible nanosheets based on monolayer clays with imidazolium and ammonium cations having long-chain alkyl groups. *J. Ceram. Soc. JAPAN* **2017,** *125*, 353-356.

45. Mayr, L.; Amschler, S.; Edenharter, A.; Dudko, V.; Kunz, R.; Rosenfeldt, S.; Breu, J., Osmotic Swelling of Sodium Hectorite in Ternary Solvent Mixtures: Nematic Liquid Crystals in Hydrophobic Media. *Langmuir* **2020,** *3*, 3814-3820.

46. van der Beek, D.; Lekkerkerker, H. N. W., Liquid crystyal phases of charged colloidal platelets. *Langmuir* **2004,** *20*, 8582-8586.

47. Hilhorst, J.; Meester, V.; Groeneveld, E.; Dhont, J. K.; Lekkerkerker, H. N., Structure and rheology of mixed suspensions of montmorillonite and silica nanoparticles. *J. Phys. Chem. B* **2014,** *118*, 11816-25.
48. Lekkerkerker, F. M. v. d. K. a. H. N. W., Liquid-Crystal Phases Formed in Mixed Suspensions of Rod- and Platelike Colloids. *Langmuir* **2000,** *16*, 10144-10149.
49. Wensink, H. H.; Lekkerkerker, H. N. W., Sedimentation and multi-phase equilibria in mixtures of platelets and ideal polymer. *Europhysi. Lett.* **2004,** *66*, 125-131.
50. Miyamoto, N.; Yamada, Y.; Koizumi, S.; Nakato, T., Extremely Stable Photoinduced Charge Separation in a Colloidal System Composed of Semiconducting Niobate and Clay Nanosheets. *Angew. Chem., Int. Ed.* **2007,** *46*, 4123-4127.
51. Nakato, T.; Yamada, Y.; Miyamoto, N.; Photoinduced Charge Separation in a Colloidal System of Exfoliated Layered Semiconductor Controlled by Coexisting Aluminosilicate Clay. *J. Phys. Chem. B* **2009**, *113*, 1323-1331
52. Nakato, T.; Yamashita, Y.; Mouri, E.; Kuroda, K., Multiphase coexistence and destabilization of liquid crystalline binary nanosheet colloids of titanate and clay. *Soft Matter* **2014,** *10*, 3161-3165.
53. Nakato, T.; Inoue, S.; Hiraragi, Y.; Sugawara, J.; Mouri, E.; Aritani, H., Decomposition of a cyanine dye in binary nanosheet colloids of photocatalytically active niobate and inert clay. *J. Mater. Sci.* **2014,** *49*, 915-922.
54. Nakato, T.; Edakubo, H.; Shimomura, T., Photoinduced electron transfer in nanostructured assemblies of layered semiconducting oxide and methylviologen: Effect of the location of acceptor molecules. *Micropor. Mesopor. Mater.* **2009,** *123*, 280-288.
55. Nakato, T.; Terada, S.; Ishiku, T.; Abe, S.; Kamimura, S.; Mouri, E.; Ohno, T., Photoinduced electron transfer in semiconductor–clay binary nanosheet colloids controlled by clay particles as a turnout switch. *Applied Catalysis B: Environmental* **2019,** *241*, 499-505.

CHAPTER2

Liquid crystal phase of clay mineral nanosheet dispersed in *N*, *N*-dimethylformamide/water mixture

CHAPTER2

Liquid crystal phase of clay nanosheet dispersed in *N*, *N*-dimethylformamide/water mixture

2.1. Introduction

Inorganic nanosheets are obtained by exfoliation of layered materials are highlighted as ultimately anisotropic nanoparticle. Nanosheets of layered clay minerals are important materials for many industrial applications such as paint, cosmetics, and plastics. In addition, the nanosheet are distinguished by the ultra-large anisotropy and 2D shape: uniform thickness of ca. 1 nm and the lateral size of up to 100 μm. Due to the large anisotropy, LC phase is formed at very low concentration as low as < 0.2 wt%.[1,2].

In those applications, dispersion in non-aqueous solvents are sometimes required; however, it is generally difficult to prepare good dispersion of fully-exfoliated nanosheets in non-aqueous solvents[3,4] because in a non-aqueous solvent, formation of electric double layer is largely hindered because salt is not dissociated so that particles aggregate. Therefore, the property of those colloids has hardly been investigated. The non-aqueous colloidal systems are also curious form the fundamental point of view because there have been few detailed studies for those system. [4] Polymer adsorption to particle for dispersion is not useful for those applications. [5 6 7 8]

Here we demonstrate successful preparation of the colloidal sols of a fluorinated layered clay mineral, fluorohectorite, dispersed in *N*,*N*-dimethylformamide (DMF)/water mixture. We investigated liquid crystallinity and structure of the colloidal sols.

2.2. Experimental

The liquid crystalline nanosheet colloid of synthetic fluorohectorite (FHT) was prepared from NHT-B2 sol supplied from Topy Industries. The colloid was purified by repeated centrifugation. The colloidal sol (1wt %, 100mL) was added with CH_3COONH_4 and stirred for 1 d to exchange the counter cation from Na^+ to $NH4^+$. The colloidal sol of $NH4^+$-exchanged FHT was then dialyzed with the solution containing 10^{-4} M of NH_4Cl in DMF/water mixtures with DMF content of 0-80. Obtained colloid was diluted to various concentrations and characterized.The nanosheet colloid was diluted to 0.001 wt%, dropped on a mica substrate, dried and observed with an atomic force microscope (AFM, SII Nano Technology Inc, Nanocute). The particle size distribution was measured by dynamic light scattering after dilution to 0.1 wt% by Otsuka Electronics DLS8000. Small-angle X-ray scattering (SAXS) was performed using NANOPIX of Rigaku. For the SAXS

measurement, the FHT nanosheet colloids were enclosed in a glass capillary having a thickness of 0.01 mm and an optical path length of 2 mm. Birefringence textures were observed by using polarized optical microscope (Olympus BX-51) and by visual observation. Birefringent index was measured by using CCD type spectrophotometer (EPP-2000 Stellar Net. Inc.) equipped on the microscopy.

2.3. Results

FHT nanosheets did not aggregate and show liquid crystallinity in H_2O/DMF mixture solution. In AFM image, single-layer nanosheets with ~1nm thickness were observed while not flocculated nanosheets (Figure 1b). Figure 1a shows SAXS-WAXS profile of FHT nanosheet colloid (H_2O:DMF=20:80, solid line) and theoretical scattering form factor (broken line) shown as *eq*. (1) of a disk particle with thickness of 0.9nm and radius of 500μm.

$$P(q) = \left(\frac{2}{q^2R^2}\right)\left[1 - \frac{J_1(2qR)}{qR}\right]\frac{sin^2(qL/2)}{(qL/2)^2} \qquad (1)$$

Here, q is scattering vector, R is radius of disk, L is thickness of disk and J_1 is first order Bessel function. Solid line agreed with the theoretical curve, therefore the single-layer FHT nanosheets dispersed in H_2O/DMF mixture solution.

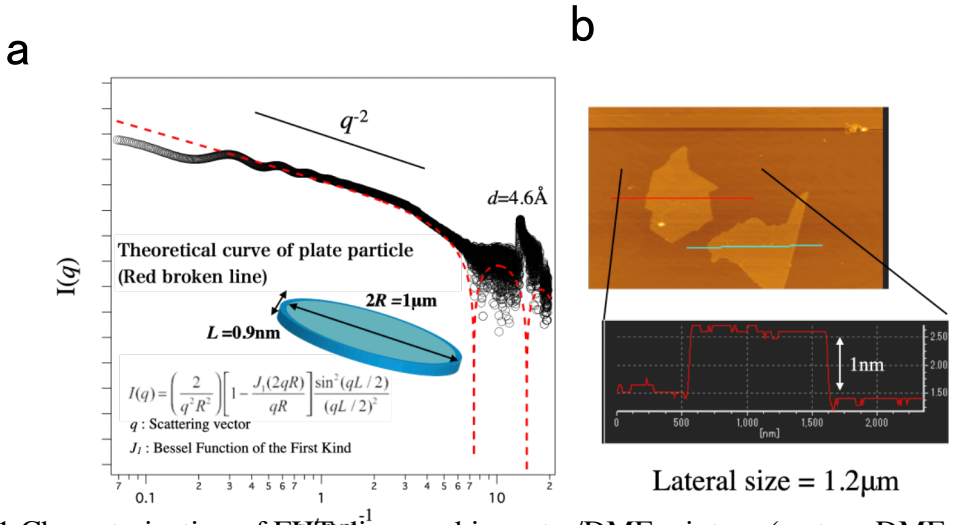

Figure 1 Characterization of FHT dispersed in water/DMF mixture (water : DMF = 20 : 80) with a: SAXS-WAXS and b: AFM.

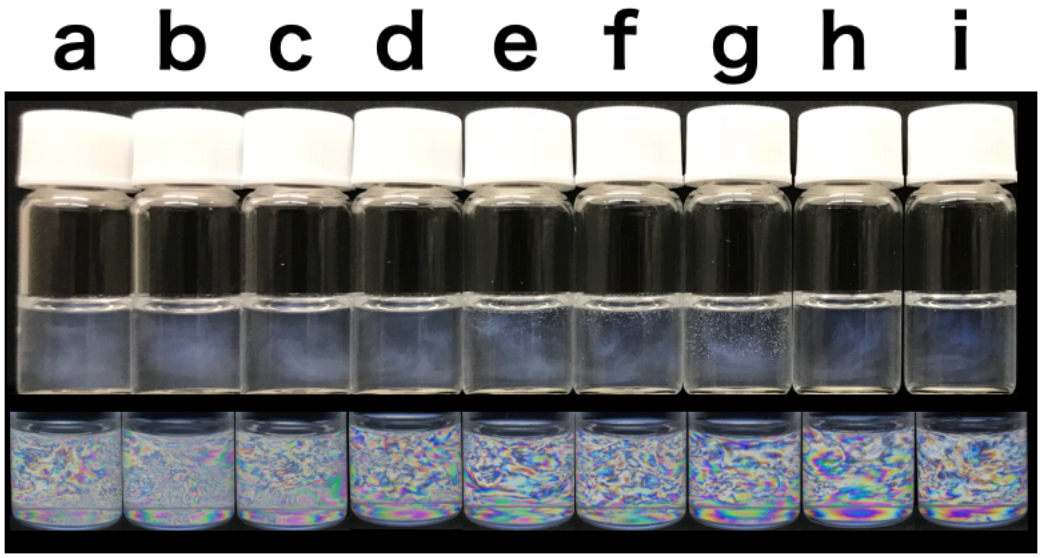

Figure 2 Visual observation under white light and crossed polarizers of 2wt% FHT nanosheet colloid. DMF ratio are a: 0%, b: 10%, c: 20%, d: 30%, e: 40%, f: 50% ,g: 60% , h: 70% , i: 80%.

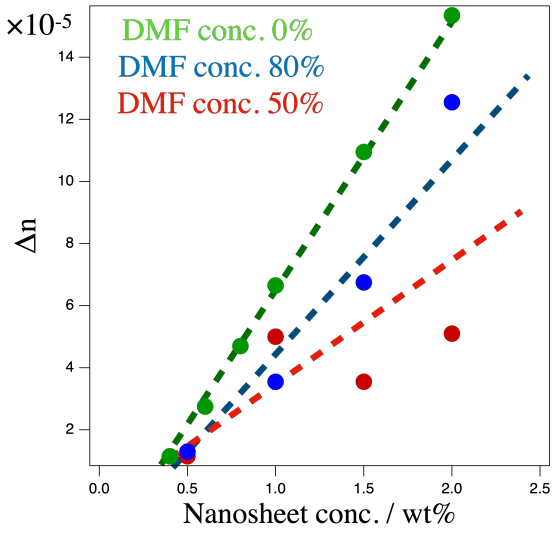

Figure 3 Birefringence measurement of FHT nanosheet colloid with various DMF ratio.

2 wt% nanosheets dispersed in H_2O/DMF mixture solvent showed nematic texture with interference colors (Figure 2). The nanosheets uniformly dispersed and all sample showed permanent birefringence and high transparency up to DMF concentration

of 80%. Stronger interference color was observed when nanosheet concentration increased. However phase separation of FHT nanosheet colloid dispersed in H_2O/DMF mixture solution was not observed. In contrast FHT nanosheet colloid dispersed in only water shows macroscopic phase separation into isotropic and nematic phases in hours or days[1]. 0.2 wt% FHT nanosheets colloid showed only flow birefringence, indicating this

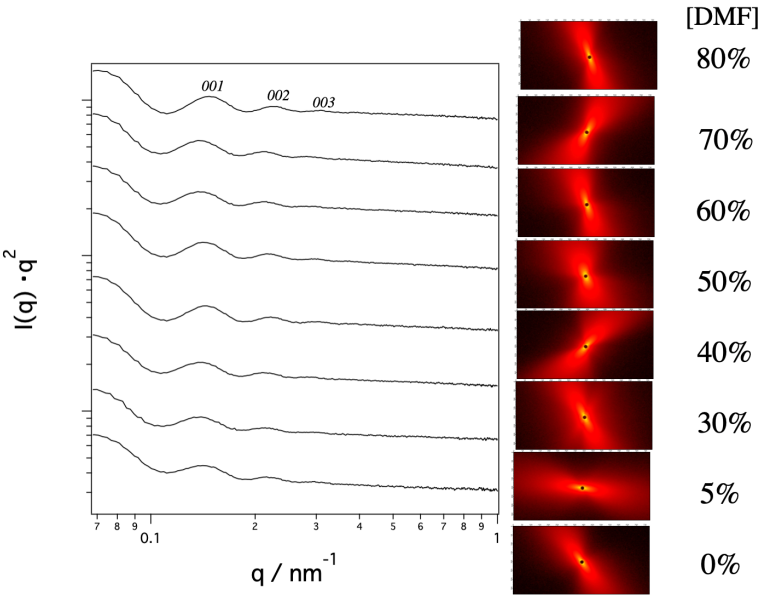

Figure 4 SAXS profile of 2wt% nanosheet dispersed in solvent of various water/DMF ratio.

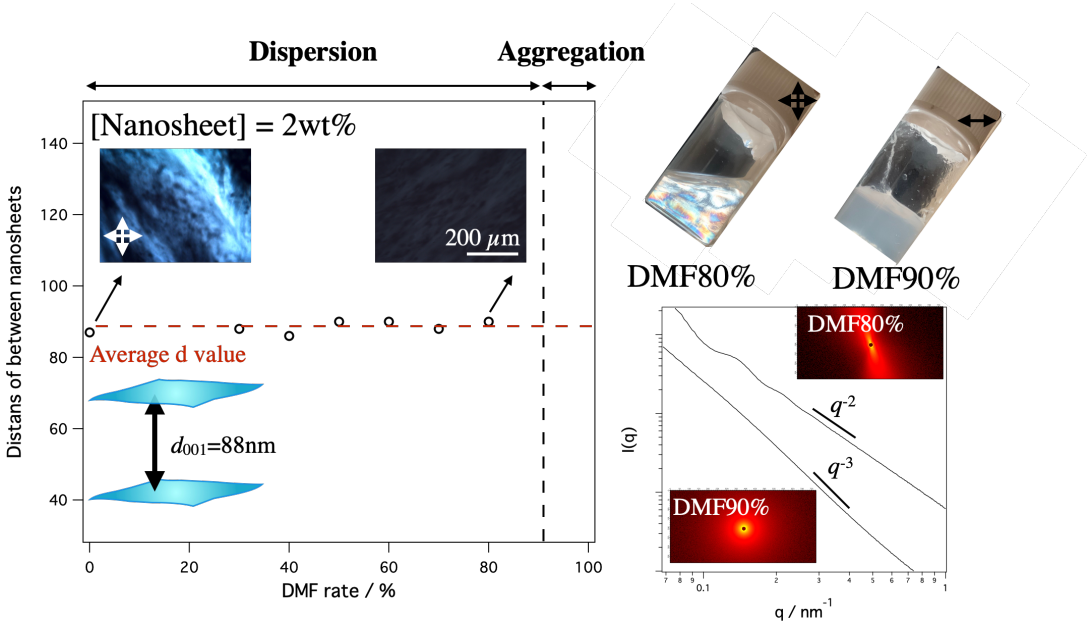

Figure 5 SAXS pattern and *d* value of nanosheet colloid dispersed in water and water/DMF

is isotropic phase. The critical concentration for isotropic to LC phase transition was determined by birefringence measurement. Figure 3 shows the relationship between the birefringence and the nanosheet concentration. The present system with or without DMF linearly increases with the increase of the nanosheet concentration. By extrapolating the plot, transitional concentration ϕ_I was determined as 0.4 wt%. This value is roughly consistent with the value calculated by Onsager theory as:

$$\phi_I = 3.3(\frac{4L}{\pi D}) \qquad (2)$$

where L is thickness D is diameter of disk particle. In present system, thickness and diameter of FHT nanosheet are 0.9nm and 1.2μm. The average particle size of the FHT nanosheet was evaluated as 1.2 nm by DLS. The different increasing of birefringence seems to be the effect of the refractive index of the solvent.

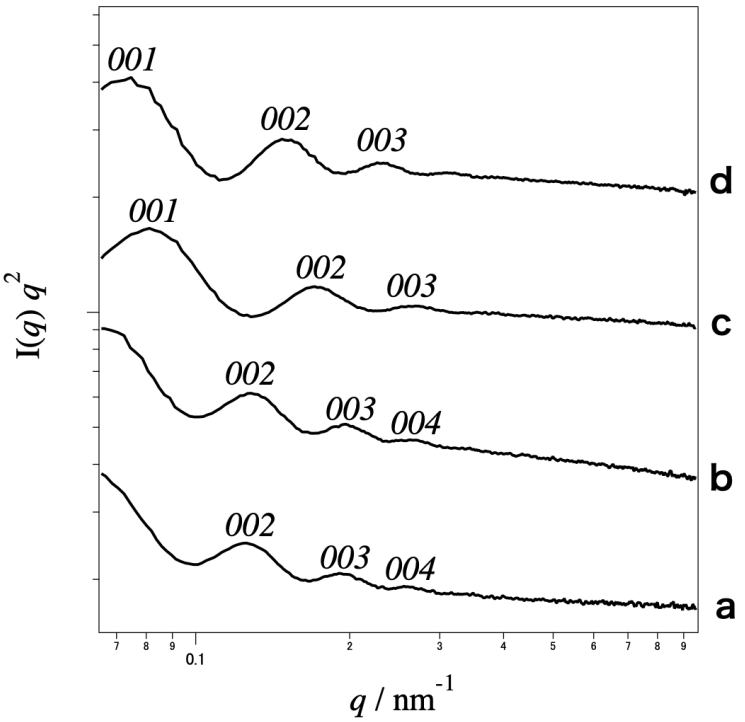

Figure 6 SAXS profile of 2 wt% nanosheet dispersed in a: water ([CH_3COONH_4]=10-4M), b: mixture of water 50% and DNF50% ([CH_3COONH_4]=10-4M), c: water ([CH_3COONH_4]=10-3M), d: mixture of water 50% and DNF50% ([CH_3COONH_4]=10-3M)

The nanosheet colloids formed lamellar-like structure and LC structure did not change when DMF ratio increased (Figure 4). All samples showed many peaks peaks ascribed to 002, 003, 004 reflections are observed. From these values d_{001} that corresponds to nanosheet-nanosheet distance is estimated as 88 nm. 2wt% nanosheets colloids dispersed in each DMF ratio showed only d_{001} = 88.0 nm and kept high structural order (Figure 5). Formation of aggregation of nanosheets is suggested at more than DMF 90%. At DMF ratio 90%, the colloid did not show birefringence and formed physical gel, Furthermore, few peaks disappeared and profile with the slope of q^{-3} was observed. The theoretical form factor (*eq*.(1)) of the nanosheets is approximated as q^{-2} for the nanosheets larger than 100 nm in the range of q in the present measurement. Influence of salt concentration were investigated with SAXS (Figure6). Figure 6a and b showed d= ～92 nm. peaks of Figure 6c and b shifted to higher q, respectively, each d were 72.6 nm and 84 nm. The salt concentration change is more remarkable in the water system than in the DMF system. Structural order did not change.

2.4. Discussion

These behaviors are considered to be qualitative with classical DLVO theory and it is explained as follows. The repulsive potential in DLVO theory is due to the excessive osmotic pressure due to the overlap of the electric double layer surrounding the particles. When two flat plates with a surface potential of Ψ_0 exist at distance h, the repulsive potential V_R in the constant charge model is following the formula.

$$V_R = \varepsilon\kappa\psi_0^2(\coth\frac{\kappa h}{2}) \qquad (3)$$

Here ε is the permittivity of the solvent and $\varkappa$ is the reciprocal of the electric double layer thickness.

$$\kappa^{-1} = \frac{\varepsilon kT}{2000N_A e^2 I} \qquad (4)$$

k is the Boltzmann constant, T is the absolute temperature, N_A is the Avogadro constant, e is the elementary charge, and I is the ionic strength in the solution.

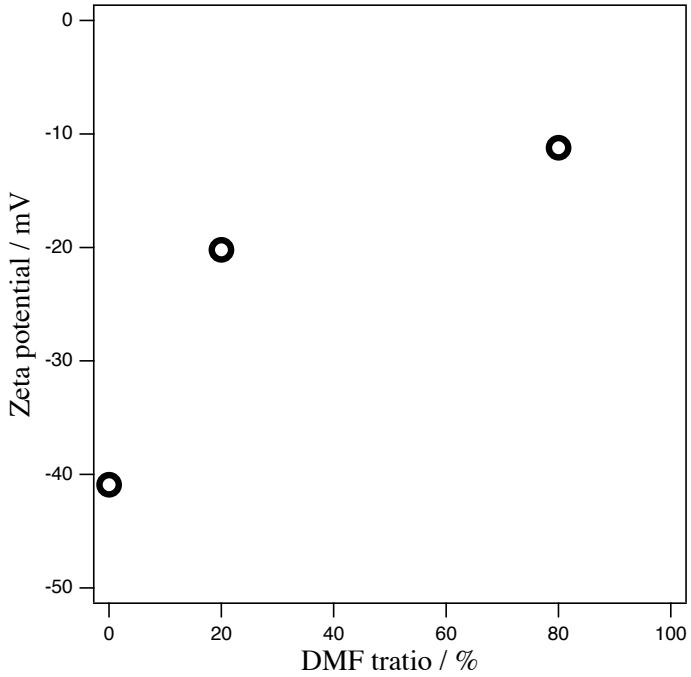

Figure 7 Zeta potential measurement of nanosheet colloid.

The repulsive potential is proportional to the square of the surface charge density and inversely proportional to the square root of the ion strength. DMF system and the water system, the relative ε is 78 and 38 at 25 ° C, respectively, the difference in ε is about two times. In addition, dissociation degree of clay nanosheets-$NH4^+$ in the water/DMF system are considerably lower than in the only water system (Figure 7). However, *d* value did not change with or without DMF. That indicating that dissociation of CH_3COONH_4 also decrease in water/DMF mixture solution. The *d* value of the water/DMF mixture system will not be higher than only water system. It is shown in SAXS measurement. Figure 8 shows relationship between the d value and various FHT nanosheet concentration. If the interactions between nanosheets are purely repulsive and nanosheets form lamellar structure, we expect that the *d* value (average nanosheet-nanosheet distance) obeys one-dimensional swelling law of the *eq*. 5 (dashed line in Figure 6).

$$d = L\,\phi^{-1} \qquad (7)$$

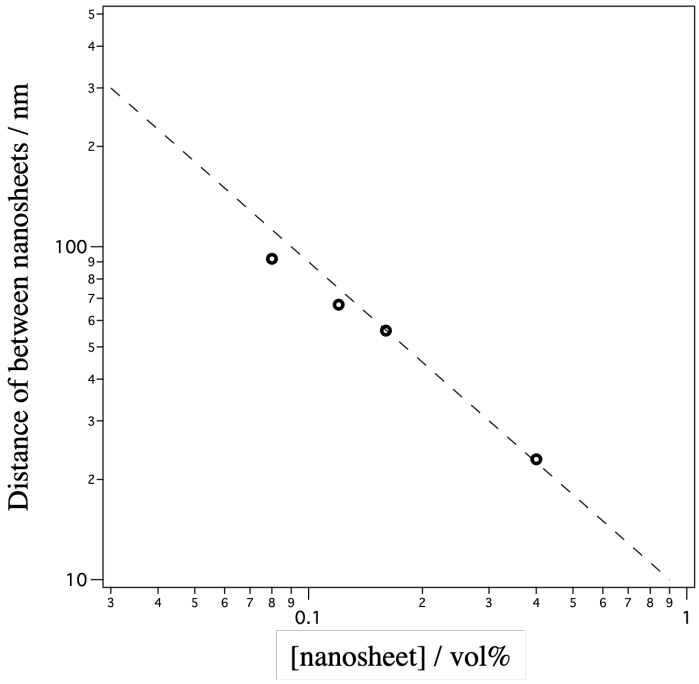

Figure 8 Relationship of *d* value and nanosheet concentration. Dashed line is one-dimensional swelling law of plate with 0.9nm-thick and 500nm-width.

Here, L is thickness of the nanosheet and ϕ is volume fraction of the nanosheets. Obtained result agree with one-dimensional swelling law. This indicates that the interactions between the nanosheets are strong repulsive force. Therefore, if the *I* decreases due to increasing DMF ratio, the *d* value can not increase.

Adding more CH_3COONH_4, dissociation of nanosheet-NH_4 decreases and the ϕ more decrease and *I* increases. Hence, the repulsive potential greatly decreases, as a result, the basal spacing and structure order are easily decreased. As described above, the degree of dissociation of the mixture system is a lower than water system, hence the decrease of repulsive force is smaller.

2.5. Conclusion

Clay mineral nanosheet dispersed in water/DMF mixture while maintaining liquid crystallinity. The liquid crystal structures with or without DMF were similar. Meanwhile, influence of salt concentration was difference. The behavior is different dissociation of CH_3COONH_4 in water/DMF mixture solution.

2.6. Reference

1. Miyamoto, N.; Iijima, H.; Ohkubo, H.; Yamauchi, Y., Liquid crystal phases in the aqueous colloids of size-controlled fluorinated layered clay mineral nanosheets. *Chem. Commun.* **2010,** *46*, 4166-4168.

2. Paineau, E.; Antonova, K.; Baravian, C.; Bihannic, I.; Davidson, P.; Dozov, I.; Impéror-Clerc, M.; Levitz, P.; Madsen, A.; Meneau, F.; Michot, L. J., Liquid-Crystalline Nematic Phase in Aqueous Suspensions of a Disk-Shaped Natural Beidellite Clay. *J. Phys. Chem. B* **2009,** *113*, 15858-15869.

3. Hernandez, Y.; Nicolosi, V.; Lotya, M.; Blighe, F. M.; Sun, Z.; De, S.; McGovern, I. T.; Holland, B.; Byrne, M.; Gun'Ko, Y. K.; Boland, J. J.; Niraj, P.; Duesberg, G.; Krishnamurthy, S.; Goodhue, R.; Hutchison, J.; Scardaci, V.; Ferrari, A. C.; Coleman, J. N., High-yield production of graphene by liquid-phase exfoliation of graphite. *Nat Nanotechnol* **2008,** *3*, 563-8.

4. Mayr, L.; Amschler, S.; Edenharter, A.; Dudko, V.; Kunz, R.; Rosenfeldt, S.; Breu, J., Osmotic Swelling of Sodium Hectorite in Ternary Solvent Mixtures: Nematic Liquid Crystals in Hydrophobic Media. *Langmuir* **2020,** *36*, 3814-3820.

5. Wong, M.; Ishige, R.; White, K. L.; Li, P.; Kim, D.; Krishnamoorti, R.; Gunther, R.; Higuchi, T.; Jinnai, H.; Takahara, A.; Nishimura, R.; Sue, H. J., Large-scale self-assembled zirconium phosphate smectic layers via a simple spray-coating process. *Nat. Commun.* **2014,** *5*, 3589-3600.

6. Suzuki, A.; Oaki, Y.; Imai, H., Synthesis of dispersible nanosheets based on monolayer clays with imidazolium and ammonium cations having long-chain alkyl groups. *Journal of the Ceramic Society of Japan* **2017,** *125*, 353-356.

7. Wong, M.; Ishige, R.; Hoshino, T.; Hawkins, S.; Li, P.; Takahara, A.; Sue, H.-J., Solution Processable Iridescent Self-Assembled Nanoplatelets with Finely Tunable Interlayer Distances Using Charge- and Sterically Stabilizing Oligomeric Polyoxyalkyleneamine Surfactants. *Chem. Mater.* **2014,** *26*, 1528.

8. TaeYoung Kim, H. L., JongEun Kim, and Kwang S. Suh, Synthesis of Phase Transferable Graphene Sheets Using Ionic Liquid Polymers. *ACS Nano* **2010,** *4*.

CHAPTER3

Rheological control of clay nanosheet colloid by adding carbonyl compound

CHAPTER3

Rheological control of clay nanosheet colloid by adding carbonyl compound

3.1. Introduction

Layered clay minerals such as saponite and montmorillonite are important in wide range of industrial applications not only due to various excellent properties (ion-exchange capability, catalytic property, etc.) but also due to their low cost, low environmental load, abundance in earth soils, and low toxicity. Especially, the superior properties originate from extremely large specific surface area and anisotropic morphology. The properties are maximized when stacked clay layers are exfoliated into single-layer nanosheets with ~1 nm thickness and sub-μm width. This ideal exfoliation is induced very easily just by dispersing the clay powders in water. In addition to the classical application as rheology modifier for paints, cosmetics, drilling fluids, catalyst, and adsorbent, many functional nanomaterials have been fabricated from clay nanosheets. Two-dimensional nano-space is suitable to immobilize and organize functional organic molecules for optical devices[1] and stable color materials[2]. Tough clay nanosheet/polymer composites with gas-barrier[3, 4] and fire-retardancy properties have been widely used for many field. Excellent gel materials with mechanical toughness and anisotropy have also been reported[5-8] and applications for soft actuators[9] and cell culture[10] .Colloidal liquid crystal phase of clay nanosheets with stimuli-responsive optical property is highlighted recently.[8, 11] Composites with biomacromolecules such as DNA,[12] tubulin,[13] and cellulose[14] are also promising.

In the process of fabricating these functional nanomaterials or using the dispersion itself as functional colloids, effective control of rheological property of the clay nanosheet colloids is indispensable because even with several wt% of clay nanosheets, the colloid becomes very viscose and forms physical gel. However, this is very problematic for homogeneous compositing with other materials and assembling the nanosheets into regulated structures. The high viscosity and gelation are not favorable also in the applications of liquid crystal colloids because good stimuli response and structure formation are hindered.

Here, we demonstrate that addition of small amount of carbonyl compounds to the aqueous colloids of a clay mineral saponite very effectively increase the fluidity and to inhibit gelation (Scheme 1), while retaining highly dispersed state and flow-birefringence property of the clay colloid. Although inorganic salts or inorganic and

organic acids,[15-17] as well as polymers[18, 19] have been reported to decrease the viscosity of clay colloids, the effect is not so large and these additives easily cause flocculation, in contrast with the present system. Haraguchi et al. reported addition of a carbonyl compound *N*-isopropylacrylamide reduces the viscosity of a clay colloid. however, no further systematic study has not been done.[20]

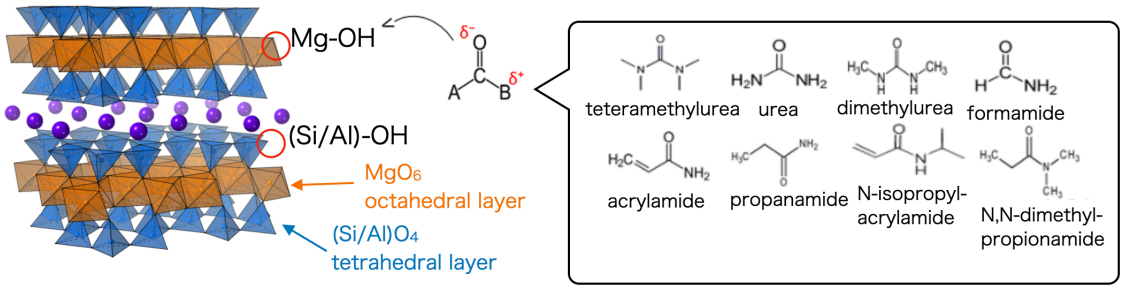

Scheme 1 The chemical structures of the saponite clay and the carbonyl compounds used in this study.

3.2. Experimental

3.2.1. Matreials. Saponite powders (Sumecton SA supplied from) were purchased from Kunimine Industries; the ideal composition of saponite is $Na_{0.33}(Mg_3)(Al_{0.33}Si_{3.67})O_{10}(OH)_2$. Trea, *N*,*N*'-dimethylurea, *N*,*N*,*N*',*N*'-tetramethylurea (TMU), and acrylamide were purchased from Tokyo Chemical and used without purification. Formaide, propionamide, *N*-isopropilacrylamide, *N*,*N*-dimethylpropionamide were purchased from Wako and used as the carbonyl compounds without purification.

3.2.2. Sample preparations. Saponite nanosheets colloid (3 wt%) was prepared by dispersing the saponite powder in water and stirring at 60 °C for 3 d. Various carbonyl compounds shown in Scheme 1 were added to the colloid, followed by dilution with pure water to adjust the saponite concentration to 2 wt%. The mixture was then stirred for 1 d. The concentration of the compounds was set as 90 mmol･g clay^{-1}, that is 1.8×10^{-4} M in the solution.

3.2.3. Characterizations. Dynamic rheology measurements were performed with the rheometer (Anton-Paar Industries, MCR303) at 25 ºC in the strain sweep mode in the range of strain ε = 0.1 - 100 % and in the frequency sweep mode in the range of frequency *f* = 0.1-100 Hz. Small/wide angle X-ray scattering (SAXS/WAXS) measurements were performed on Rigaku NANOPIX.

3.3. Results

3.3.1. Appearance and mesoscopic structure of the colloid

Figure 1 shows the photographs of the saponite colloids added with TMU observed with crossed polarizers. All the samples seem homogeneous with no obvious aggregates even with the addition of 90 mmol/g clay of TMU. While 1 wt% colloid fall down when the glass tube was placed upside down, the 2 wt% samples with or without TMU did not fall down, indicating they are in a gel state. Weak birefringent textures are observed in the 2 wt% samples regardless of addition of TMU, indicating that the nanosheets are partially macroscopically oriented, while 1 wt% colloid was isotropic liquid without birefringence.

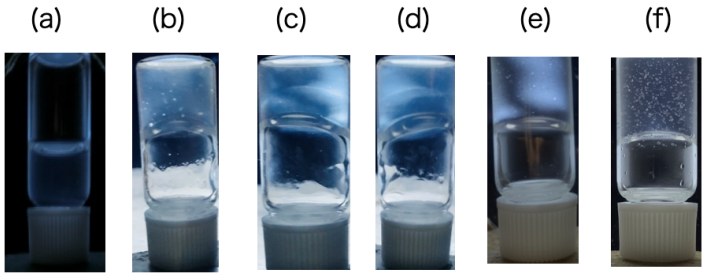

Figure 1. Crossed polarizer observations of the (a) 1 wt% and (b)-(d) 2 wt% saponite colloids (2 wt%) added with (a)(b)0, (c)4.17, (d)16.67, (e) 40 and 90 mmol/g clay of tetramethylurea. The glass tube was placed upside down for observation after the colloid was loaded.

Figure 2 shows the SAXS-WAXS profiles of the saponite colloids. Regardless of the addition of TMU, the profile obeys the power law of q^{-2} in the range 0.2 $nm^{-1} < q < 6$ nm^{-1}, while they show minimum and broad maximum at around q = 8.0 and 16 nm^{-1}, respectively. These profiles are in accordance with the theoretical form factor of a thin disk expressed as:

$$P(q) = \left(\frac{2}{q^2R^2}\right)\left[1 - \frac{J_1(2qR)}{qR}\right]\frac{sin^2(qL/2)}{(qL/2)^2} \qquad (1)$$

where J_1 is the Bessel function of the first kind, R is the radius of the disk, and L is the thickness of the disk. The absence of excess scattering at lower-q region confirms that the

nanosheets are dispersed without aggregations even with the addition of TMU. Sharp diffraction peak around q = 6 nm^{-1} (d ~ 1 nm) is neither observed, indicating that there are no stacked layers.

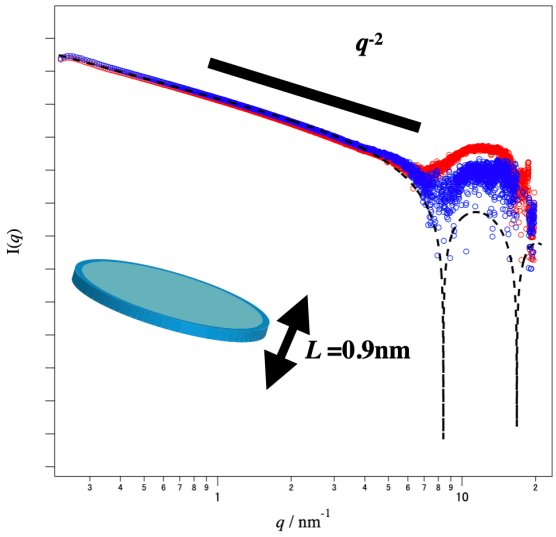

Figure 2. SAXS-WAXS profiles of the saponite colloids (2 wt%) added without TMU (red line) and with 90 mmol g clay-1 of TMU (blue line). The black dashed curbe is the theoretical form factor for a thin disk with thickness of 0.9 nm.

3.3.2. Rheological properties

Figure 3 shows the frequency f response of G' and G'' of the 2 wt% saponite colloids. The moduli are mostly constant in the range of 0.3 Hz < f < 10 Hz. Hence, we set the f = 1 Hz in the following measurements in strain sweeping mode. Note that the significant drops of moduli at higher strain are the artifacts caused by slipping between sample and the cone plate.

Figure 4a and a' show strain response of G' and G'' of a 2 wt% saponite colloid, respectively. In the smaller strain region, G' is larger than G'' with G' ~ 4 x 10^4 Pa, indicating that the colloid is a weak physical gel. With the increases of the strain, G' curve crosses with G'' curve so that G' is larger than G'' above the strain of 12 %. This indicates the transition from the gel to viscose sol above this strain. The modulus and strain at the cross-point is defined as the gel-sol transition strain $\varepsilon_{(gel\text{-}sol)}$ and modulus $G_{(gel\text{-}sol)}$. Remarkably, as shown in Figure 2b and b', addition of TMU to the saponite colloid resulted in significant decrease of the moduli over whole the strain range, while $\varepsilon_{(gel\text{-}sol)}$ shifted to higher strain (22 %).

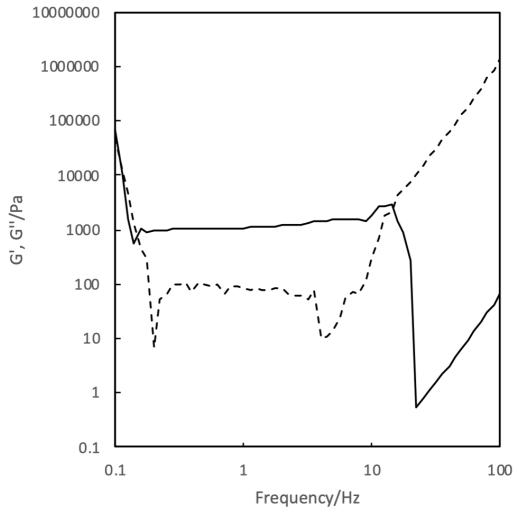

Figure 3 Frequency response of G' and G'' measured with 1% strain of 2 wt% saponite colloid. Solid and dashed lines show G' and G'', respectively.

TMU concentration dependence on the rheological property was then evaluated. Figure 5b and c show *G*' and *G*'' measured at the strain of 1% (gel state) and 100% (sol state) as the function of the TMU concentration. The moduli drastically decreased by the addition of small amount of the compound, followed by gradual increase after the minimum value at around 30 mmol▪g clay^{-1}. The *G*' in the gel state and *G*'' in the sol state of the sample added with TMU were significantly lower than that without TMU. As shown in Figure 5a, $G_{(gel\text{-}sol)}$ also decreased with addition of TMU and the turned to increase above the maximum around 30 mmol/g clay, while $\varepsilon_{(gel\text{-}sol)}$ increased with the addition of TMU and turned to decrease.

The rheological property of the present systems showed significant time-dependence, that is hardening with time. Figure 4 shows the time-course of the absolute value of the complex viscosity $|\eta^*|$ defined by the eq. 2, that is an index of fluidity of the colloid (more fluid colloid has smaller $|\eta^*|$), during continuous measurement at 1 Hz and 1% strain.

$$|\eta^*| = \sqrt{[G'/(2\pi f)]^2 + [G''/(2\pi f)]^2} \qquad (2).$$

In the 2 wt% saponite colloid without the additive, $|\eta^*|$ increased gradually until 1000 s, and increased more steeply later. The samples added with TMU also showed similar trends. Similar hardening has been generally observed in clay colloid systems[21] and are explained by slow structure formation through clay-clay interactions.[22-26]

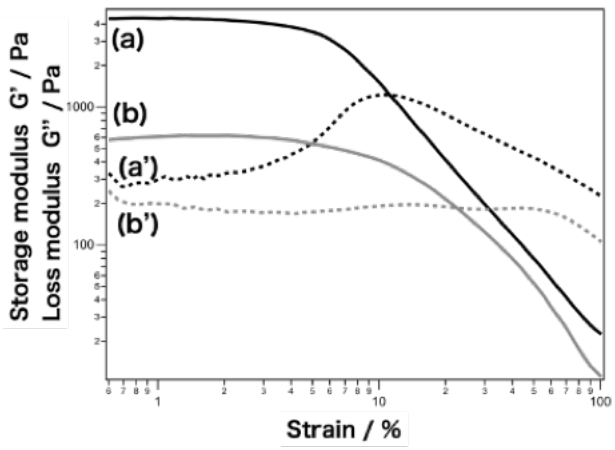

Figure 4 Strain response of G' and G'' of 2 wt% saponite colloid (a)(a)' without TMU and (b)(b)' with the addition of 20 mmol/$g_{saponite}$ of TMU. The frequency was set as 1 Hz. Solid and dashed lines show G' and G'', respectively.

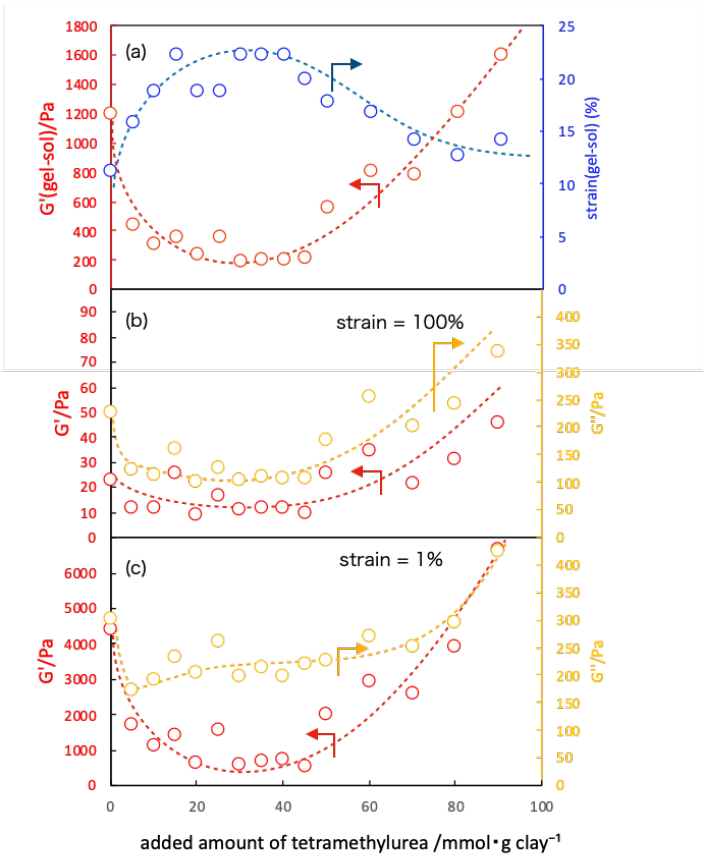

Figure 5 (a) The strain and G' of gel-sol transition, and the moduli at strain of (b) 1% and (c) 100% of the 2 wt% saponite colloid as the function of added amount of tetramethylurea. The frequency was set as 1 Hz. Solid and dashed lines show G' and G'', respectively.

Other kinds of carbonyl compounds (*N*-isopropylacrylamide, urea, propionamide, *N*,*N*'-dimethylurea, formamide) also affected the rheological property of the saponite colloid; Figure 7 compares the G' and G'' at 1% strain as the function of concentration of the added compounds. All the compounds give similar trends that the moduli decrease by the addition of small amount of the compound, followed by gradual increase. The reduction of the moduli was in the order of: TMU > N-isopropylacrylamide > urea > propanamide > *N*,*N*'-dimethylurea > formamide. In the cases of *N*,*N*'-dimethylurea and formamide, the moduli was larger than the saponite without addition of the compound.

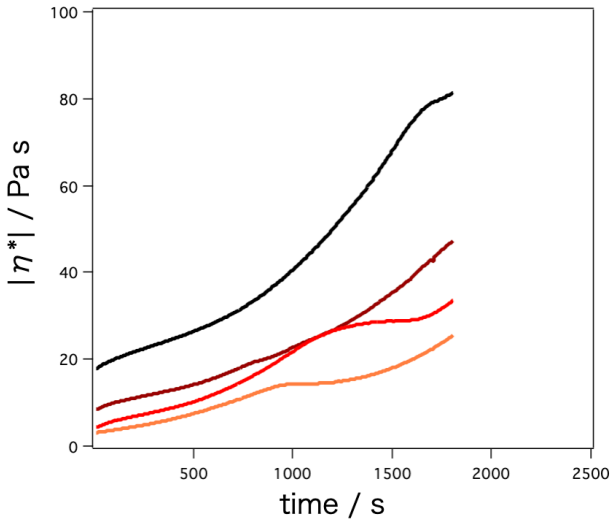

Figure 6 Time course of the absolute value of complex viscosity $|\eta^*|$ of the 2 wt% saponite colloids added with (a) 0, (b) 8.3, (c) 16.7, and (d) 33.3 mmol/g clay of TMU. The measurement was performed at 1% strain and the frequency of 1 Hz,

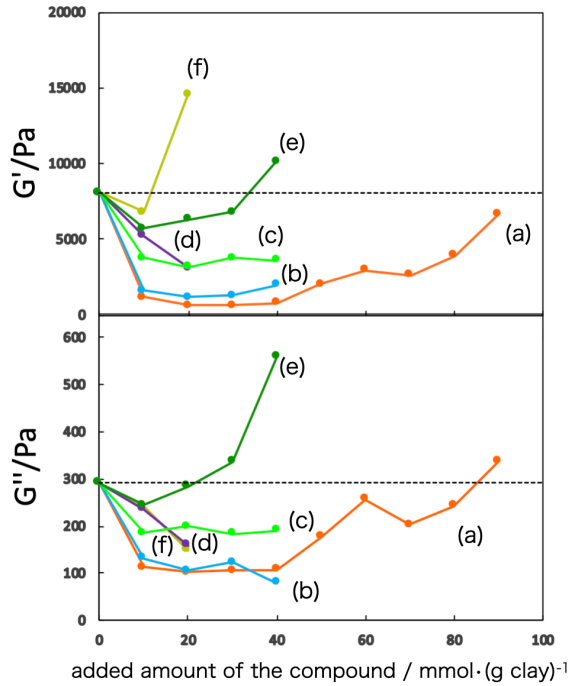

Figure 7 G' and G'' 2 wt% saponite colloid as the function of added amount of carbonyl compounds: (a) ***N***,***N***,***N***',***N***'-tetramethylurea, (b) ***N***-isopropylacrylamide, (c) urea, (d) propionamide, (e) *N*,*N*'-dimethylurea, and (f) formamide.

3.4. Discussion

Generally, rheological property of any kind of colloidal system of small particles depends on the size, shape and concentration of particles as theoretically expressed in the classical Einstein's equation:

$$\eta_r = 1 + K\phi \quad (1)$$

where η_r is the relative viscosity, ϕ is the volume fraction of particles, and K is the constant related to particle shape (2.5 for sphere and >2.5 for anisotropic particles). However, clay colloids show very complicated rheological properties such as unexpectedly high viscosity, thixotropy (time-dependent change of rheological property), and formation of physical gel.[27] [28] The complicated rheological behavior of clay colloids have been investigated by many researchers and several mechanisms have been proposed: colloidal glass model[29] and card house[27] (or empty liquid[30]) model.

The important points to be considered in these models are the charges on the layer surface and the edges as well as very anisotropic shape of the clay sheets. Clay

layers have permanent negative charge due to isomorphous substitution in octahedral and/or tetrahedral layers, while the -OH groups on the layer edges are present as $-OH^{(\delta+)}$ or even MOH_2^+ as well as $-O^-$, depending on pH and point of zero charges of the MOH group. In the colloidal glass model, the clay particle is simply considered as negatively charged particle surrounded by electric double layer of counter cations that cause strong repulsive interactions between the clay particles. Above a certain nanosheet concentration, motion of the particles is significantly restricted due to that repulsion, resulting in higher viscosity or gelation. According to the DLVO theory,[28, 31] addition of salt screens this repulsion so that the viscosity of colloid decreases. However, at very high salt concentration, the layers are partly restacked to form inhomogeneous attractive gel or flocculation. On the other hand, in the card house model, the positive charges on the edges are also considered. Weak attractive interactions between the positively charged edges and negatively charged surfaces results in the formation of network structure spread over whole the colloid, recently termed as empty colloid, that contribute to high viscosity or gelation. The very anisotropic shape contributes to the formation of this network at very low concentration.

The layer of saponite used in the present study is ideally composed of two $(Si/Al)O_4$ tetrahedral layers sandwiching a MgO_6 octahedral layer (Scheme 1). Considering the generally known point of zero charge values of SiO_2 (2-3), Al_2O_3 (5-9) and MgO (~12) and the pH value of the 2 wt% saponite colloid (pH ~ 9-10), part of the edges should have considerable amount of positive charges, while the particle have net negative charge. Thus, in the saponite colloid without addition of the compounds, it is likely that the empty colloid gel is form through weak attractive interaction between edge and surface of clay nanosheets.

The decrease of the moduli by the addition of carbonyl compounds to saponite colloid is explained by the reduction of attractive interaction between clay nanosheets through adsorption of the compounds. Carbonyl compounds can be weakly adsorbed through weak ion-dipole or dipole-dipole interaction between the $>C=O^{(\delta-)}$ group and the positive sites of the clay edges. Adsorption of negatively charged species such as phosphoric acid and deoxyribonucleic acid on smectite clays have also been reported.[12] The adsorbed carbonyl compounds can block the edge-surface interactions between the clay nanosheets, resulting in lowering of the viscosity and inhibition of gelation

3.5. Conclusion

G' and G'' of aqueous saponite colloid was effectively lowered by adding carbonyl compounds, while retaining highly dispersed state and flow-birefringence

property of the clay colloid. Among various carbonyl compounds, *N*,*N*,*N*',*N*'-tetramethylurea most effectively lowered G' and G''. The low-viscosity clay colloids are applicable for many applications such as nanocomposite synthesis, liquid crystalline colloid with optical property.

3.6. References

1. Ogawa, M.; Kuroda, K., Photofunctions of Intercalation Compounds. *Chem. Rev.* **1995,** *95*, 399-438.
2. Hata, H.; Mallouk, T. E.; Kuroda, K., Color Tuning of an Acidic Blue Dye by Intercalation into the Basic Interlayer Galleries of a Poly(allylamine)/Synthetic Fluoromica Nanocomposite. *Chem. Mater.* **2009,** *21*, 985-993.
3. Schilling, T.; Habel, C.; Rosenfeldt, S.; Röhrl, M.; Breu, J., Impact of Ultraconfinement on Composite Barriers. *ACS Appl. Polym. Mater.* **2020,** *2*, 3010-3015.
4. Ebina, T.; Mizukami, F., Flexible Transparent Clay Films with Heat-Resistant and High Gas-Barrier Properties. *Adv. Mater.* **2007,** *19*, 2450-2453.
5. Haraguchi, K.; Takehisa, T., Nanocomposite Hydrogeis: A Unique Organic-Inorganic Network Structure with Extraordinary Mechanical, Optical,and Swelling/De-swelling Properties. *Adv.Mater.* **2002,** *14*, 1120-1124.
6. Miyamoto, N.; Shintate, M.; Ikeda, M.; Hoshida, Y.; Yamauchi, Y.; Annaka, M., Liquid Crystalline Inorganic Nanosheets for Facile Synthesis of Polymer Hydrogels with Anisotropies in Optical Property, Structure, Swelling/Deswelling, and Ion Transport/Fixation. *Chem. Commun.* **2013,** *49*, 1082-1084.
7. Inadomi, T.; Ikeda, S.; Okumura, Y.; Kikuchi, H.; Miyamoto, N., Photo-Induced Anomalous Deformation of Poly(N-Isopropylacrylamide) Gel Hybridized with an Inorganic Nanosheet Liquid Crystal Aligned by Electric Field. *Macromol. Rapid Commun.* **2014,** *35*, 1741-1746.
8. Miyamoto, N.; Iijima, H.; Ohkubo, H.; Yamauchi, Y., Liquid crystal phases in the aqueous colloids of size-controlled fluorinated layered clay mineral nanosheets. *Chem. Commun.* **2010,** *46*, 4166-4168.
9. Kino, H.; Kiyota, A.; Inadomi, T.; Kato, T.; Fujioka, H.; Miyamoto, N., Step Response Characteristics of Anisotropic Gel Actuator Hybridized with Nanosheet Liquid Crystal. *J. Robotics Mechatronics* **2019,** *31*, 647-656.
10. Haraguchi, K.; Takehisa, T.; Ebato, M., Control of Cell Cultivation and Cell Sheet Detachment on the Surface of Polymer/Clay Nanocomposite Hydrogels. *Biomacromolecules* **2006,** *7*, 3267-3275.

11. Michot, L. J.; Bihannic, I.; Maddi, S.; Funari, S. S.; Baravian, C.; Levitz, P.; Davidson, P., Liquid–crystalline aqueous clay suspensions. *Proc. Nat. Acad. Sci.* **2006,** *103*, 16101-16104.
12. Yamguchi, N.; Anraku, S.; Paineau, E.; Safinya, C. R.; Davidson, P.; Michot, L. J.; Miyamoto, N., Swelling Inhibition of Liquid Crystalline Colloidal Montmorillonite and Beidellite Clays by DNA. *Sci. Rep.* **2018,** *8*, 4367.
13. Kato, R.; Kakugo, A.; Shikinaka, K.; Ohsedo, Y.; Kabir, A. M. R.; Miyamoto, N., Liquid Crystalline Colloidal Mixture of Nanosheets and Rods with Dynamically Variable Length. *ACS Omega* **2018,** *3*, 14869–14874.
14. Yamamoto, S.; Ohsedo, Y.; Yamada, E.; Sonoda, K.; Mita, H.; Miyamoto, N., Cultivation of Cellulose-Producing Bacteria in the Nanosheet Liquid Crystal of Na-fluorohectorite. *Clay Sci.* **2015,** *19*, 73-77.
15. Penner, D.; Lagaly, G., Influence of anions on the rheological properties of clay mineral dispersions. *Appl. Clay Sci.* **2001,** *19*, 131-142.
16. Abend, S.; Lagaly, G., Bentonite and double hydroxides as emulsifying agents. *Clay Minerals* **2001,** *36*, 557-570.
17. Permien, T.; Lagaly, G., The rheological and colloidal properties of bentonite dispersions in the presence of organic compounds. IV. Sodium montmorillonite and acids. *Appl. Clay Sci.* **1994,** *9*, 251-263.
18. Labanda, J.; Sabaté, J.; Llorens, J., Rheology changes of Laponite aqueous dispersions due to the addition of sodium polyacrylates of different molecular weights. *Colloids and Surfaces A* **2007,** *301*, 8-15.
19. Pozzo, D. C.; Walker, L. M., Reversible shear gelation of polymer–clay dispersions. *Colloids and Surfaces A* **2004,** *240*, 187-198.
20. Haraguchi, K.; Li, H.-J.; Matsuda, K.; Takehisa, T.; Elliott, E., Mechanism of Forming Organic/Inorganic Network Structures during In-situ Free-Radical Polymerization in PNIPA-Clay Nanocomposite Hydrogels. *Macromolecules* **2005,** *38*, 3482-3490.
21. Bonn, D.; Kellay, H.; Tanaka, H.; Wegdam, G.; Meunier, J., Laponite: What Is the Difference between a Gel and a Glass? *Langmuir* **1999,** *15*, 7534-7536.
22. Pignon, F. d. r.; Magnin, A.; Piau, J.-M., Butterfly Light Scattering Pattern and Rheology of a Sheared Thixotropic Clay Gel. *Phys. Rev. Lett.* **1997,** *79*, 4689-4692.
23. Pignon, F.; Magnin, A.; Piau, J.-M.; Cabane, B.; Lindner, P.; Diat, O., Yield stress thixotropic clay suspension: investigations of structure by light, neutron, and x-ray scattering. *Phys. Rev. E* **1997,** *56*, 3281-3289.

24. Tanaka, H.; Jabbari-Farouji, S.; Meunier, J.; Bonn, D., Kinetics of ergodic-to-nonergodic transitions in charged colloidal suspensions: aging and gelation. *Phys. Rev. E* **2005,** *71*, 021402.
25. Jabbari-Farouji, S.; Wegdam, G. H.; Bonn, D., Gels and glasses in a single system: evidence for an intricate free-energy landscape of glassy materials. *Phys. Rev. Lett.* **2007,** *99*, 065701.
26. Jabbari-Farouji, S.; Wegdam, G. H.; Bonn, D., multiple nonergodic disordered states in Laponite suspensions: A phase diagram. *Phys. Rev. E* **2008,** *78*, 061405.
27. Ruzicka, B.; Zaccarelli, E., A fresh look at the Laponite phase diagram. *Soft Matter* **2011,** *7*, 1268.
28. Michot, L. J.; Bihannic, I.; Porsch, K.; Maddi, S.; Baravian, C.; Mougel, J.; Levitz, P., Phase Diagrams of Wyoming Na-Montmorillonite Clay. Influence of Particle Anisotropy. *Langmuir* **2004,** *20*, 10829-10837.
29. Tanaka, H.; Meunier, J.; Bonn, D., Nonergodic states of charged colloidal suspensions: Repulsive and attractive glasses and gels. *Phys. Rev. E* **2004,** *69*, 031404.
30. Bailey, L.; Lekkerkerker, H. N.; Maitland, G. C., Smectite clay-inorganic nanoparticle mixed suspensions: phase behaviour and rheology. *Soft Matter* **2015,** *11*, 222-36.
31. Gabriel, J. C. P.; Camerel, F.; Lemaire, B. J.; Desvaux, H.; Davidson, P.; Michael, W.; Batail, P., Swollen liquid-crystalline lamellar phase based on extended solid-like sheet. *Nature* **2001,** *413*, 504-508.

CHAPTER4

MMT nanosheet colloid showing non defect huge liquid crystallinity domain

CHAPTER4

MMT nanosheet colloid showing non defect huge liquid crystallinity domain at mm-scale

4.1. Introduction

Polymer nanocomposite of polymers with anisotropic nanoparticles is expected to improve mechanical strength, thermal stability and function based on elements and shapes of nanoparticle[1, 2]. Uniformly organization of nanoparticles is necessary for realization of materials having high mechanical strength like abalone shell [3]. Using anisotropic particle as a filler is one of the methods for achieving. It is possible to easily self-assembled because it forms liquid crystal (LC) phase by entropic force when particle concentration is higher. Among them, nanosheet from layered crystals is excellent fillers due to large aspect ratio and specific large surface area. The large surface area became many cross linking points in polymer matrix, and show high mechanical strength even small amount[4 5]. In addition, horizonal orientation nanosheet improves high gas barrier property [6-9], anisotropic thermo transmittance[10] and anisotropic mechanical property[10, 11].

However, it seem that inhomogeneous fill of nanosheets are present in those excellent materials. Because anisotropic particles form LC droplets and it causes phase separation[12-17]. LC phase transition of colloidal LC is caused from isotropic phase to isotropic phase/LC phase to LC phase when increasing anisotropic particle concentration. In isotropic phase/LC phase, it is always in a state of microphase separation of LC droplet even if it looks like a uniform dispersed solution. Even perfectly LC phase is mixture of sub-micron LC droplet of anisotropic particles. The forming droplet and phase separation of colloidal LC is inevitable behavior, so it may be defect in polymer matrix. Applying external field such as shear[18, 19], electric field[11, 16, 20], magnetic field[14, 16, 21], optical tweezer[22] to nanosheets colloid are good methods for inducing of uniformly orientation, but the orientation is only nanosheet LC droplet unit, so sub-micron phase separation were observation. Applying very high magnetic field, uniformly orientation of nanosheets was showed[21], but Industrial application is difficult and there is no realistic example.

In this study, we demonstrate montmorillonite nanosheets colloid having cm scale orientational LC domain. Colloidal property such as rheological property, LC structure is controlled by elements of particle, particle size, counter ion and salt concentration. cm scale LC phase without phase separation was obtained by controlled those property. Further, uniformly orientational the LC phase was fixed in polymer gel without using external field and more organized structure was also obtained when electric

field was applied. We also propose a new type inorganic/organic hybrid film dried uniformly organizational montmorillonite nanosheets / polymer composite gel.

4.2. Experimental

Natural MMT powder (made in Tsukinuno) 2 g was mixed to 0.2 M NaCl solution and stirred for 1 day, impurities were removed by centrifugation. The process was repeated 3 times. The suspension was dialyzed from 10^{-4} to 10^{-1}M NaCl solution. Monolayer MMT nanosheet was observed that the nanosheet colloid was diluted to 0.001 wt%, dropped on a mica substrate, dried and observed with an atomic force microscope (AFM, SII Nano Technology Inc, Nanocute). The particle size distribution was measured by dynamic light scattering diluted with 0.1 wt% (Otsuka Electronics DLS8000). Small-angle X-ray scattering (SAXS) was performed using NANOPIX of Rigaku. The MMT nanosheet colloid were measured by being enclosed in a glass capillary having a thickness of 0.01 mm and an optical path length of 2 mm, while the composite fiber was measured without a capillary. Birefringence textures were observed by using polarized optical microscope (Olympus BX-51) and by visual observation. Birefringent index was measured by using CCD type spectrophotometer（EPP-2000 Stellar Net. Inc.）equipped on the microscopy.

4.3. Results

Uniformly dispersed monolayer MMT nanosheet colloid was obtained from layered crystal (Figure 1). In the AFM image (Figure 1a), the nanosheets with ~1 nm thickness were observed while not exfoliated layered crystal nor flocculated nanosheets were observed. In the XRD pattern of the dried powders of the purified MMT (Figure 1b), the peaks ascribed to Na-montmorillonite were observed. The peak due to impurity (quartz) at $2\theta=26.6$ was not observed, indicating that the impurity is removed. In Figure 1c, SAXS-WAXS profiles of the MMT nanosheet colloid (solid line) is shown with the theoretical scattering profile (broken line) for a disk particle with thickness of 0.9 nm and diameter of 250 nm. Nanosheet colloid profile agreed with the theoretical curve, further confirming the formation of single-layer MMT nanosheets. The average particle size of the MMT nanosheet was evaluated as ~520 nm by DLS (Figure.1d).

2 wt% MMT nanosheet colloid formed the LC phase that is different from the previously reported nanosheet systems[14,15,17,23,24] as follows. The colloid spontaneously formed cm-scale nematic domains (Figure 2b) that is much larger than the other systems; in the POM image (from μm to mm scale), no defect nor optical textures were observed. (Figure 1e) The present colloid did not show phase separation even after half a year

despite the colloid possesses high fluidity, in contrast with other systems that show macroscopic phase separation into isotropic and nematic phases in hours or days.

The concentration dependence of the LC phase formation was similar to the other nanosheets. 1 wt% MMT nanosheet colloid (Figure 2a) showed only flow birefringence, indicating this is isotropic phase. The critical concentration for isotropic to LC phase transition was determined by birefringence measurement. Figure 3 shows the relationship between the birefringence and the nanosheet concentration. The birefringence linearly increases with the increase of the nanosheet concentration. By extrapolating the plot, transitional concentration ϕ_I was determined as 1.2 wt%. This value is roughly consistent with the value calculated by Onsager theory as:

$$\phi_I = 3.3\left(\frac{4L}{\pi D}\right) \qquad (1)$$

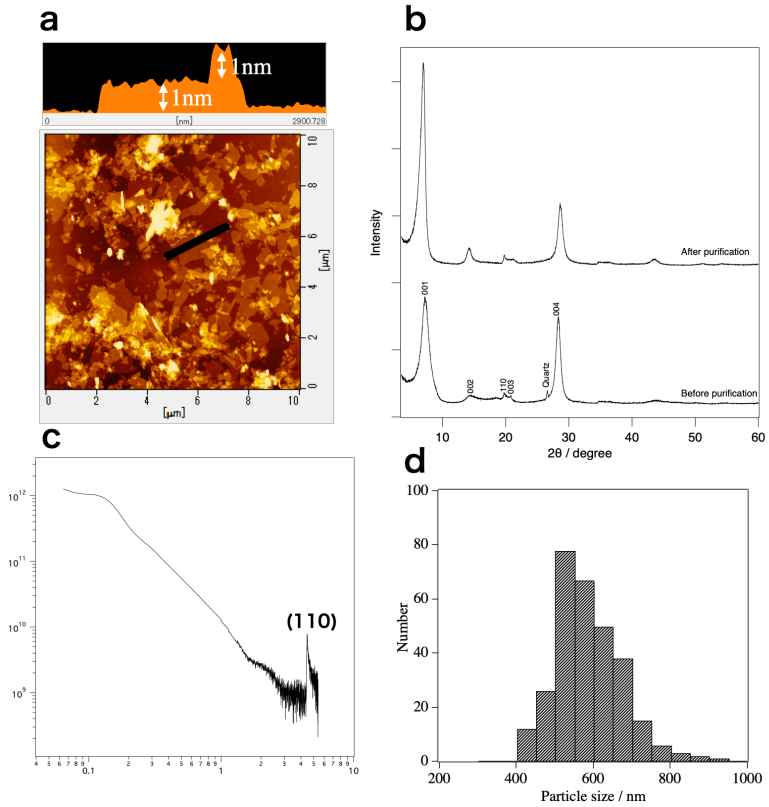

Figure 1 Characterization of MMT nanosheet with a : AFM, b : XRD, c : SAXS-WAXS, d : DLS measurement.

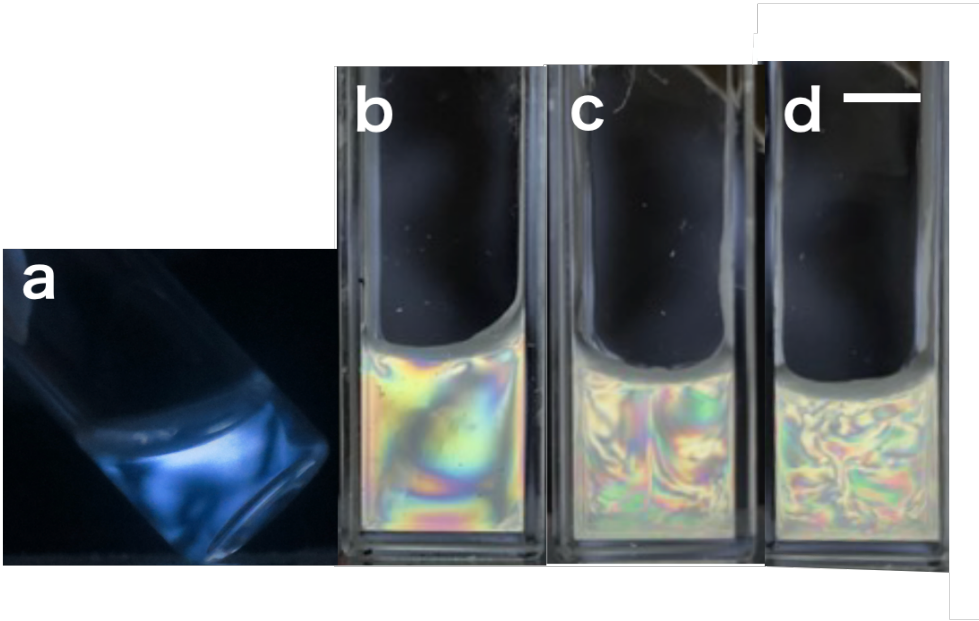

Figure 2 Observation of MMT nanosheet colloid under cross nicoles. MMT nanosheet concentration is a : 1 wt%, b : 2 wt%, c : 3 wt%, d : 4 wt%. Scale bar is 1 cm.

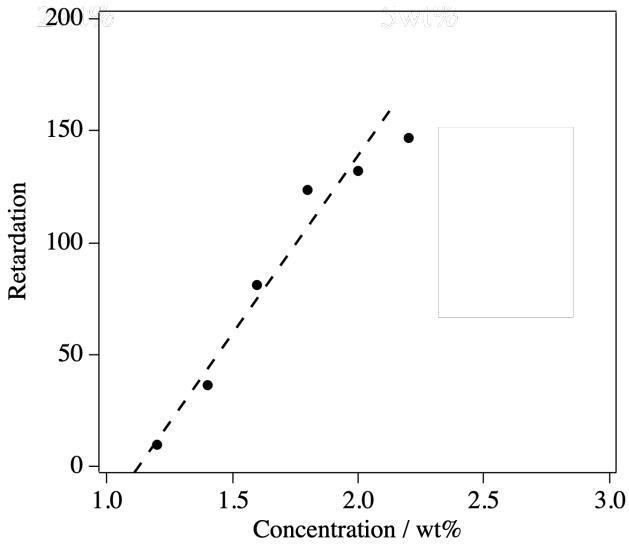

Figure 3 Birefringence measurement of MMT nanosheet colloid.

where L is thickness, D is diameter of disk particle. In present system, thickness and diameter of MMT nanosheet are 0.9nm and 500nm. Thus, the nematic phase formation is basically explained by the similar framework as the previous system, while the large domain formation and phase separation behavior was different. The size of the nematic

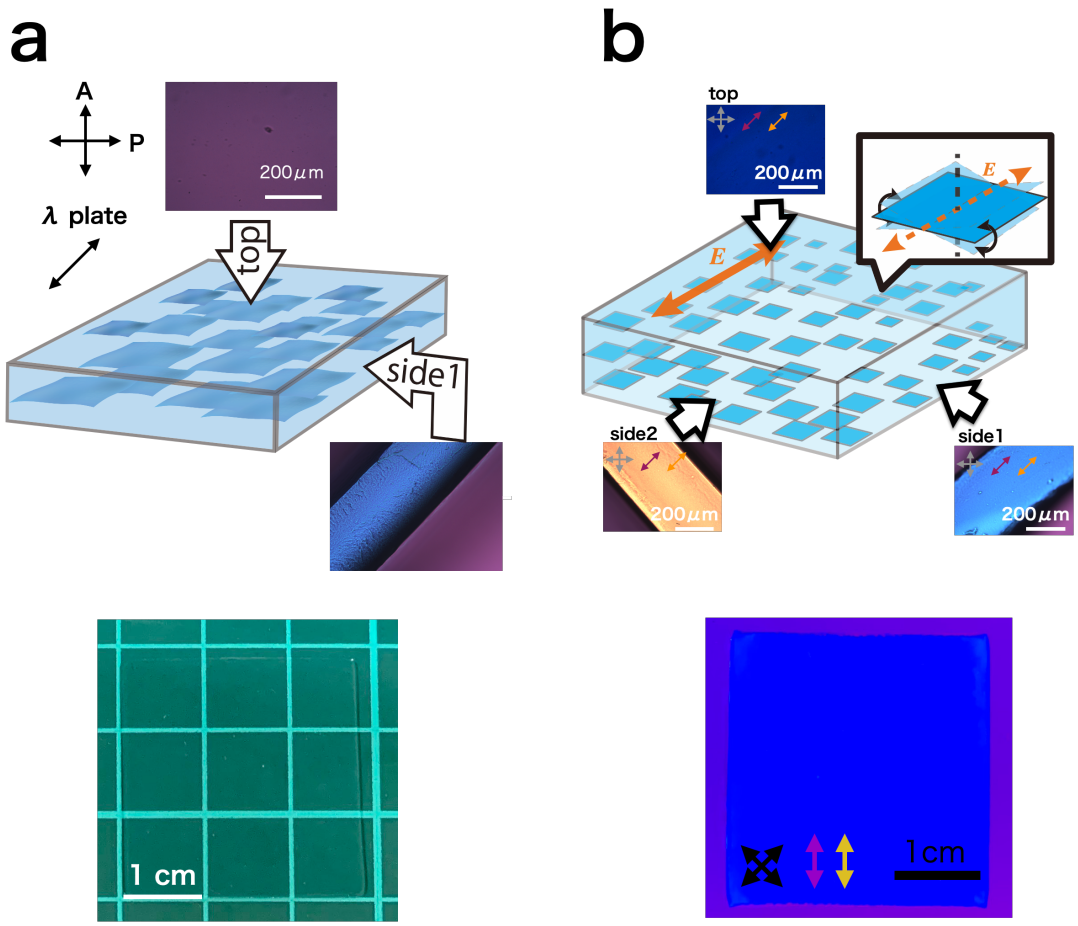

Figure 4 Model image of MMT nanosheet/pNIPA composite gel and image of POM observation or visual. a: not applied electric field, b: applied electric field.

domain decreased to several tens of μm when the nanosheet concentration increased to 3 or 4wt% (Figure 2c, d). Its results will be detailed in discussion section.

As the MMT nanosheet colloid is loaded into 0.3 mm-thick glass cell, the nanosheets were perfectly aligned along the cell surface and formed large mono-domain with no defect; this structure was successfully fixed in a polymer gel network. The gel was observed with crossed polarizers and a wave plate. With this setup, interference color of blue or yellow is observed if the nanosheet plane is parallel or perpendicular, respectively, to the fast axis of the wave plate. Purple is observed if isotropic phase or nothing sample the nanosheet plane is parallel to the cell surface. In the cross-sectional image (Figure 4a side1), uniform interference color of blue was observed when the direction of the wave-plate and the gel surface is parallel. In the top view (Figure 4a top), interference color was purple. These observations suggest that the nanosheets are aligned parallel to the cell surface and formed large mono-domain with no defect as schematically

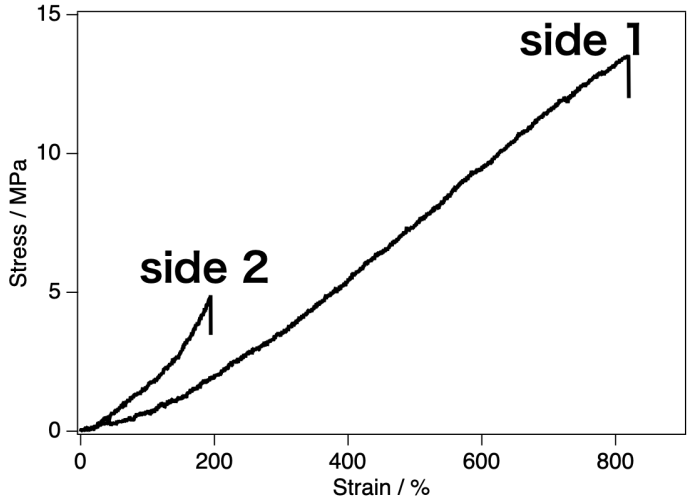

Figure 5 Tensile test of electric field applied MMT nanosheet/pNIPA composite gel.

shown in Figure 4a. It is notable that the monodomain is as large as 30 mm × 30 mm and the size can be easily extended to much larger size, e.g. > 1 m^2, because the structure is spontaneously formed through the interaction of the nanosheets with the top and bottom surfaces of the glass cell.

Mono-domain of MMT nanosheet LC in pNIPA gel was controlled by electric field and the gel had anisotropic mechanical property. In crossed polarizers, top of the gel was showed uniformly blue without yellow and purple (Figure 4b, top). In orthogonal (Figure 4b, side1) and parallel (Figure 4b, side2) directions to the electric field, the gel showed also uniformly blue and yellow. Those results suggested slightly tilted around direction to electric field without broken horizonal orientation structure of MMT

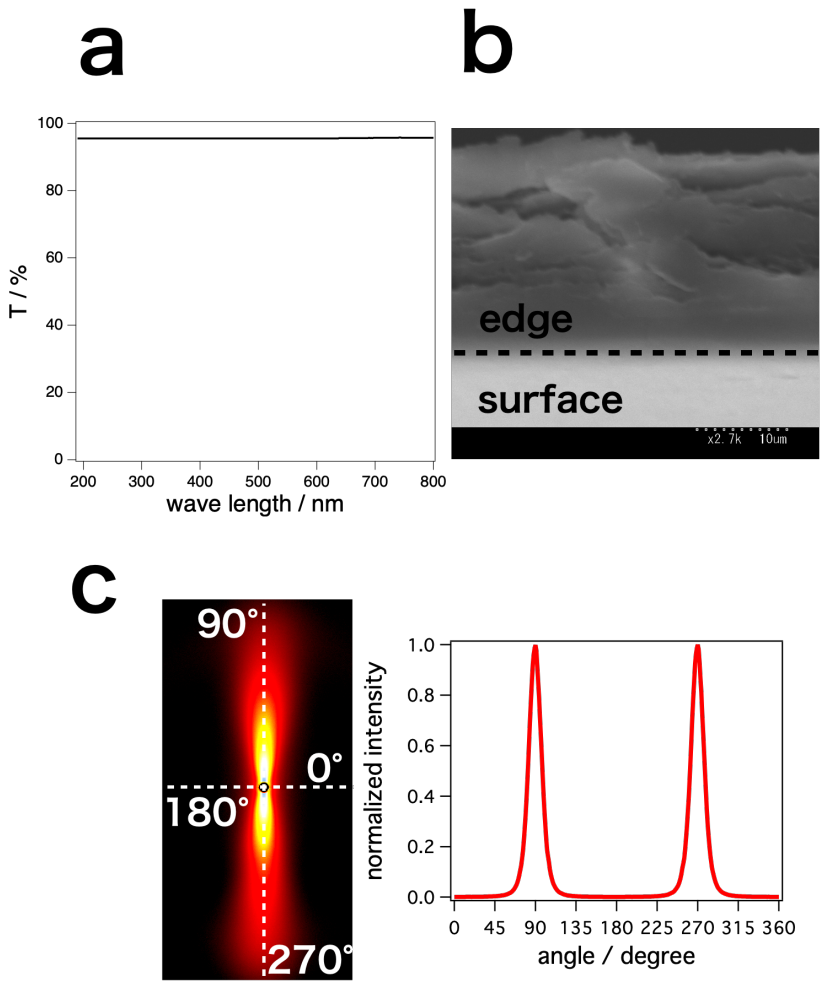

Figure 6 Characterization of dried film of MMT nanosheet / pNIPA composite gel with a: Spectral analysis, b: SEM, c: SAXS.

nanosheet. It the slightly tilted MMT nanosheet gave anisotropic mechanical property to pNIPA gel (Figure 5). Breaking stress σ and Breaking strain ε of side1 were ~2 times higher than side2 although E was equivalence.

Thin film dried horizonal aligned MMT nanosheet/pNIPA gel showed high transparency and mechanical property. The film showed 95 % transmission from 200 nm to 800 nm of wavelength despite contain 60 wt% MMT nanosheet (Figure 6a). In addition, it showed high mechanical strength while having flexibility. MMT nanosheets were uniformly orientated in horizontal direction of the gel, so the gel showed shrink only vertical direction of the gel by drying. As a result, uniformly orientated MMT nanosheets and nematic structure in film were kept. The uniformly orientation yield smooth surface and cracked edge along the orientation of nanosheets (Figure 6b). Orientation of nanosheet and structure were observed with SAXS. The anisotropic 2D scattering pattern

(Figure 6c) and the sharp peaks in the intensity vs χ profile indicate the strong alignment of the nanosheets. From the intensity vs χ profile, nematic order parameter S = 0.94 was estimated.

4.4. Discussion

As above, MMT nanosheet system has characteristic property that is spontaneously formed huge orientational nematic domain and did not show phase separation. We investigated rheological property of MMT nanosheet colloid for understanding of the behavior. Figure 3 is strain sweep measurement results. 1.5 wt% MMT nanosheet colloid showed G'' > G' in measurement region, so it is sol. 1.7 wt% MMT nanosheet colloid showed showed G'' < G' on less than strain 19%, formed gel. And it broke to sol on more than strain 19 %. Elastic modulus of colloid depended on nanosheet concentration. However, strain of gel-sol transition (cross point of G' and G'') increased until 3.4 wt%, decreased more 3.4 wt%. Other clay nanosheet (High fluidity nanoseets colloid: FHT, no fluidity nanosheets colloid: Saponite) existed different region from MMT nanosheet showing the huge orientational domain. Elastic modulus of FHT nanosheets colloid is smaller than MMT nanosheet. In addition, nanosheet concentration increased, strain of gel-sol transition decreased. Although saponite nanosheet colloid has high elastic modulus, strain of gel-sol transition decreased depending on the nanosheet concentration some as FHT nanosheet colloid.

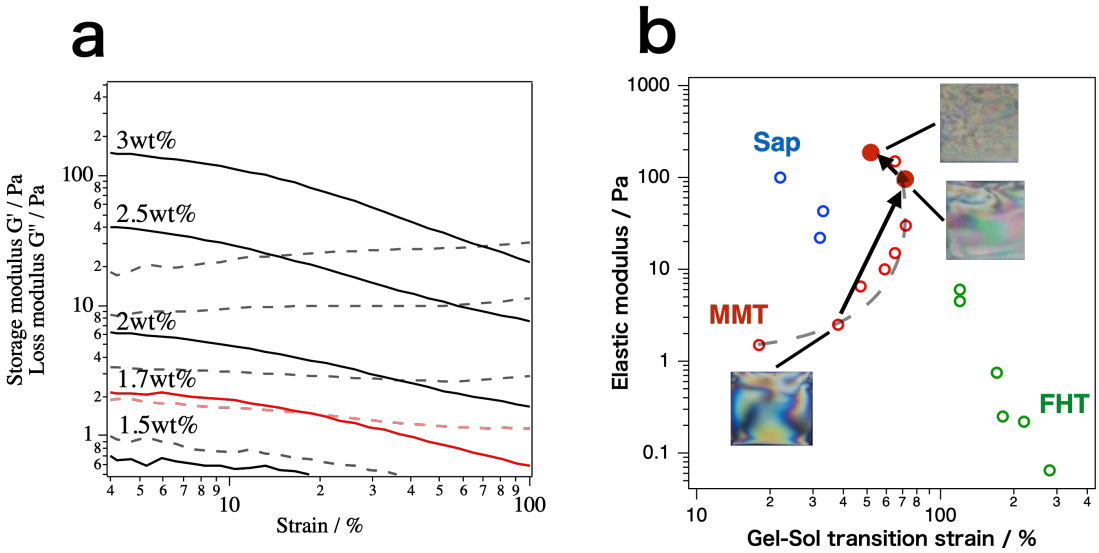

Figure 7 Rheological measurement of MMT nanosheet colloid. a: Strain sweep measurement b: Relationship of gel-sol transition strain and elastic modulus

2 wt% MMT nanosheet colloid formed physical gel and low strain of gel-sol transition compared to other nanosheets colloid. Here, low strain of gel-sol transition indicates the easily deform of the nematic domain. Larger LC droplets also seems to be easily deformed by weaker external shear stress. Deformed LC droplets fuse and form lager droplets because the colloid is physical gel. It suggested that orientational nematic domain of 2 wt% MMT nanosheet colloid easily broke, reoriented, and coalesced, eventually fixed as soft gel. In contrast, more 3 wt% MMT nanosheet colloid could be broken but not reoriented for high elastic modulus, and fixed. It was also confirmed with SAXS (Figure 8). Structural order of generally lyotropic LC system is depended on particle concentration. In this system, structural order decreased with increasing particle concentration. That suggested that the nanosheets could not reorientate due to high elastic modulus. The relationship between elastic modulus and orientation nematic domain was further investigated. That is, the MMT nanosheet colloid system formed fragile soft gel and then brittle hard gel. The increasing of salt in the colloid is expected to increase the elastic modulus with decreasing of diffusion electric double layer between the MMT nanosheet colloids. There, the effect of elastic modulus was investigated by increasing the NaCl concentration of the 2 wt% nanosheet colloid. The elastic modulus increased from 2.5 Pa to 27.2 Pa and 121.1 Pa in the system from 10^{-4} M NaCl concentration to 10^{-3} M and 10^{-2} M. Along with that, the orientation domains observed to became tiny. In addition, decreasing of distance between nanosheets and structural order were observed as the elastic modulus increased. Therefore, from these facts, there is a clear relationship

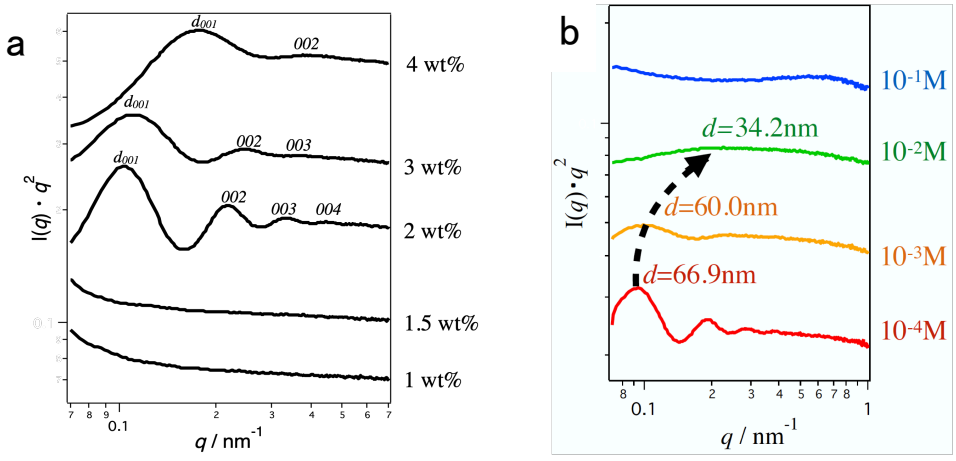

Figure 8 SAXS profiles of a: MMT nanosheets colloid of various nanosheet concentration and b: 2 wt% MMT nanosheet colloid with various salt concentration.

between the size of the alignment domain formed by the nanosheet and the elastic modulus, and by controlling this, similar results are expected in other colloidal LC system.

4.5. Conclusion

Relationship between the size of LC orientational domain and rheological property of colloid was revealed, MMT nanosheet colloid formed LC orientational domain up to mm scale. Montmorillonite nanosheet is typical industrial material and special material, machine and technic did not use, so this present system is simple. Hence, this presented system is not only the montmorillonite nanosheet, it may be possible to apply it to other lyotropic LC. In addition, Functional materials can be developed into better systems by huge orientational LC domain.

4.6. Reference

1. Kojima, Y.; Usuki, A.; Kawasumi, M.; Okada, A.; Fukushima, Y.; Kurauchi, T.; Kamigaito, O., Mechanical properties of nylon 6-clay hybrid. *J. Mater. Res.* **1993,** *8*, 1185-1189.
2. Usuki, A.; Kojima, Y.; Kawasumi, M.; Okada, A.; Fukushima, Y.; Kurauchi, T.; Kamigaito, O., Synthesis of of nylon 6-clay hybrid. *J. Mater. Res.* **1993,** *8*, 1179-1184.
3. Arakaki, A.; Shimizu, K.; Oda, M.; Sakamoto, T.; Nishimura, T.; Kato, T., Biomineralization-inspired synthesis of functional organic/inorganic hybrid materials: organic molecular control of self-organization of hybrids. *Org. Biomol. Chem.* **2015,** *13*, 974-89.
4. Haraguchi, K.; Takehisa, T.; Fan, S., Effects of Clay Content on the Properties of Nanocomposite Hydrogels Composed of Poly(N-isopropylacrylamide) and Clay. *Macromolecules* **2002,** *35*, 10162-10171.
5. Haraguchi, K.; Li, H.-J., Hydrophobic Surface Characteristics of Nanocomposite Hydrogels. *Macromolecular Symposia* **2010,** *291-292*, 159-167.
6. Ebina, T.; Mizukami, F., Flexible Transparent Clay Films with Heat-Resistant and High Gas-Barrier Properties. *Adv. Mater.* **2007,** *19*, 2450-2453.
7. Schilling, T.; Habel, C.; Rosenfeldt, S.; Röhrl, M.; Breu, J., Impact of Ultraconfinement on Composite Barriers. *ACS Appl. Polym. Mater.* **2020,** *2* (7), 3010-3015.
8. Wong, M.; Ishige, R.; White, K. L.; Li, P.; Kim, D.; Krishnamoorti, R.; Gunther, R.; Higuchi, T.; Jinnai, H.; Takahara, A.; Nishimura, R.; Sue, H. J.,

Large-scale self-assembled zirconium phosphate smectic layers via a simple spray-coating process. *Nat. Commun.* **2014,** *5*, 3589-3600.

9. Xia, Y.; Mathis, T. S.; Zhao, M. Q.; Anasori, B.; Dang, A.; Zhou, Z.; Cho, H.; Gogotsi, Y.; Yang, S., Thickness-independent capacitance of vertically aligned liquid-crystalline MXenes. *Nature* **2018,** *557* (7705), 409-412.

10. Wang, Z.; Rolle, K.; Schilling, T.; Hummel, P.; Philipp, A.; Kopera, B. A. F.; Lechner, A. M.; Retsch, M.; Breu, J.; Fytas, G., Tunable Thermoelastic Anisotropy in Hybrid Bragg Stacks with Extreme Polymer Confinement. *Angew. Chem. Int. Ed.* **2020,** *59*, 1286-1294.

11. Inadomi, T.; Ikeda, S.; Okumura, Y.; Kikuchi, H.; Miyamoto, N., Photo-Induced Anomalous Deformation of Poly(N-Isopropylacrylamide) Gel Hybridized with an Inorganic Nanosheet Liquid Crystal Aligned by Electric Field. *Macromol. Rapid. Commun.* **2014,** *35*, 1741-1746.

12. Bruggen, M. P. B. v.; Lekkerkerker, H. N. W., Metastability and Multistability: Gelation and Liquid Crystal Formation in Suspensions of Colloidal Rods. *Langmuir* **2002,** *18*, 7141-7145.

13. Luo, Z.; Song, H.; Feng, X.; Run, M.; Cui, H.; Wu, L.; Gao, J.; Wang, Z., Liquid crystalline phase behavior and sol-gel transition in aqueous halloysite nanotube dispersions. *Langmuir* **2013,** *29*, 12358-66.

14. Gabriel, J. C. P.; Camerel, F.; Lemaire, B. J.; Desvaux, H.; Davidson, P.; Michael, W.; Batail, P., Swollen liquid-crystalline lamellar phase based on extended solid-like sheet. *Nature* **2001,** *413*, 504-508.

15. Miyamoto, N.; Iijima, H.; Ohkubo, H.; Yamauchi, Y., Liquid crystal phases in the aqueous colloids of size-controlled fluorinated layered clay mineral nanosheets. *Chem. Commun.* **2010,** *46*, 4166-4168.

16. Paineau, E.; Antonova, K.; Baravian, C.; Bihannic, I.; Davidson, P.; Dozov, I.; Impéror-Clerc, M.; Levitz, P.; Madsen, A.; Meneau, F.; Michot, L. J., Liquid-Crystalline Nematic Phase in Aqueous Suspensions of a Disk-Shaped Natural Beidellite Clay. *J. Phys. Chem. B* **2009,** *113*, 15858-15869.

17. Michot, L. J.; Bihannic, I.; Maddi, S.; Funari, S. S.; Baravian, C.; Levitz, P.; Davidson, P., Liquid–crystalline aqueous clay suspensions. *Proc. Nat. Acad. Sci.* **2006,** *103*, 16101-16104.

18. Kiriya, D.; Kawano, R.; Onoe, H.; Takeuchi, S., Microfluidic control of the internal morphology in nanofiber-based macroscopic cables. *Angew. Chem., Int. Ed.* **2012,** *51*, 7942-7947.

19. Miyamoto, N.; Shintate, M.; Ikeda, M.; Hoshida, Y.; Yamauchi, Y.; Annaka, M., Liquid Crystalline Inorganic Nanosheets for Facile Synthesis of Polymer Hydrogels with Anisotropies in Optical Property, Structure, Swelling/Deswelling, and Ion Transport/Fixation. *Chem. Commun.* **2013,** *49*, 1082-1084.
20. Nakato, T.; Nakamura, K.; Shimada, Y.; Shido, Y.; Houryu, T.; Iimura, Y.; Miyata, H., Electrooptic Response of Colloidal Liquid Crystals of Inorganic Oxide Nanosheets Prepared by Exfoliation of a Layered Niobate. *J. Phys. Chem B* **2011,** *115*, 8934–8939.
21. Kim, Y. S.; Liu, M.; Ishida, Y.; Ebina, Y.; Osada, M.; Sasaki, T.; Hikima, T.; Takata, M.; Aida, T., Thermoresponsive actuation enabled by permittivity switching in an electrostatically anisotropic hydrogel. *Nat. Mater.* **2015,** *14*, 1002-1007.
22. Tominaga, M.; Nagashita, T.; Kumamoto, T.; Higashi, Y.; Iwai, T.; Nakato, T.; Suzuki, Y.; Kawamata, J., Radiation Pressure Induced Hierarchical Structure of Liquid Crystalline Inorganic Nanosheets. *ACS Photonics* **2018,** *5*, 1288-1293.
23. Miyamoto, N.; Yamamoto, S.; Shimasaki, K.; Harada, K.; Yamauchi, Y., Exfoliated Nanosheets of Layered Perovskite $KCa_2Nb_3O_{10}$ as an Inorganic Liquid Crystal. *Chem. Asian J.* **2011,** *6*, 2936-2939.
24. Kim, J. E.; Han, T. H.; Lee, S. H.; Kim, J. Y.; Ahn, C. W.; Yun, J. M.; Kim, S. O., Graphene Oxide Liquid Crystals. *Angew. Chem., Int. Ed.* **2011,** *50*, 3043-3047.

CHAPTER5

Liquid crystal phase of clay nanosheet/cellulose nanofiber

CHAPTER5

Liquid crystal phase of clay mineral nanosheet/natural cellulose nanofiber mixture

5.1. Introduction

Colloidal sol of anisotropic particles forms liquid crystal phase by increasing concentration. Liquid crystal that forms depending on mesogen concentration is called lyotropic LC. Lyotropic LC have been used to fabricate various functional materials such as structural color gel,[1, 2] anisotropic gel,[3-5] and tough Kevlar vest. In many applications, highly regulated structure of the liquid crystal phase in hierarchical manner from macroscopic to nanoscopic affords better materials properties. Applying external fields such as shear [6, 7], electric field [3 8 9 10], magnetic field [10 11 12] are good method to regulate macroscopic orientation. The use of optical tweezer was also reported as an excellent method.[13] Nanoscopic and mesoscopic scale structure is spontaneously formed by self-assembly through entropic and attractive interactions of the mesogens.

Double-component colloidal mixture system of different shape particles show further intriguing liquid crystalline phase formation behaviors compared to single component ones. The repulsive rod/plate, rod/sphere, and plate/sphere mixtures shows various liquid crystalline phases depending on the concentration of each components and the particle shapes; the structure formation is explained by only by entropic interactions among the particles.[14, 15 16 17] Introduction of attractive interactions to double-component colloidal, in addition to the entropic one, leads to more sophisticated structure formation, although such system have rarely been reported. However, if particles with positive and negative charges are mixed, a strong attractive interaction is induced and the particles form aggregates with non-regulated structures. Hence, it is favorable that particles-particle interaction is totally repulsive but partially and weakly attractive. Biopolymers having hydrogen bonds as weak attractive interactions and liquid crystallinity due to entropic interaction should be suitable in this sense. Liquid crystalline clay mineral nanosheets are also interesting system because the nanosheet surface carries a negative charge due to isomorphic substitutions, whereas nanosheet edges partially have positive charges, so that similar interactions are expected. Clay nanosheet is also distinguished by the ultra-large anisotropy and 2D shape: uniform thickness of ca. 1 nm and the lateral size of up to 100 μm. Due to the large anisotropy, LC phase is formed at very low concentration as low as < 0.2 wt%. Many applications of liquid crystalline nanosheets for anisotropic composite gel, [3 2] fibers, [18 19] and optical devices, [20] have been investigated.

So far, only a few liquid crystal systems of mixture of biopolymer and clay mineral have been reported. In the clay nanosheet + DNA system,[21] significant enhancement of liquid crystallinity was observed by the addition of DNA to clay nanosheets. In the clay mineral nanosheet + microtubules system,[22] the nanosheet-nanosheet distance in the liquid crystal phase was effectively controlled through biochemical microtubule formation induced by temperature change. We expect further development of this kind of mixture system.

Here, we demonstrate a new type double-component mixture system of liquid crystalline biopolymer and liquid crystalline clay mineral. Cellulose nanofibers (CNF) [23] with ~4 nm diameter and ~several μm length are adopted as the biopolymer. The CNF colloid has liquid crystallinity and high transparency. Recently, applications of CNF for fabrication of mechanically tough and transparent films have been attracting interests. Meanwhile, among several kinds of anisotropic particles, fluorohectorite nanosheets (FHT) was adopted as the clay counterpart. FHT colloid possess lower viscosity than other clay minerals and suitable for the fundamental studies as well as for future applications.

5.2. Experimental

Purified FHT nanosheets colloid was prepared, according to the previously reported process from NHT-B2 sol supplied from Topy Industries.[24]

Cellulose nanofiber colloid was prepared from commercially available pine tips. First, impurities such as protein, lignin, hemicellulose and non-crystalline cellulose were removed through the following process. Pine tips were immersed in toluene/ethanol (2:1) mixture solution for 6 h. Then the pine tips were immersed in 1 M sodium chlorite solution at 70 °C for 1 h. The process was repeated until the tips were bleached to white. Further, this bleached sample was immersed in 6 wt% potassium hydroxide solution for 1 d and then heated for 2 h at 80 °C, to obtain purified cellulose sample. Second, the purified cellulose was oxidized through TEMPO oxidation method.[23] The purified cellulose (4 g) was suspended in 150 mL of the aqueous solution containing 2,2,6,6-tetramethyl-1-piperidinyloxy (0.05 g), sodium bromide (0.5 g) and $NaClO \cdot 5H_2O$ (20 g) and stirred at room temperature. The pH was maintained at 10.5 by adding 0.5 M NaOH. When no more decrease in pH was observed, we considered that the reaction was finished and adjusted the pH to 7 by adding 0.5 M HCl. The oxidized sample was washed with water by centrifugation. Finally, defibration to cellulose nanofibers was conducted by ultrasonication (3 h) treatment.

Salt concentration of the FHT nanosheets colloid and cellulose nanofiber colloid were adjusted to 10^{-4} M by dialysis in NaCl solution. The FHT nanosheet colloid and the cellulose nanofiber colloid were mixed at various ratios for evaluation.

For the polarized optical microscopy observation (POM; Olympus BX 51), the samples were sealed in 0.5 mm thickness glass cell. For phase separation observation, the sample were sealed in 2 cm thickness glass cell. Structural analyses by small angle X-ray scattering (SAXS) were performed with the Rigaku NANOPIX (CuKα radiation at 30 V and 40 mA) with the camera distance of 720 mm. For the SAXS measurements, the samples were introduced into a thin glass capillary of 1.5 mm.

5.3. Results and discussion

Decreasing and increasing of LC phase were observed depending on cellulose nanofiber concentration when cellulose nanofiber was added to isotropic/LC mixture phase of FHT. Figure 1 shows phase separation observation. All the sample just sealed in the cells showed the textures with permanent interference colors over whole the sample domain. Single-component FHT colloid (0.2 vol%) separated to isotropic phase and LC phase and the volume fraction of LC phase did not significantly change after 72 h (Figure 1a). Phase separation of double-component system (FHT 0.2 vol% + CNF 0.008 vol%) (Figure 1b) was slower owing to higher viscosity caused by the cellulose nanofiber; it continued for 168 h until equilibrium state. In the equilibrium state, the volume fraction of the LC phase was smaller than the single-component FHT colloid. Interestingly, with further increasing CNF concentration (Figure 1c and d), the fraction of LC phase turned to increase. It is notable that the system with FHT 0.2 vol% + CNF 0.008 vol% (72 h and 120 h in Figure 1b), showed apparently different phase separation process compared to other system. Interference colors of blue, purple, yellow and white are observed from bottom to the top of the LC phase, indicating that the FHT concentration is high at the bottom in the intermediate state.

Double-component system was further investigated with SAXS (Figure 2a); it was revealed that even a small amount of CNF dramatically improves the structural order of the LC phase of FHT. The single-component FHT colloid (0.2 vol%) showed anisotropic 2D SAXS pattern with no peak (Figure 2a), indicating that this colloid is nematic phase with low structural regularity. As the [CNF] increases to 0.008 vol% (Figure 2c), weak peaks ascribed to 002, 003, 004 reflections are observed. From these values d_{001} that corresponds to nanosheet-nanosheet distance is estimated as 120 nm. As [CNF] is increased to 0.03 vol% or more (Figure 2e-i), the peak intensity dramatically increases and higher order peaks up to 10^{th} reflection is observed, indicating very high

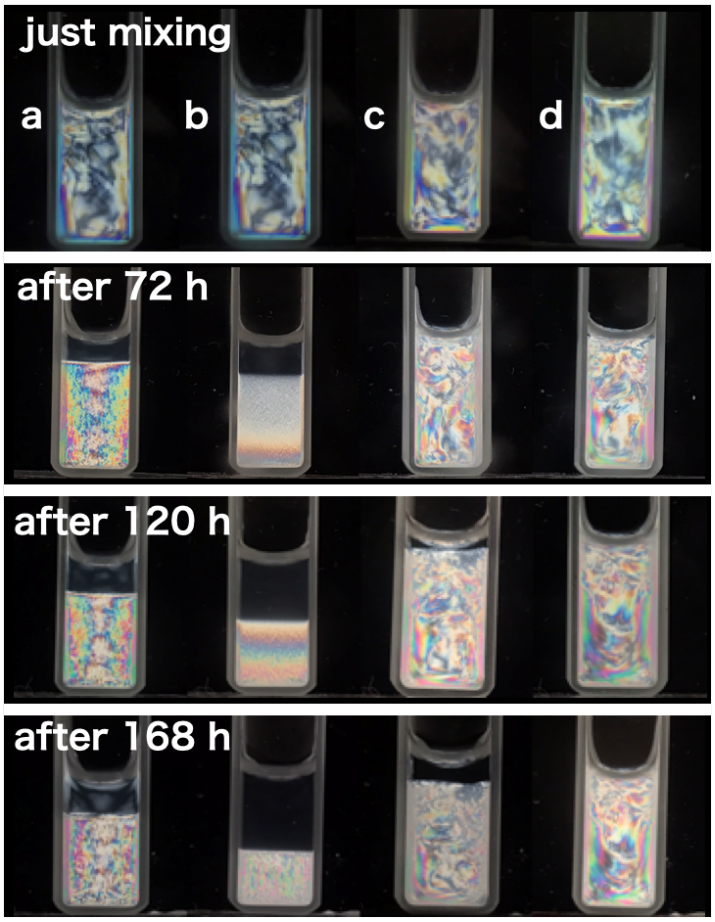

Figure 1 Phase separation observation of (a)single-component colloid of FHT and (b-d) double-component colloids of FHT and CNF. All the samples contain 0.2 vol% of FHT. CNF concentrations are (b) 0.008 vol %, (c) 0.04 vol% and (d) 0.08 vol%.

structural order. The peaks gradually shifted to higher-q with increasing [CNF], indicating the decrease of d_{001} down to 26 nm with [CNF]=0.15 vol%. The relationship between d_{001} and [CNF] is shown in Figure 3. The d_{001} value initially decrease linearly but approaches to constant value at higher [CNF]. The d values of the colloids with 0.8 vol% FHT were smaller than those with 0.2 vol% FHT, but the trend is similar.

Dependence of the SAXS profiles on FHT concentration was then investigated with the double-component colloids containing 0.04 vol% of CNF (Figure 4). With 0.005 vol% of FHT (Figure 4b), nine reflection peaks (d_{001}=77.4 nm) are observed, indicating very high structural order. In contrast, single-component 0.005 vol% FHT colloid showed no peak. As [FHT] is increased up to 0.8 vol%, the very high structural order is retained,

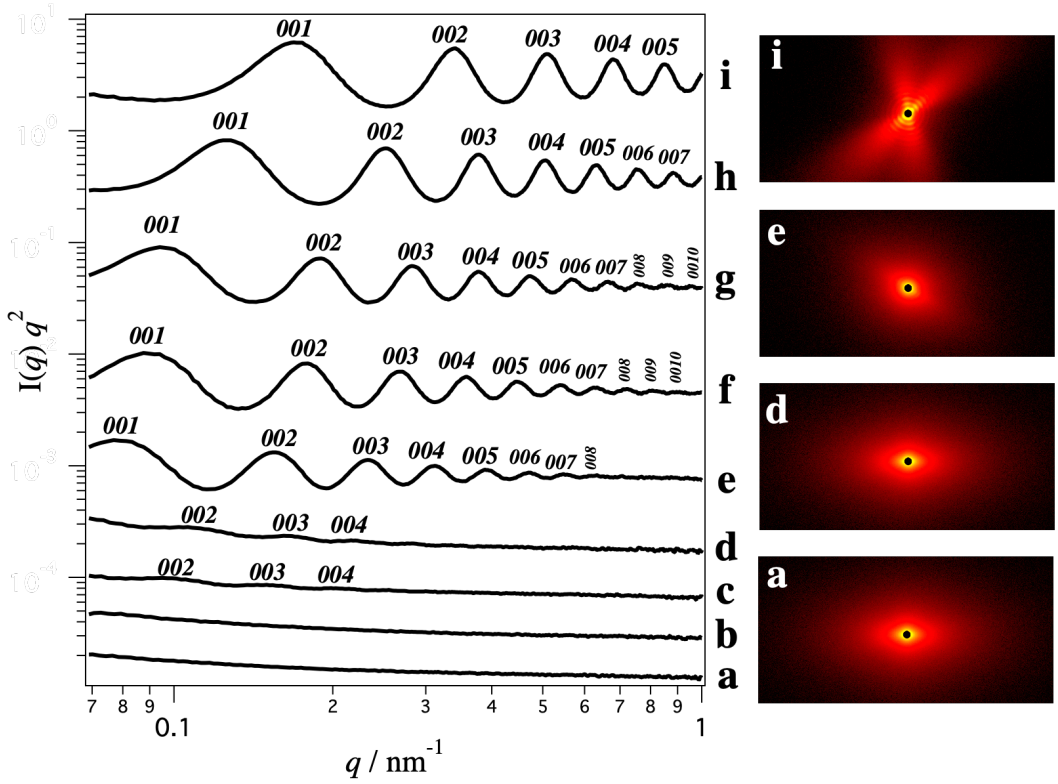

Figure 2 SAXS profiles of the double-component colloids of 0.2 vol% FHT added with CNF (a:0 vol%, b: 0.001 vol%, c:0.004 vol%, d:0.008 vol%, e:0.02 vol%, f:0.03 vol%, g:0.04 vol%, h:0.08 vol%, i:0.15 vol%).

while the d value gradually decreases. Figure 5 shows the relationship between the d value and [FHT]. With [CNF] = 0.004 vol% and 0.04 vol%, the *d* value decreases with the increase of [FHT]. However, with [CNF] = 0.15 vol.%, the d-value was almost constant, independent of [FHT]. Meanwhile, the *d* values decreased with the increase of [CNF], as already confirmed in Figure 3.

The observed d-values were much smaller than expected in swelling-law. In the case of lower nanosheet concentration, if the interactions between nanosheets are purely repulsive, we expect that the *d* value (average nanosheet-nanosheet distance) obeys isotropic swelling law of the *eq*. 1 (dashed line in Figure 4).

$$d = \left(\frac{\pi D^2 L}{4}\right)^{\frac{1}{3}} \phi^{-\frac{1}{3}} \qquad eq.\ 1$$

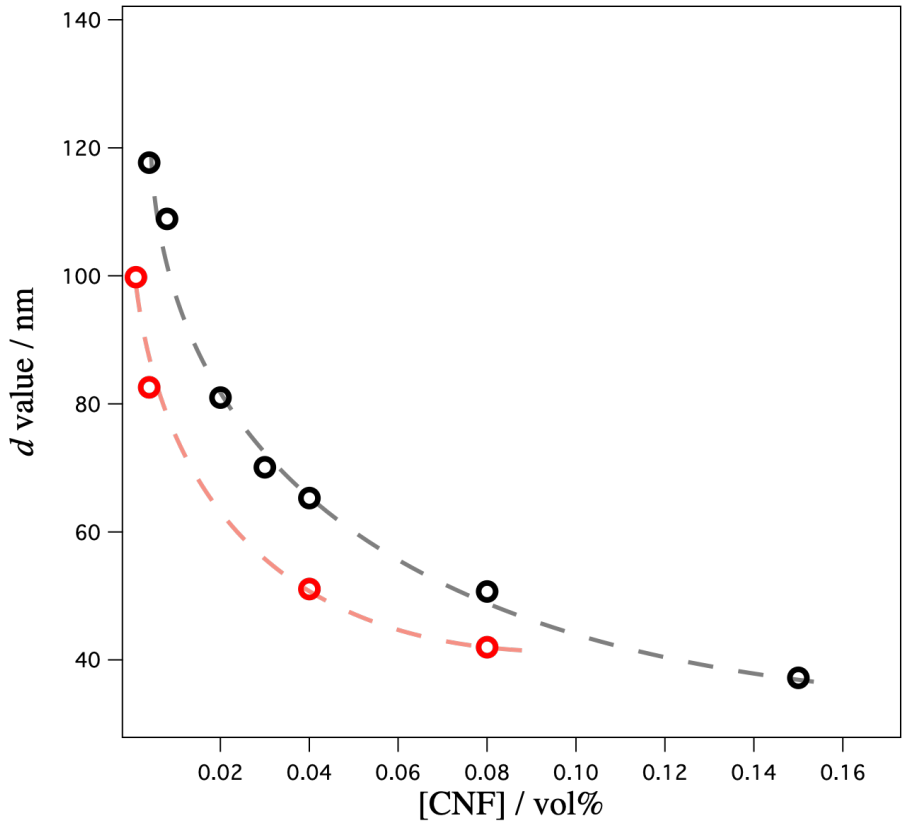

Figure 3 Relationship between the *d*-value and CNF concentration in the double-component colloids containing 0.2 vol% (black plots) and 0.8 vol% (red plots), respectively.

where L is thickness of nanosheet, D is the diameter of the nanosheet, and ϕ is volume fraction of the nanosheets. The experimental values are much smaller than the theoretical value. This indicates that the interactions between the nanosheets are not simply repulsive but partly attractive. We suppose the attractive interaction is caused by CNF adsorbed on FHT.

Adsorption of CNF to FHT was actually confirmed by using UV-Vis spectroscopy. We prepared the double-component colloid containing 0.2 vol% of FHT and 0.016 vol% of CNF. After centrifugation (15000 rpm, 1h) to remove all the FHT nanosheets, the supernatant contained only 0.006 vol% of CNF. Note that single-

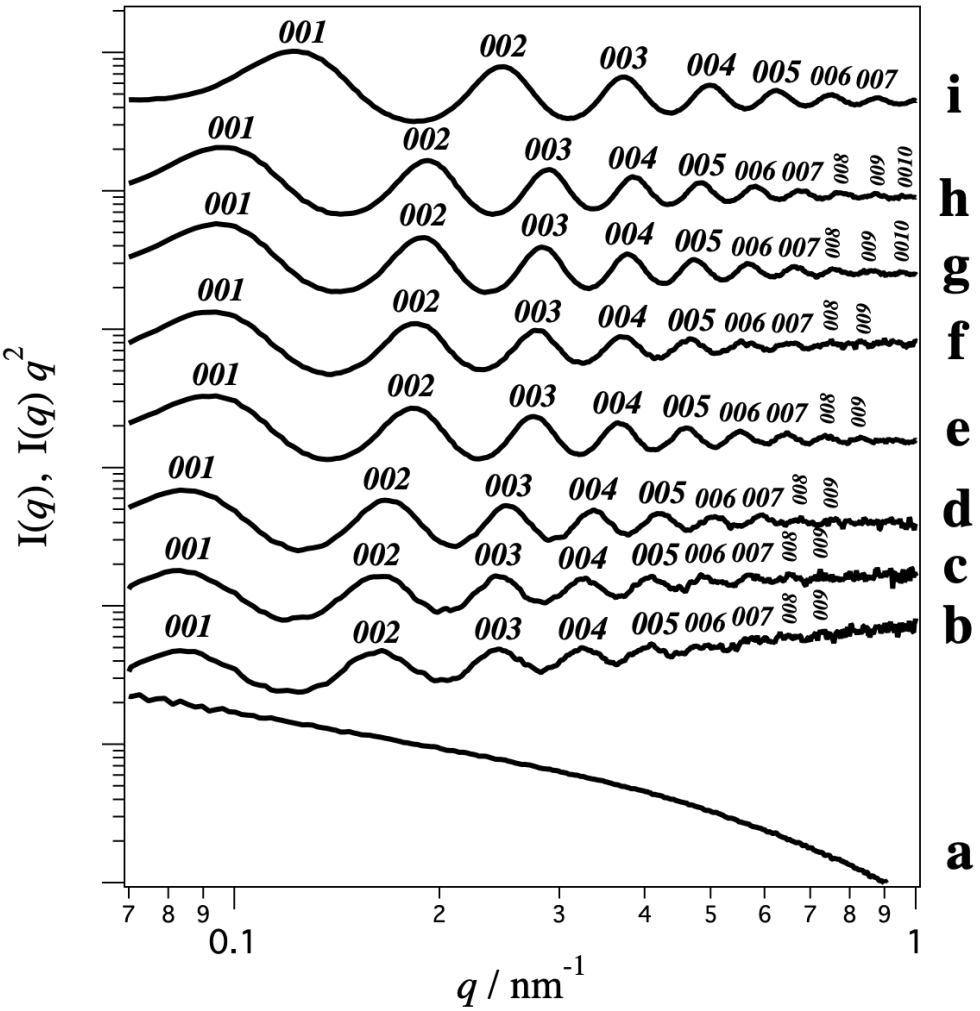

Figure 4 SAXS profiles of the double-component colloids containing 0.04 vol% of CNF and FHT (a: 0 vol%, b:0.005 vol%, c: 0.01 vol%, d:0.02 vol%, e:0.04 vol%, f:0.08 vol%, g:0.12 vol%, h:0.2 vol%, i:0.8 vol%). a is I(q) vs q plots and other samples are I(q) q^{-2} vs q plots.

component solution of CNF did not precipitate in this centrifugation condition. This result indicates that 37 % (0.006 of 0.016) of initially loaded CNF is adsorbed to FHT. This is equivalent to 5.4 x 10^{-2} mmol of $C_6H_{10}O_6$ unit per a g of clay. Considering the pH of zero charge of MgO (~12) and the pH of the present dilute colloid (~8), MgOH groups on the edge of the octahedral layer of FHT is positively charged. It is probable that the CNF are weakly adsorbed to FHT through the interaction between COO- on groups on CNF and $MgOH_2^+$/$MgOH^{(\delta+)}$ on the edge of FHT.

Considering the above result, we would propose the following model for the present system. Without addition of CNF, the interaction between the FHT nanosheets

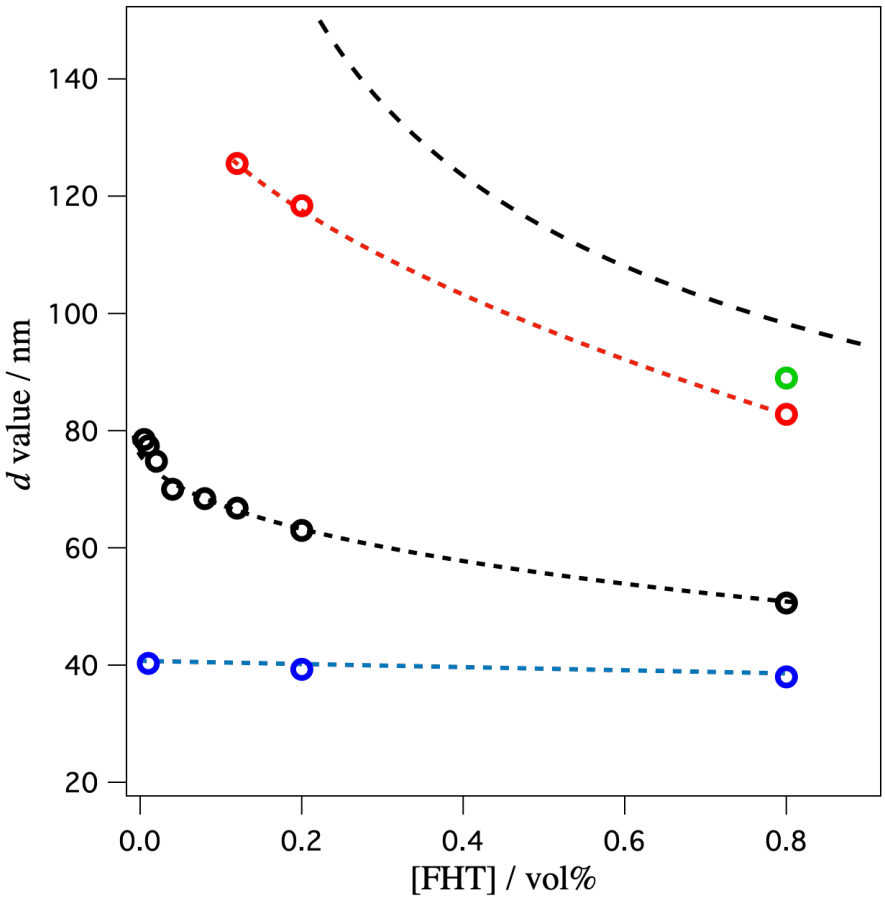

Figure 5 Relationship between the *d*-value and FHT concentration of the double-component colloid. The CNF concentration is 0 vol% (green plot), 0.004 vol% (red plots), 0.04 vol% (black plot), and 0.15 vol% (blue plot). Dashed line is the theoretical value calculated based on the swelling law expressed as *eq*. 1.

are strongly repulsive due to the electric double layer repulsion originating from the strong surface layer. The nanosheets are partly aligned due to entropic interactions to form liqud crystal-isotropic biphase. With the addition of small amount of CNF, the CNF adsorbs on the edge of nanosheets and weakly bridges the nanosheets, resulting in introduction of partly attractive interaction between the nanosheets. This causes decrease of the average nanosheet-nanosheet distance and highly regulated lamellar structure as well as the decrease of the macroscopic volume fraction of liquid crystal phase. With adding more CNF, although *d* value continued to decrease, the volume fraction of liquid crystal turned to increase. This result seems very strange and actually very unusual compared to reported double-component colloidal systems. We suppose the adsorption of CNF to FHT is saturated in this stage. However, rather than forming macroscopically

separated CNF phase and FHT phases, CNF is included in the liquid crystalline FHT phase and present as mesoscopically phase-separated state between the FHT liquid crystal domains and compress the FHT liquid crystal domains.

5.4. Conclusion

Double-component colloidal liquid crystal with highly regulated lamellar structure was obtained by addition of small amount of CNF to dilute FHT nanosheets. We considered that the unusual structural formation was caused by attractive interaction between the nanosheets mediated by CNF adsorbed to nanosheets. Based on the present results, we expect development of CNF/nanosheet nanocomposite materials with very high mechanical property and gas barrier property owing to the regulated structures.

5.5. Reference

1. Haque, M. A.; Kamita, G.; Kurokawa, T.; Tsujii, K.; Gong, J. P., Unidirectional alignment of lamellar bilayer in hydrogel: one-dimensional swelling, anisotropic modulus, and stress/strain tunable structural color. *Adv. Mater.* **2010,** *22*, 5110-5114.
2. Yang, W.; Yamamoto, S.; Sueyoshi, K.; Inadomi, T.; Kato, R.; Miyamoto, N., Perovskite Nanosheet Hydrogels with Mechanochromic Structural Color. *Angew. Chem. Int. Ed.* **accepted for publication**.
3. Inadomi, T.; Ikeda, S.; Okumura, Y.; Kikuchi, H.; Miyamoto, N., Photo-Induced Anomalous Deformation of Poly(N-Isopropylacrylamide) Gel Hybridized with an Inorganic Nanosheet Liquid Crystal Aligned by Electric Field. *Macromol. Rapid Commun.* **2014,** *35*, 1741-1746.
4. Shintate, M.; Inadomi, T.; Yamamoto, S.; Kuboyama, Y.; Ohsedo, Y.; Arimura, T.; Nakazumi, T.; Hara, Y.; Miyamoto, N., Anisotropic self-oscillating reaction in liquid crystalline nanosheets hydrogels. *J. Phys. Chem. B* **2018,** *122*, 2957–2961.
5. Miyamoto, N.; Shintate, M.; Ikeda, M.; Hoshida, Y.; Yamauchi, Y.; Annaka, M., Liquid Crystalline Inorganic Nanosheets for Facile Synthesis of Polymer Hydrogels with Anisotropies in Optical Property, Structure, Swelling/Deswelling, and Ion Transport/Fixation. *Chem. Commun.* **2013,** *49*, 1082-1084.
6. Kiriya, D.; Kawano, R.; Onoe, H.; Takeuchi, S., Microfluidic control of the internal morphology in nanofiber-based macroscopic cables. *Angew. Chem. Int. Ed.* **2012,** *51*, 7942-7947.

7. Miyamoto, N.; Shintate, M.; Ikeda, S.; Hoshida, Y.; Yamauchi, Y.; Motokawa, R.; Annaka, M., Liquid crystalline inorganic nanosheets for facile synthesis of polymer hydrogels with anisotropies in structure, optical property, swelling/deswelling, and ion transport/fixation. *Chem. Commun.* **2013,** *49* (11), 1082-4.
8. Hong, S.-H.; Shen, T.-Z.; Song, J.-K., Electro-optical Characteristics of Aqueous Graphene Oxide Dispersion Depending on Ion Concentration. *J. Phys. Chem. C* **2014,** *118*, 26304-26312.
9. Nakato, T.; Nakamura, K.; Shimada, Y.; Shido, Y.; Houryu, T.; Iimura, Y.; Miyata, H., Electrooptic Response of Colloidal Liquid Crystals of Inorganic Oxide Nanosheets Prepared by Exfoliation of a Layered Niobate. *J. Phys. Chem. C* **2011,** *115*, 8934-8939.
10. Paineau, E.; Antonova, K.; Baravian, C.; Bihannic, I.; Davidson, P.; Dozov, I.; Impéror-Clerc, M.; Levitz, P.; Madsen, A.; Meneau, F.; Michot, L. J., Liquid-Crystalline Nematic Phase in Aqueous Suspensions of a Disk-Shaped Natural Beidellite Clay. *J. Phys. Chem. B* **2009,** *113*, 15858-15869.
11. Commeinhes, X.; Davidson, P.; Bourgaux, C.; Livage, J., Orientation of Liquid-Crystalline Suspensions of Vanadium Pentoxide Ribbons by a Magnetic Field. *Adv. Mater.* **1997,** *9*, 900-903.
12. Gabriel, J. C. P.; Camerel, F.; Lemaire, B. J.; Desvaux, H.; Davidson, P.; Michael, W.; Batail, P., Swollen liquid-crystalline lamellar phase based on extended solid-like sheet. *Nature* **2001,** *413*, 504-508.
13. Tominaga, M.; Nagashita, T.; Kumamoto, T.; Higashi, Y.; Iwai, T.; Nakato, T.; Suzuki, Y.; Kawamata, J., Radiation Pressure Induced Hierarchical Structure of Liquid Crystalline Inorganic Nanosheets. *ACS Photonics* **2018,** *5*, 1288-1293.
14. van der Kooij, F. M.; Lekkerkerker, H. N. W., Liquid-Crystalline Phase Behavior of a Colloidal Rod-Plate Mixture. *Phys. Rev. Lett.* **2000,** *84*, 781-784.
15. Adams, M.; Dogic, Z.; Keller, S. L.; Fraden, S., Entropically driven microphase transitions in mixtures of colloidal rods and spheres. *Nature* **1998,** *393*, 349-352.
16. Wensink, H. H.; Vroege, G. J.; Lekkerkerker, H. N. W., Isotropic-nematic phase separation in asymmetrical rod-plate mixtures. *J. Chem. Phys.* **2001,** *115*, 7319-7329.
17. Woolston, P.; van Duijneveldt, J. S., Three-Phase Coexistence in Colloidal Rod-Plate Mixtures. *Langmuir* **2015,** *31*, 9290-9295.

18. Morooka, T.; Ohsedo, Y.; Kato, R.; Miyamoto, N., Structure-regulated tough elastomer of liquid crystalline inorganic nanosheets/polyurethane nanocomposite. *Mater. Adv.* **2021,** *2*, 1035-1042.
19. Liu, Z.; Xu, Z.; Hu, X.; Gao, C., Lyotropic liquid crystal of polyacrylonitrile-grafted graphene oxide and its assembled continuous strong nacre-mimetic fibers. *Macromolecules* **2013,** *46*, 6931−6941.
20. Miyamoto, N.; Kuroda, K.; Ogawa, M., Exfoliation and film preparation of a layered titanate, $Na_2Ti_3O_7$, and intercalation of pseudoisocyanine dye. *J. Mater. Chem.* **2004,** *14*, 165-170.
21. Yamguchi, N.; Anraku, S.; Paineau, E.; Safinya, C. R.; Davidson, P.; Michot, L. J.; Miyamoto, N., Swelling Inhibition of Liquid Crystalline Colloidal Montmorillonite and Beidellite Clays by DNA. *Sci. Rep.* **2018,** *8*, 4367.
22. Kato, R.; Kakugo, A.; Shikinaka, K.; Ohsedo, Y.; Kabir, A. M. R.; Miyamoto, N., Liquid Crystalline Colloidal Mixture of Nanosheets and Rods with Dynamically Variable Length. *ACS Omega* **2018,** *3*, 14869−14874.
23. Tsuguyuki Saito, Y. N., Jean-Luc Putaux, Michel Vignon, and Akira Isogai, Homogeneous Suspensions of Individualized Microfibrils from TEMPO-Catalyzed Oxidation of Native Cellulose. *Bio MACROMOLECULES* **2006,** *7*, 1689-1691.
24. Miyamoto, N.; Iijima, H.; Ohkubo, H.; Yamauchi, Y., Liquid crystal phases in the aqueous colloids of size-controlled fluorinated layered clay mineral nanosheets. *Chem. Commun.* **2010,** *46*, 4166-4168.

CHAPTER6

Liquid Crystalline Colloidal Mixture of Nanosheets and Rods with Dynamically Variable Length

CHAPTER6

Liquid Crystalline Colloidal Mixture of Nanosheets and Rods with Dynamically Variable Length

6.1. Introduction

Anisotropic and hierarchical structures composed of inorganic and organic nanocomponents, such as abalone shell (protein + calcium carbonate) and human body (muscle + bone), are key for sophisticated functions of living organisms.[1] The complex architectures of living organisms are assembled through consumption of energy and exchange of molecules. Inspired by living systems, many kinds of artificial materials with regulated superstructures and functions have been fabricated by controlling electrostatic force, hydrogen bond, Van der Waals interactions and coordination bond: DNA-origami,[2] mesophases of liquid crystals (LC), surfactant micelles, and metal-organic-framework[3] are old and new examples. In addition to those interactions, entropic interactions are also important to regulate the assembly of the nano-components. Prominent examples are the ordered structures found in colloidal systems [4] such as colloid crystals and colloidal liquid crystals.[5] Further, combination of components with dissimilar morphology such as rod/plate,[6] rod/sphere,[7] plate/sphere,[8] nanosheet/rod,[9] nanosheet/nanosheet,[10] and plate/polymer [11] types of particles also facilitates formation of variety of well-ordered structures. Thus, complexity of the system is a key to develop highly organized and hierarchical structures.

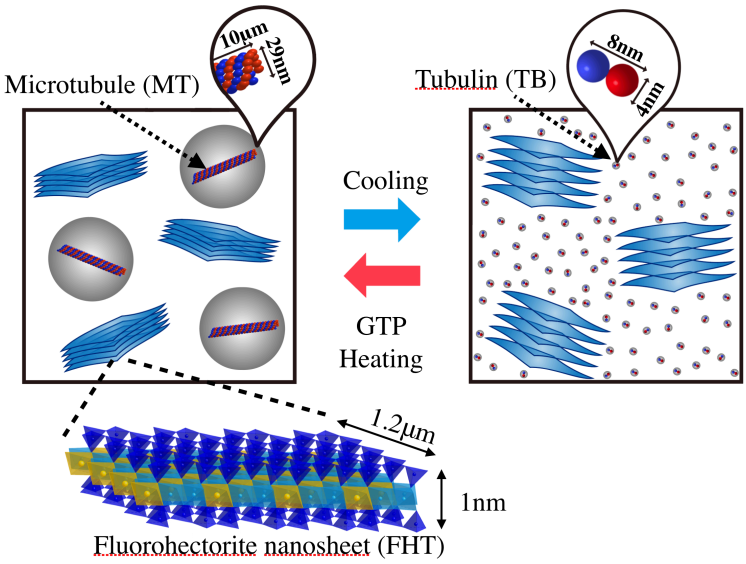

Scheme 1. Overview of this study.

Herein, we demonstrate a new-type double-component colloidal system composed of two types of colloidal LC mesogens (Scheme 1): one is a thin platy particle and the other is a rigid hollow rod with the length reversibly controllable in-situ in response to temperature. As the platy particle, we use inorganic nanosheets obtained by exfoliation of a layered clay mineral fluorohectorite (FHT).[12] Among several kinds of anisotropic particles, nanosheets [13] [14] are distinguished by the ultra-large anisotropy and 2D shape: uniform thickness of ca. 1 nm and the lateral size of up to 100 μm. Due to the large anisotropy, LC phase is formed at very low concentration as low as < 0.2 wt%.[15] Many applications of liquid crystalline nanosheets for anisotropic composite gel[16], fibers[17], optical devices[18], and anisotropic medium for spectroscopy[19] have been investigated. High biocompatibility of the clay nanosheets[20] allows us to choose a living biopolymer, microtubule (MT), as the counterpart. MT is a hollow rod with the diameter of 25 nm, length of up to several tens of μm, and high rigidity (the persistent length on the order of millimeters).[21, 22] MT is actively formed by polymerization of tubulin dimers (TBs) through biochemical reaction that consume biochemical energy obtained from hydrolysis of guanosine triphosphate (GTP) at ~37 °C , while it reversibly dissociates to TBs by cooling. Due to the large excluded volume of the rigid hollow tube, the solution of microtubules forms a nematic LC phase. Organization of microtubules into well-defined structure is valuable for future applications as artificial muscle, sorting device, and biosensors. The present system will not only give new insights to mixed colloidal systems controlled by entropic interactions but also lead to various active molecular devices of which structures are hierarchically regulated both by the mesogenic nanosheets and MT rods.

6.2. Experimental

The liquid crystalline nanosheet colloid of synthetic fluorohectorite (FHT) was prepared, according to the previously reported process from NHT-B2 sol supplied from Topy Industries.[12] This colloidal solution was diluted with pure water to 2 wt%. Average particle size of the nanosheets were 1.2 μm with the standard deviation of 0.14 μm. TB was extracted and purified from porcine brain according to the previously reported process[23], using aqueous buffer solution (pH 6.8) containing 1 M of 1,4-piperazinediethanesulfonic acid (PIPES), 20 mM of ethylene glycol tetraacetic acid (EGTA), and 10 mM of $MgCl_2$. To polymerize the TB to MT, the TB solution was added with GTP and dimethylsulfoxide (the final concentrations are 0.1 mM and 5 vol %, respectively) and incubated at 37 ºC for 30 min. The nanosheet colloid and MT solution

were mixed at various ratios to obtain the samples for evaluation. For all the samples, including single component FHT colloid, the concentrations of the buffer constituents were adjusted to 0.08 M of PIPES, 0.001 M of EGTA, and 0.001 M of $MgCl_2$ for the polarized optical microscopy observation (POM; Nikon ECLIPSE LV100POL), the samples were sealed in a glass capillary. Structural analyses by small angle X-ray scattering (SAXS) were performed with the Bruker Nanostar (CuKα radiation at 30 V and 40 mA) with the camera distance of 1070 mm or with the Rigaku NANOPIX (CuKα radiation at 30 V and 40 mA) with the camera distance of 750 mm. For the SAXS measurements, the samples were introduced into a thin glass capillary or a cell with the thickness of 1.5 mm. The SAXS and POM observations were conducted under controlled temperature of 4 or 37 °C.

6.3. Results and discussion

FHT and MT were uniformly mixed and polymerization /depolymerization of MT proceeded without being disturbed by the presence of the nanosheets. The single-component colloids of FHT (2 wt%) (Figure 1a) and MT (120 μM) (Figure 1b) showed permanent birefringence due to the LC phase in which nanosheets[12] or MTs are oriented.[24] Due to the flow of the sample when it was introduced into the capillary, the optical axis is preferentially oriented along the capillary wall. No specific textures like Schlieren texture were observed. The double-component system containing both FHT and MT (Figure 1c) showed birefringent image similar to the single-component FHT system. It is notable that we did not observe phase separation or aggregation of the nanosheets, confirming that the two components are mixed homogeneously. Generally, in double-component colloidal liquid crystalline systems, macroscopic phase separations is observed after storing the sample for sufficiently long time[25] or by centrifugation,[26] which is valuable to investigate the system more in detail. However, this phenomenon was not observed in our system although we stored the sample up to 24h; we cannot store the sample longer at the present condition since MT dissociate into TBs when GTP is exhausted. Gravity-induced sedimentation also sometimes prevents us from clear observation of the phase separation.

The birefringence was weakened when the double-component sample was cooled at 4 ºC for 30 min (Figure 1d). This indicates depolymerization of MTs to TBs.The birefringence of the double component system was weaker than the single-component nanosheet colloid containing same concentration of the nanosheet, suggesting that TBs interact with the nanosheets and partly disturbed the formation of LC phase of the nanosheets.

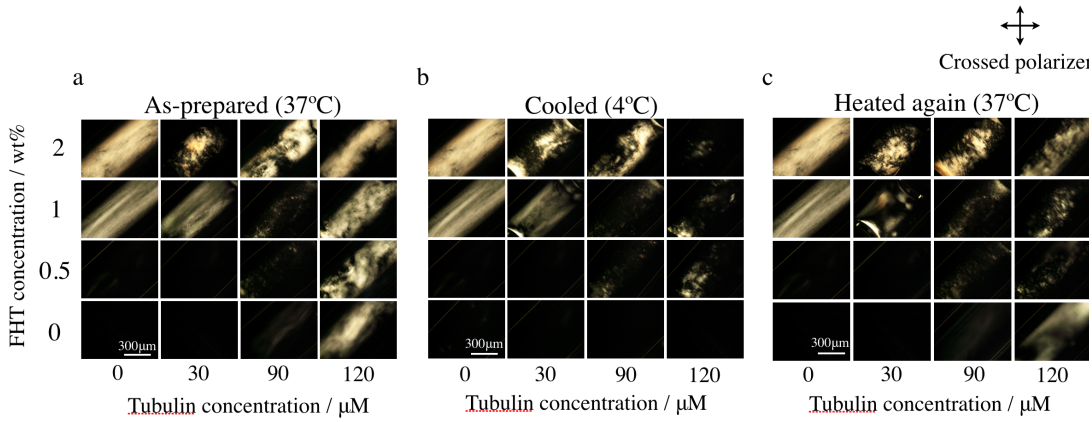

Figure 2 POM images of the FHT/MT mixtures at various mixing ratio. The observation was made (a) as-prepared (37℃), (b) after cooling (4℃), and (c) after heating again (37℃).

Effects of the concentrations of FHT and MT were then examined. Figure 2 shows the POM images of the solutions containing various concentrations of FHT and MT. The single-component FHT systems showed the LC phase at above 1 wt% and the birefringence increased with increasing FHT concentration. They did not show temperature dependence. Meanwhile, the single component MT system showed LC phase at above 90 μM, and birefringence increased with increase in MT concentration. In the double-component system, the stronger birefringence was observed at higher MT or FHT concentrations. The samples containing MT showed response to temperature with or without the nanosheets.

SAXS measurements revealed the structural change on the mesoscale induced by temperature change, corresponding to the macroscopic change observed by POM. The profile of MT solution (Figure 3a) agrees with the theoretical form factor[27] shown as *eq*. (1) (Figure 3a') of hollow cylinder with the outer and inner diameters of 29 and 21 nm, respectively.

$$P(q) = \frac{A}{V_{shell}} \int_0^{\frac{\pi}{2}} f^2(q,\alpha) \sin\alpha \, d\alpha \qquad (1)$$

where $f(q,\alpha) = 2\Delta\rho V_{core} J_0(qH\cos\alpha) \frac{J_1(qr\sin\alpha)}{(qr\sin\alpha)}$

$$+2\Delta\rho V_{core} J_0[q(H+t)\cos\alpha)] \frac{J_1[q(r+t)\sin\alpha)]}{[q(r+t)\sin\alpha)]}$$

$$J_0(x) = \frac{\sin(x)}{x}, V_{core} = \pi r^2 L, V_{shell} = \pi(r+t)^2 L$$

Here, q is scattering vector, r is core radius, $r+t$ is shell radius, L is length of MT, $\Delta\varrho$ is the scattering contrast between the core and the shell, A is the factor related to the particle volume and concentration, and J_1 is the first order Bessel function. This geometrical size corresponds to the microtubules composed of 15 TBs in one lap, while it is known that the MTs with various diameter is formed depending on the condition.[28] The nanosheet colloid (Figure 3c) and mixture of nanosheet and MT (Figure 3b) showed profiles with the slope of q^{-2}. This indicates that the most of the nanosheets are present as single layers because the theoretical form factor (*eq*.(2)) (Figure 3c') of the nanosheets is approximated as q^{-2} for the nanosheets larger than 100 nm in the range of q in the present measurement.[10]

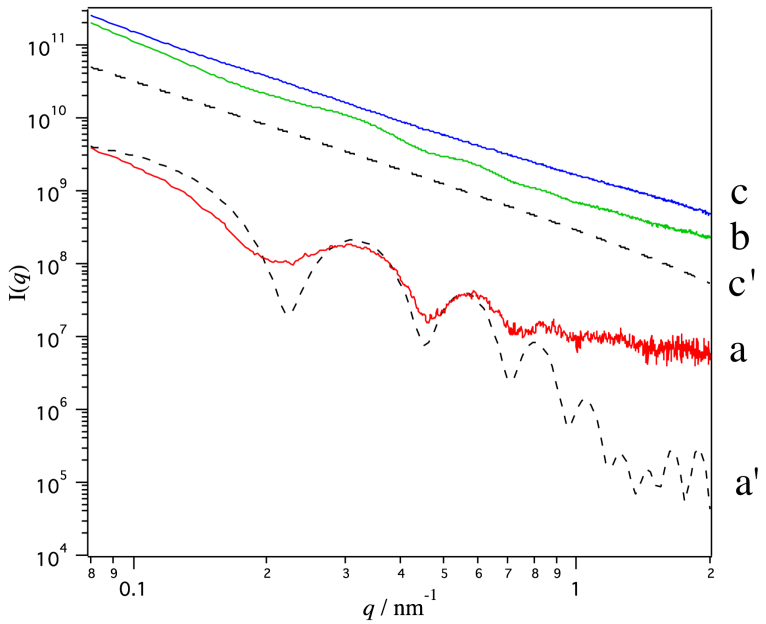

Figure 3 The SAXS patterns of (a) MT solution (from 75 μM of TB), (b) the mixture of FHT (4wt.%) and MT (from 75 μM of TB), and (c) FHT colloid (4 wt.%). The theoretical form factors for (a') hollow cylinder and (c') thin disk are also shown as doted lines.

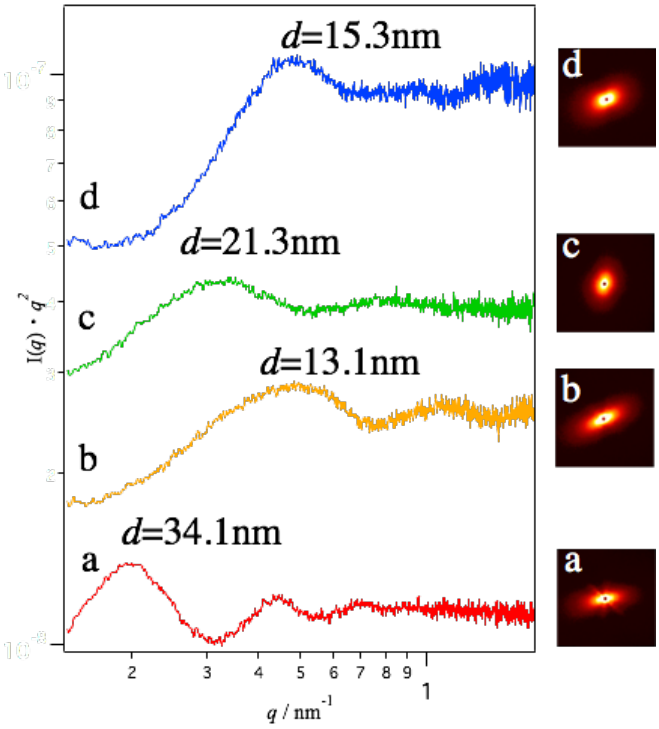

Figure 4 SAXS patterns of (a) single component FHT colloid, (b) as-prepared FHT/MT mixture (37 °C), (c) FHT/TB obtained by cooling the FHT/MT to 4°C, and (d) FHT/MT mixture obtained heating to at 37 °C again. Concentrations of FHT and MT/TB are 4 wt% and 75 μM of TB, respectively.

$$P(q) = \left(\frac{2}{q^2R^2}\right)\left[1 - \frac{J_1(2qR)}{qR}\right]\frac{sin^2(qL/2)}{(qL/2)^2} \qquad (2)$$

Note that the profile in the double component system mainly reflects the scattering from nanosheets because scattering capability of the inorganic nanosheets is more than one order of magnitude higher than MTs which is composed only of organic atoms.

From the SAXS patterns, the superstructures in the double component colloids were evaluated after eliminating the effect of form factor. The as-observed scattering profile $I(q)$ is expressed as

$$I(q) = A\, S(q)\, P(q) \qquad (3)$$

where $S(q)$ is the structure factor, $P(q)$ is the form factor and A is a factor determined by scattering power and number of the particles.

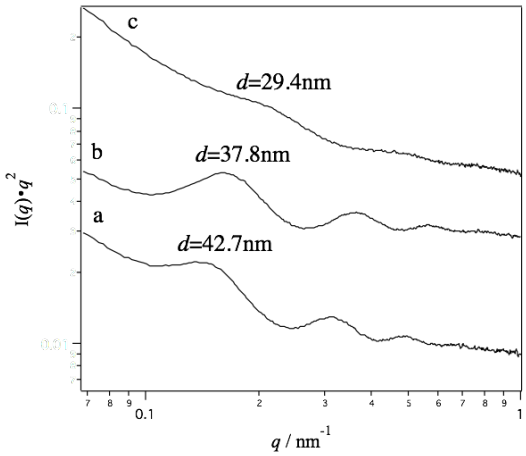

Figure 5 SAXS patterns of (a) FHT only, (b) FHT +1% buffer (0.01 M of PIPES, 0.0002 M of EGTA, and 0.0001 M of $MgCl_2$) and (c) FHT + 10% buffer 1 (0.1 M of PIPES, 0.002 M of EGTA, and 0.001 M of $MgCl_2$) in FHT.

Since the form factor $P(q)$ of the nanosheets is approximated as q^{-2}, $S(q)$ is calculated as $S(q) = I(q)\ q^2$ with A=1. As the consequence, we show $I(q)\ q^{-2}$ vs q plots in Figure 4 to discuss the structure of the colloid. Single component FHT colloid (Figure 4a) showed the peaks due to the structure with the basal spacing d = 34.1nm.[12] In the double component system of FHT and MT (Figure 4b), the peak shifted to higher q (d = 13.1nm). After cooling, the peak shifted to lower q (d = 21.3nm) again. The temperature-triggered change is reversible reaction and the peak shifted to higher q (d = 15.3 nm) after heating again. Although basal spacing significantly changes by salt effect (Figure 5), we have adjusted the concentration of the buffer constituents in all the samples examined. Hence, the observed peak shift is explained that the coexisting MTs deprive the free volume for nanosheets so that the nanosheet LC phase was compressed. The 2D-SAXS patterns (right side of Figure 4) are more or less anisotropic for all the cases, indicating the presence of anisotropic liquid crystalline domains. Although the concentrations were adjusted to exactly the same, the peak position in Fig. 3b and 4b are different because these samples were prepared from different batch of tubulin purified on different date. Because the present system is a biochemical system, the obtained data largely depend on the sample batch.

Structural formation in response to temperature found in the double-component system is driven by entropic interactions explained based on the Onsager theory.[31] Onsager theory consider hard core *repulsive* force between the cylindrical particles (D>>L is disk or D<<L is rod) of diameter D and length L. The particles occupy

considerably larger excluded volume b as compared with their own actual volume v_p (= $\pi D^2 L/4$) when the anisotropic particles are freely rotating. The b/v_p is calculated by the following equation:

$$\frac{b}{v_P} = \frac{1}{v_p}\frac{1}{4}\pi D\left(L^2 + \frac{1}{2}(\pi + 3)DL + \frac{1}{4}\pi D^2\right) \quad (4)$$

When the sum of the excluded volume b becomes larger than a certain value, the particles cannot keep free rotation so that liquid crystal phase is formed. It has been reported so far that the formation of liquid crystal phase of nanosheet colloids can roughly be explained by this theory.[32, 33] Since both the FHT nanosheets and MTs are negatively charged, repulsive force is dominant in the system, so that Onsager theory can be applied in this double component system. Usually, when treating with Onsager theory, electrostatic repulsion between the charged particles is taken into account, for example, by considering effective size of particles defined as the sum of the size of particle core and the additional size related to Debye length and charge density. However, here we ignore this effect because ionic strength is adjusted at high value (>0.2 M) and the high ionic strength screens the electrostatic interaction.

If the MT is regarded as a cylinder with D_{MT} = 29 nm and L_{MT} = 10^4 nm, the excluded volume b per one MT unit is calculated as 2.5 × 10^9 nm^3 from the eq. (4). Meanwhile, the b for one TB dimer is 5.5 × 10^2 nm^3 if we model the dimer as a cylinder with D_{TB} = 4 nm and L_{TB} = 8 nm. The number of the dimers consisting one MT is calculated as L_{MT} / 8 × 15= 1.9 × 10^4, considering that the dimer is 8 nm in height and there are 15 dimers per a lap. Thus, when one microtubule is cooled and dissociates into TBs, the total excluded volume reduces to (1.9 × 10^4) × (5.5 × 10^2) = 1.0×10^7 nm^3, that is 250 times smaller than the value for the MT. Therefore, when TBs polymerize to MTs, the free volume for nanosheets is largely deprived. Considering the SAXS result that the spacing between the nanosheets in the double component system is smaller than the diameter of the MT (29 nm), MTs cannot be present between the nanosheets forming the LC phase. This indicates that nanosheets and MTs are forming separated LC domains although they seem to be homogeneously mixed on the macroscopic scale as observed by POM. The decrease in the basal spacing in the double component system compared to the single component FHT nanosheets colloid is ascribable to the compression of the liquid crystal phase of nanosheet by coexisting MTs.

6.4. Conclusion

FHT nanosheet colloid and MT were mixed uniformly, and biochemical polymerization/ depolymerization of MT proceeded without being disturbed by the presence of nanosheets. The present system is highlighted as the first system that nanosheets are mixed with rods that reversibly change their length triggered by external factors. Such the system will be a good model system for fundamental studies of anisotropic colloidal systems composed of multiple mesogenic components. Since microtubules constitutes molecular motor system with kinesin, the present system will be further developed as a new molecular motor system or artificial muscle with hierarchical ordered structure formed by synergy of the mesogenic nanosheets and the biological MTs.

6.5. Reference

1. Arakaki, A.; Shimizu, K.; Oda, M.; Sakamoto, T.; Nishimura, T.; Kato, T., Biomineralization-inspired synthesis of functional organic/inorganic hybrid materials: organic molecular control of self-organization of hybrids. *Org. Biomol. Chem.* **2015,** *13*, 974-89.
2. Rothemund, P. W. K., Folding DNA to create nanoscale shapes and patterns. *Nature* **2006,** *440*, 297-302.
3. Zhou, H. C.; Kitagawa, S., Metal-organic frameworks (MOFs). *Chem. Soc. Rev.* **2014,** *43*, 5415-8.
4. Lekkerkerker, H. N.; Vroege, G. J., Liquid crystal phase transitions in suspensions of mineral colloids: new life from old roots. *Philosophical Transactions. Series A, Mathematical, physical, and engineering sciences* **2013,** *371* (1988), 20120263.
5. van der Kooij, F. M.; Kassapidou, K.; Lekkerkerker, H. N. W., Liquid crystal phase transition in suspensions of polydisperse plate-like particles. *Nature* **2000,** *406*, 868-871.
6. van der Kooij, F. M.; Lekkerkerker, H. N. W., Liquid-Crystal Phase Formed in Mixed Suspensions of Rod- and Platelike Colloids. *Langmuir* **2000,** *16*, 10144-10149.
7. Adams, M.; Dogic, Z.; Keller, S. L.; Fraden, S., Entropically driven microphase transitions in mixtures of colloidal rods and spheres. *Nature* **1998,** *393* (6683), 349-352.
8. Kleshchanok, D.; Petukhov, A. V.; Holmqvist, P.; Byelov, D. V.; Lekkerkerker, H. N. W., Structures and phase behavior in mixtures of charged colloidal spheres and platelets. *Langmuir* **2010,** *26* (16), 13614-21.

9. Woolston, P.; van Duijneveldt, J. S., Three-Phase Coexistence in Colloidal Rod-Plate Mixtures. *Langmuir* **2015,** *31* (34), 9290-9295.
10. Yamaguchi, D.; Miyamoto, N.; Koizumi, S.; Nakato, T.; Hashimoto, T., Hierarchical structure of niobate nanosheets in aqueous solution. *J. Appl. Cryst.* **2007,** *40*, s101–s105.
11. Wensink, H.; Lekkerkerker, H., Sedimentation and multi-phase equilibria in mixtures of platelets and ideal polymer. *Europhys. Lett. 66*, 125-131.
12. Miyamoto, N.; Iijima, H.; Ohkubo, H.; Yamauchi, Y., Liquid crystal phases in the aqueous colloids of size-controlled fluorinated layered clay mineral nanosheets. *Chem. Commun.* **2010,** *46*, 4166-4168.
13. Sasaki, T.; Watanabe, M.; Hashizume, H.; Yamada, H.; Nakazawa, H., Macromolecule-like Aspects for a Colloidal Suspension of an Exfoliated Titanate. Pairwise Association of Nanosheets and Dynamic Reassembling Process Initiated from It. *J. Am. Chem. Soc.* **1996,** *118*, 8329-8335.
14. Osada, M.; Sasaki, T., Two-Dimensional Dielectric Nanosheets: Novel Nanoelectronics From Nanocrystal Building Blocks. *Adv. Mater.* **2012,** *24*, 210-228.
15. Miyamoto, N.; Nakato, T., Liquid Crystalline Inorganic Nanosheet Colloids Derived From Layered Materials. *Israel J. Chem.* **2012,** *52*, 881-894.
16. Inadomi, T.; Ikeda, S.; Okumura, Y.; Kikuchi, H.; Miyamoto, N., Photo-Induced Anomalous Deformation of Poly(N-Isopropylacrylamide) Gel Hybridized with an Inorganic Nanosheet Liquid Crystal Aligned by Electric Field. *Macromol. Rapid Commun.* **2014,** *35*, 1741-1746.
17. Liu, Z.; Xu, Z.; Hu, X.; Gao, C., Lyotropic liquid crystal of polyacrylonitrile-grafted graphene oxide and its assembled continuous strong nacre-mimetic fibers. *Macromolecules* **2013,** *46*, 6931–6941.
18. Miyamoto, N.; Kuroda, K.; Ogawa, M., Exfoliation and film preparation of a layered titanate, $Na_2Ti_3O_7$, and intercalation of pseudoisocyanine dye. *J. Mater. Chem.* **2004,** *14*, 165-170.
19. Gabriel, J. C. P.; Camerel, F.; Lemaire, B. J.; Desvaux, H.; Davidson, P.; Michael, W.; Batail, P., Swollen liquid-crystalline lamellar phase based on extended solid-like sheet. *Nature* **2001,** *413*, 504-508.
20. Yamamoto, S.; Ohsedo, Y.; Yamada, E.; Sonoda, K.; Mita, H.; Miyamoto, N., Cultivation of Cellulose-Producing Bacteria in the Nanosheet Liquid Crystal of Na-fluorohectorite. *Clay Sci.* **2015,** *19*, 73-77.

21. Wada, S.; Kabir, A. M.; Ito, M.; Inoue, D.; Sada, K.; Kakugo, A., Effect of length and rigidity of microtubules on the size of ring-shaped assemblies obtained through active self-organization. *Soft Matter* **2015,** *11*, 1151-7.
22. Luria, I.; Crenshaw, J.; Downs, M.; Agarwal, A.; Seshadri, S. B.; Gonzales, J.; Idan, O.; Kamcev, J.; Katira, P.; Pandey, S.; Nitta, T.; Phillpot, S. R.; Hess, H., Microtubule nanospool formation by active self-assembly is not initiated by thermal activation. *Soft Matter* **2011,** *7*, 3108-3115.
23. Castoldi, M.; Popov, A. V., Purification of brain tubulin through two cycles of polymerization–depolymerization in a high-molarity buffer. *Protein Expression and Purification* **2003,** *32*, 83-88.
24. Kakugo, A.; Tamura, Y.; Shikinaka, K.; Yoshida, M.; Kawamura, R.; Furukawa, H.; Osada, Y.; Gong, J. P., Formation of Well-Oriented Microtubules with Preferential Polarity in a Confined Space under a Temperature Gradient. *J. Am. Chem. Soc.* **2009,** *131*, 18089–18095.
25. van der Kooij, F. M.; Lekkerkerker, H. N. W., Liquid-Crystalline Phase Behavior of a Colloidal Rod-Plate Mixture. *Phys. Rev. Lett.* **2000,** *84*, 781-784.
26. Beek, D. v. d.; Radstake, P. B.; Petukhov, A. V.; Lekkerkerker, H. N. W., Fast Formation of Opal-like Columnar Colloidal Crystals. *Langmuir* **2007,** *23*, 11343-11346.
27. Shigehara, K.; Kudoh, H.; Mori, S.; Tamura, Y.; Kakugo, A.; Kawamura, R.; Furukawa, H.; Gong, J. P.; Masunaga, H.; Masui, T.; Koizumi, S.; Shikinaka, K., Nematic growth of microtubules that changed into giant spiral structure through partial depolymerization and subsequent dynamic ordering. *Soft Matter* **2012,** *8*, 11544.
28. Wade, R. H.; Chrétien, D.; Job, D., Characterization of Microtubule Protofilament Numbers How Does the Surface Lattice Accommodate? *J. Mol. Biol.* **1990,** *212*, 775-786.

CHAPTER7

CHAPTER7

Conclusion

The results of this thesis demonstrated control of liquid crystallinity and rheological property of clay mineral nanosheet by adding organic double-component such as poor solvent, carbonyl compound, polymer, cellulose nanofiber, tubulin.

In viewpoint of rheological property, It was revealed that the addition of carbonyl compound is a useful means for rheological property control. Furthermore, strong relationship between the rheological property of the nanosheet colloid with forming the LC phase was revealed, montmorillonite nanosheets colloid automatically forming non defect liquid crystalline structure at cm-scale. Uniformly orientated nanosheet / polymer composite gel immobilized the liquid crystal phase showed high mechanical strength. Functional materials can be developed into better systems by uniformly dispersing the filler. Montmorillonite nanosheet is typical industrial material, special material, machine and technic did not use, so this present system is simple. This present system may be not only the montmorillonite nanosheet, It may be possible to apply it to other systems.

In viewpoint of liquid crystallinity, behavior of forming LC structure of nanosheets in water/DMF mixture was observation without aggregation. The system is expected to filler of composite materials such as elastomer, hydrophobic plastic and gas barrier film. High ordered structure was formed by adding different shape liquid crystallinity semi-rigid polymer. Composite material using the structure also was considered. Nanosheet / tubulin system is highlighted as the first system that nanosheets are mixed with rods that reversibly change their length triggered by external factors. Such the system will be a good model system for fundamental studies of anisotropic colloidal systems composed of multiple mesogenic components. Since microtubules constitutes molecular motor system with kinesin, the present system will be further developed as a new molecular motor system or artificial muscle with hierarchical ordered structure formed by synergy of the mesogenic nanosheets and the biological tubulin.

List of publication

1 “Various function and application of inorganic nanosheet”
Science and industry、Vol.91、No.4、pp.85-95 (2017)
Nobuyoshi Miyamoto, Riki Kato

2 “Liquid Crystallin Colloidal Mixture of Nanosheets and Rods with Dynamically Variable Length”
ACS Omega, Vol. 3, No. 11, pp.14869-14874 (2018)
Riki Kato, Akira Kakugo, Kazuhiro Shikinaka, Yutaka Ohsedo, Arif Md. Kabir, Nobuyoshi Miyamoto

3 “Design and phase transition behavior of siloxane-based monomeric liquid crystals bearing cholesteryl mesogenic groups”
Journal of Organometallic Chemistry, Vol. 886, No. 15 pp.34-39 (2019)
Kaito Katsuki, Kosuke Kaneko, Kimiyoshi Kaneko, Riki Kato, Nobuyoshi Miyamoto, Tomonori Hanasaki

4 “High Virus Removal by Self-Organized Nanostructured 2D lLiquid-Crystalline Smectic Membranes for Water Treatment”
Small, Vol. 16, No. 23, pp.2001721-2001725 (2020)
Daniel Kuo, Miaomiao Liu, K. R. Sunil Kumar, Kazuma Hamagichi, Kian Ping Gan, Takeshi Sakamoto, Takafumi Ogawa, Riki Kato, Nobuyoshi Miyamoto, Hiroki Nada, Masahiro, Kimura, Masahiro Henmi, Hiroyuki, Katayama, Takashi Kato

5 “Stsucture-regulated tough elastomer of liquid crystalline inorganic nanosheets/polyurethane nanocomposite”
Materials Sciences, Vol.2, pp.1035-1042, (2021)
Toki Morooka, Yutaka Ohsedo, Riki Kato and Nobuyoshi Miyamoto

6 “Perovskite Nanosheet Hydrogels with Mechanochromic Structural Color”
Angewante Chemie International Edition, accepted for publication. (2021)
Wenqi Yang, Shinya Yamamoto, Keiichiro Sueyoshi, Takumi Inadomi, Riki Kato, Nobuyoshi Miyamoto

Acknowledgement

I would like to express my acknowledgement and appreciation to associate professor Nobuyoshi Miyamoto for discussion, variable advice, continuous encouragement. Thanks to you, I could do research, I could write the thesis.

Special thanks are due to associate professor Akira Kakugo, senior researcher Kazuhiro Shikinaka, associate professor Yutaka Ohsedo, assistant professor Kosuke Kaneko, professor Takashi Kato, Dr. Daniel Kuo, professor Patrick Davidson, Dr. Erwan Paineau Dr. Shinya Anraku for discussion and advice of joint research.

Finally, I thank laboratory member, friends, my parents, my family, my grandparents for understanding and support.